

**NASA Contractor Report 3023**

(NASA-CR-3023) WORKBOOK FOR ESTIMATING  
EFFECTS OF ACCIDENTAL EXPLOSIONS IN  
PROPELLANT GROUND HANDLING AND TRANSPORT  
SYSTEMS Final Report (Southwest Research  
Inst.) 274 p HC A12/MF A01

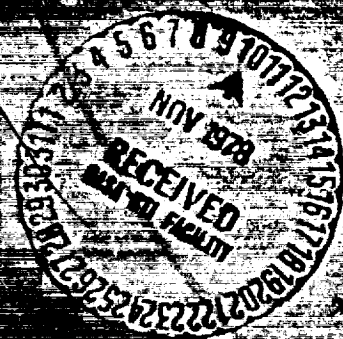
N79-10226

Unclas  
CSCI 21D H1/28 36434

**Workbook for Estimating Effects  
of Accidental Explosions in  
Propellant Ground Handling  
and Transport Systems**

V. E. Baker, J. J. Kulcsz, R. E. Ricker,  
P. S. Westine, V. B. Parr, L. M. Vargas,  
and P. K. Moseley

CONTRACT NAS3-2049  
AUGUST 1978



**NASA**

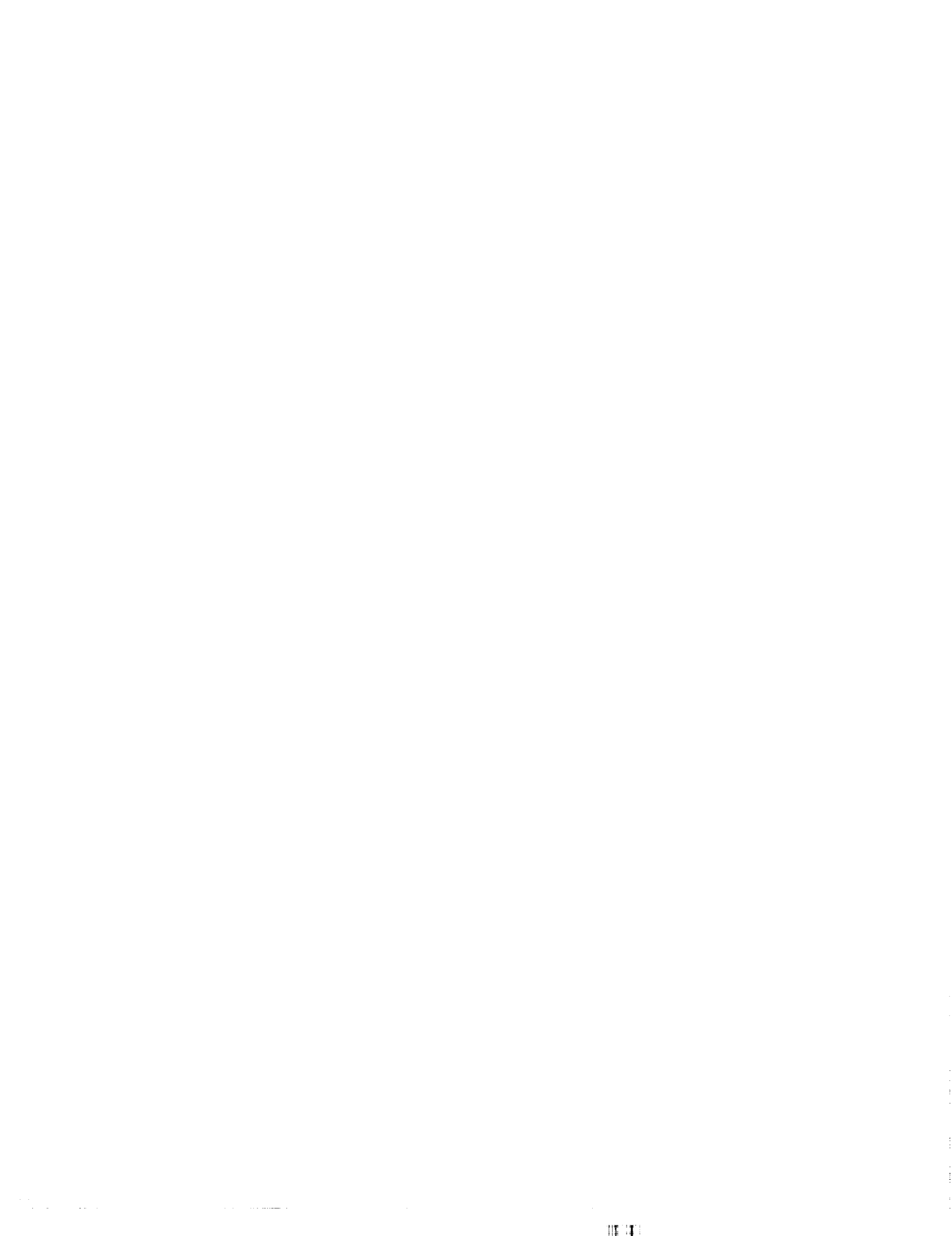


WORKBOOK FOR ESTIMATING EFFECTS OF  
ACCIDENTAL EXPLOSIONS IN PROPELLANT  
GROUND HANDLING AND TRANSPORT SYSTEMS

W. E. Baker, et al

Lewis Research Center  
San Antonio, Texas

Aug 78



N79-10226

NASA Contractor Report 3023

# Workbook for Estimating Effects of Accidental Explosions in Propellant Ground Handling and Transport Systems

W. E. Baker, J. J. Kulesz, R. E. Ricker,  
P. S. Westine, V. B. Parr, L. M. Vargas,  
and P. K. Moseley

*Southwest Research Institute  
San Antonio, Texas*

Prepared for  
Lewis Research Center  
under Contract NAS3-20497

**NASA**

National Aeronautics  
and Space Administration

**Scientific and Technical  
Information Office**

1978

REPRODUCED BY  
**NATIONAL TECHNICAL  
INFORMATION SERVICE**  
U.S. DEPARTMENT OF COMMERCE  
SPRINGFIELD, VA. 22161



U U U E E A E E E E E E E E E E E E E E E E



И И И И И И И И И И И И И И И И И И И И





## TABLE OF CONTENTS

	<u>Page</u>
SUMMARY	1
INTRODUCTION	2
I. ESTIMATES OF EXPLOSIVE YIELD	8
1-1 General	8
1-2 Compressed Gas Bursts	8
1-3 Flash-Evaporating Liquid Bursts	10
1-4 Vapor Cloud Explosions	16
References, Chapter I	20
II. CHARACTERISTICS OF PRESSURE WAVES	22
2-1 General	22
2-2 Two-Dimensional Blast Wave Characteristics	22
2-3 Blast Waves from Bursting Frangible Spheres	31
References, Chapter II	49
III. EFFECTS OF PRESSURE WAVES	50
3-1 General	50
3-2 Additional Beam Response Predictions	50
3-3 Buckling of Axially-Loaded Members	59
References, Chapter III	62
IV. CHARACTERISTICS OF FRAGMENTS	63
4-1 General	63
4-2 Analytical Predictions of Fragment Velocity Distributions	64
4-3 Analytic Predictions of Fragment Trajectories, Ranges and Impact Conditions	75
4-4 Statistical Analysis of Fragments	77
References, Chapter IV	92
V. EFFECTS OF FRAGMENTS AND RELATED TOPICS	93
5-1 General	93
5-2 Penetration Effects of Massive Missiles	94
5-3 Effects of Barricades on Blast Waves	105
References, Chapter V	112
VI. DISCUSSION AND RECOMMENDATIONS	113



APPENDIX A - Calculations of Blast Wave Properties for Pressure Vessel Bursts	116
APPENDIX B - Development of Additional Prediction Methods for Structural Response to Blast Wave Loading	123
APPENDIX C - Model Analysis for Bursting Containment Vessels	133
APPENDIX D - Estimate of Initial Velocities of Fragments from Spheres and Cylinders Bursting Into Two Unequal Fragments	140
APPENDIX E - Model Analysis for Fragment Trajectories	166
APPENDIX F - Rocketing of Storage and Transportation Vessels	169
APPENDIX G - Model Analysis for Rocketing of Storage and Transportation Vessels	193
APPENDIX H - Accident Data and Statistical Fitting to Fragment Data	198
LIST OF SYMBOLS	251
BIBLIOGRAPHY OF DATA SOURCES FOR MISSILE MAPS	258
CONVERSION FACTORS	260
GLOSSARY OF TERMS	262
BIBLIOGRAPHY	265





## INTRODUCTION

### General Discussion

This workbook is a companion to an earlier NASA workbook [Baker, et al (1975)], NASA CR-134906, which was prepared to aid designers and safety engineers in predicting damage and hazards from accidental explosions involving liquid propellants and compressed gases in flight hardware. This book, in contrast, is devoted to blast and fragment hazards for the same classes of accidental explosion sources in propellant ground handling and transport systems. Prediction methods which were thoroughly covered in the earlier workbook and which apply without change will not be repeated here. Instead, explosion hazards peculiar to ground storage and transport systems, or ranges of input parameters specific to these systems, will be emphasized. For completeness, the reader should use the earlier workbook in conjunction with this one.

A microfiche supplement of the workbook is attached to the back cover for the convenience of the reader.

### Nature of the Hazards

The general nature of the hazards from accidental explosions in propellant and industrial gases ground handling systems is similar in many respects to the hazards which occur in such explosions in flight vehicles. These accidents cause damage by air blast loading, fragment or appurtenance impact, radiation from fireballs, or fire from ignition of combustible materials following an explosion. Damage can occur to buildings and other facilities, vehicles, and flora and fauna--including humans. Depending on the severity, type and location of an explosion accident, the damage can range from minor to extensive.

The sequences of events or causes of accidental explosions in ground handling systems for liquid propellants and compressed gases can be quite similar to those which can occur in flight vehicles, or can differ markedly. Failure by material fatigue on overstress can occur in either case. But, many of the possible causes of flight vehicle explosions such as loss of thrust during launch, guidance system failure, or rupture of a bulkhead separating a fuel from an oxidizer, are inapplicable for ground handling systems. Conversely, transportation accidents followed by explosions are causes which are absent in flight vehicle accidents.

Ground handling systems usually have less serious weight constraints than do flight vehicles. This difference dictates some of the differences in the nature of the hazards. Ground sys-





but also the estimation of the probability that the event will occur and cause some level of damage. We do not address here the overall problem of risk assessment, but instead cover only the prediction of the effects. Throughout, we assume that some postulated explosive accident can and has happened. This workbook therefore covers only the more deterministic aspects of explosions and their effects, but can serve as inputs to the probabilistic models used in complete risk assessment studies.

#### Scope and Significance of Material Presented

From the material presented in this workbook, one should be able to make predictions of blast and fragment characteristics and effects for a wide range of possible explosion accidents in ground systems. The body of the workbook gives the prediction methods in the form of graphs, equations, or tables. All detailed development and some computer programs are given in appendices. Given a number of accident scenarios, the material should allow prediction of:

- 1) Explosive energy yield or energy release.
- 2) Characteristics of blast pressure waves generated by spherical and non-spherical explosions.
- 3) Effects of pressure waves on certain classes of targets or for blast loading conditions not covered in Baker, et al (1975).
- 4) Characteristics of fragments generated by ground equipment explosions. This includes massive vessel parts which "rocket."
- 5) Effects of fragment impact not covered in Baker, et al (1975), including effects of fragment revetments on blast waves.

The scope of the material presented here is deliberately limited to avoid duplication with the previous workbook [Baker, et al (1975)]. As noted earlier, it should be used in conjunction with that reference. (Microfiche)

Significant advances presented here are:

- 1) Prediction of blast wave characteristics for non-spherical sources.
- 2) Some additional methods for rapid prediction of structural damage from blast waves and massive fragment impact.





Applications to Areas Other Than Aerospace  
Propellant and High Pressure Gas  
Handling Facilities

This workbook can be as easily applied to many types of industrial explosive accidents as to those limited to aerospace propellants and high pressure gases. There have been many gas pressure vessel failures, road and rail tanker accidents with fuels such as LPG (liquified petroleum gas) followed by explosion and fire, and piping failures in chemical plants followed by vapor cloud explosions. For all such accidents, the methods presented here can be applied to estimation of blast and fragment hazards.

Additional Areas of Research

The methods given here are based on the best test data, analysis methods, and accident reports available to us. But, in many of these areas, the data base is quite sketchy and the governing physical processes are as yet poorly understood. We feel that additional work is needed in the following areas:

- 1) A better understanding and better methods of prediction of conditions under which vapor cloud explosions will occur, and the blast wave properties for such explosions.
- 2) A more thorough study of non-spherical accidental explosion effects.
- 3) Extension of the pressure-impulse (P-I) damage concept to typical blast waves for accidental explosions. In particular, the pronounced negative phase characteristics of such explosions should be considered.
- 4) Better definition of impact effects for large, massive fragments or objects.
- 5) Establishment of a more comprehensive and accurate system or method for reporting of explosion accidents. In particular, good industrial accident reporting could greatly increase the data base for comparison with these prediction methods or for judging explosion severity.







discussed in some detail and analyzed by Adamczyk and Strehlow (1977). They include an estimate based on isentropic expansion from initial burst pressure to atmospheric pressure [Baker (1973), Brinkley (1969)],

$$E = \frac{P_1 V_1}{\gamma_1 - 1} \left[ 1 - \left( \frac{P_a}{P_1} \right)^{\frac{\gamma_1 - 1}{\gamma_1}} \right] \quad (1-2)$$

and, as a lower limit, the energy released by constant pressure addition of energy to the explosion source region [Adamczyk and Strehlow (1977)],

$$E = P_a (V_f - V_1) \quad (1-3)$$

where  $V_f$  is the final volume occupied by the gas which was originally in the vessel. These three equations are given in descending order of total blast energy, with eq. (1-3) representing the energy release for a process which is so slow that no blast wave is formed.

Adamczyk and Strehlow (1977) show that the blast yield must lie between eqs. (1-2) and (1-3). However, eq. (1-1) gives only slightly higher values than does (1-2), and is simpler. So, realizing that its use results in an overestimate of blast yield, we retain it for this workbook. The reader can use eq. (1-2), however, for a somewhat more accurate estimate which is still an overestimate, and hence is conservative.

The equations given here for blast yield are all based on the assumption that all of the energy which can drive a blast wave does so, depending only on the energy release rate. For real vessels, some energy must be absorbed by the vessel as it fractures, both in the fracturing process itself and in accelerating the vessel pieces or fragments to their maximum velocity. For failure of a compressed gas vessel, the energy absorbed in the fracture process is negligible because the vessel is already stressed to failure. But, the energy absorbed in accelerating vessel fragments can be significant. In experiments such as those of Esparza and Baker (1977a) and Boyer, et al (1958) with pressurized glass spheres and Pittman (1972), (1975) with metal pressure vessels, the fragments were observed with high speed cameras or other velocity measuring systems. In accidental vessel bursts, the velocities of fragments can be estimated by methods to be presented in Chapter IV. Knowing mean fragment velocity  $U$  and total mass  $M$  of the vessel, one can then compute the kinetic energy of the vessel fragments

$$E_k = M U^2 / 2 \quad (1-4)$$





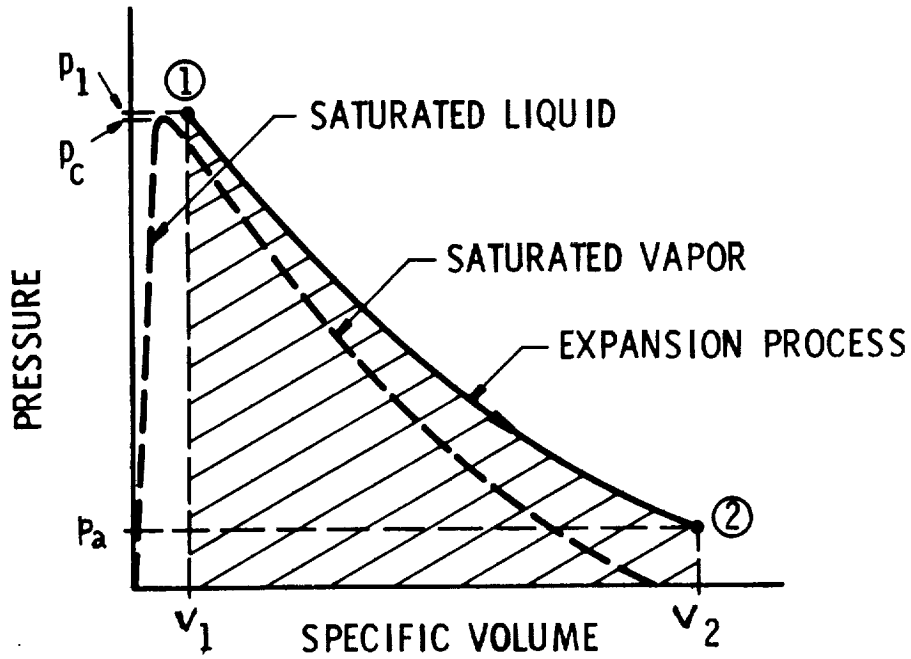


FIGURE 1-1. P-V DIAGRAM OF EXPANSION

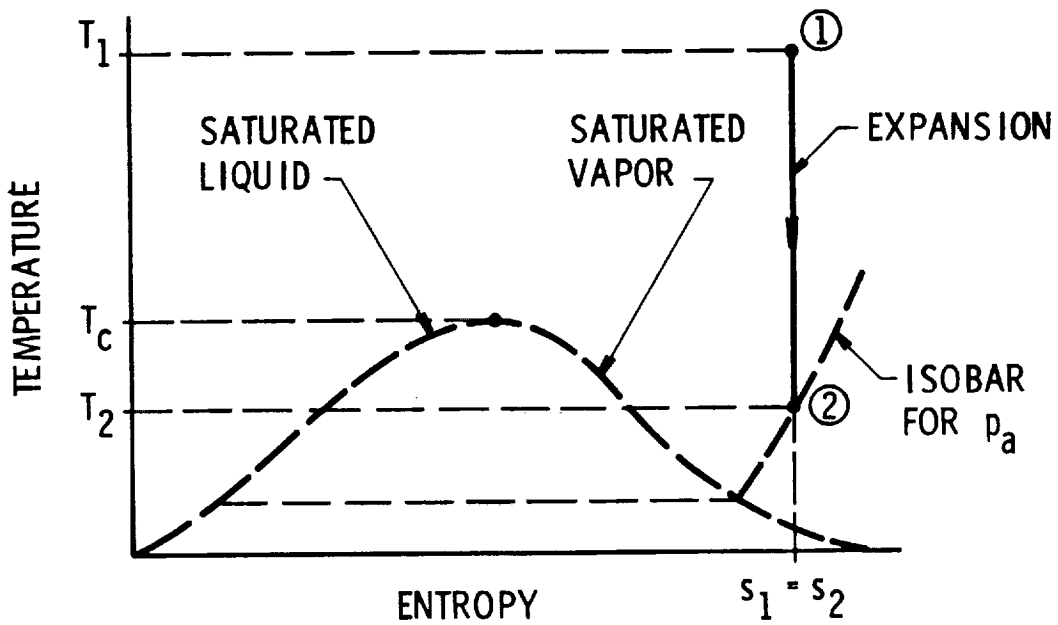


FIGURE 1-2. T-s DIAGRAM OF EXPANSION



ternal energy  $u$  or enthalpy  $h$  defined as

$$h = u + pv \quad (1-7)$$

are tabulated for the entire wet vapor region and the superheat region, as functions of pressure and specific volume, or temperature and entropy. When an initial or a final state falls within the wet vapor region, an important parameter is the quality of the vapor, defined as

$$x = \frac{v-v_f}{v_g-v_f} = \frac{s-s_f}{s_g-s_f} = \frac{u-u_f}{u_g-u_f} = \frac{h-h_f}{h_g-h_f} \quad (1-8)$$

where subscript  $f$  refers to fluid (saturated liquid) and subscript  $g$  refers to gas (saturated vapor). Also, within the wet vapor region, a given pressure uniquely defines a corresponding temperature, and vice versa.

In bursts of vessels containing flash-evaporating fluids, three combinations of state variables are possible at states 1 and 2. These are:

- Case 1) Superheated vapor at state 1 and at state 2 (as for the process shown in Figs. 1-1 and 1-2)
- Case 2) Superheated vapor at state 1 and wet vapor at state 2
- Case 3) Wet vapor (including both saturated liquid and saturated vapor) at state 1, and wet vapor at state 2.

The process of estimating  $e$  and total blast yield  $E$  is basically the same, but, depending on where state 1 lies, the procedure for entering the thermodynamic tables differs somewhat. The basic procedure is as follows:

- Step 1) Estimate the initial state variables, including  $p_1$ ,  $v_1$ ,  $s_1$ ,  $u_1$ , or  $h_1$
- Step 2) Assume isentropic expansion to atmospheric pressure  $p_a$ , i.e.,  $s_2 = s_1$ . Determine  $v_2$ ,  $u_2$ , or  $h_2$ .
- Step 3) Calculate specific work  $e$  from eq. (1-6)
- Step 4) Calculate total blast yield  $E$  by multiplying  $e$  by mass  $m$  of fluid initially present in the vessel.

In Step 4, we use the basic definition of specific volume to obtain



the mass  $m$  of fluid from the known vessel volume  $V_1$ ,

$$v_1 = V_1/m \quad (1-9)$$

and compute  $E$  from

$$E = m(u_2 - u_1) \quad (1-10)$$

Let us describe the differences in the three cases enumerated above. In Cases 1 and 2, the initial state conditions must be obtained from superheat tables for the fluid, usually entering with knowledge of the pressure and temperature together. In Case 1, superheat tables are also used for  $p_2 = p_a$ ,  $s_2 = s_1$ , to obtain the final state conditions; while in Case 2, the saturated vapor tables must be used with the definition of final quality  $x_2$ , determined from final entropy  $s_2$ , being the most important factor. In case 3, all values are found in the saturated vapor table, with initial quality  $x_1$  usually being determined from a real or fictitious initial specific volume. This case is probably the most common for flash-evaporating fluid vessel bursts. The fictitious initial specific volume for a vessel which is partially filled is obtained simply from eq. (1-9) by using  $m$  as the mass of liquid in the vessel of volume  $V_1$ .

Some tables of thermodynamic properties for fluids which can be used to estimate blast yields by the process just described are the ASHRAE Handbook of Fundamentals for refrigerants, Keenan, et al (1969) for steam, Din (1962) for a number of fluids including fuels such as propane and ethylene, and Goodwin (1974) and Goodwin, et al (1976) for methane and ethane. In many instances, these tables do not include internal energy  $u$  directly, but instead include  $h$ ,  $p$  and  $v$ . One then has to use eq. (1-7) to calculate  $u$ . Also, most of tables are given in English units, so calculations are usually made in these units. SI units are shown, and a conversion table is provided.

Several example calculations of blast energy for Freon 12 refrigerant, using tables from the ASHRAE handbook, follow:

Isentropic expansion of Freon-12 liquid at  $p_1/p_a = 20.3$  and room temperature  $\theta = 76^\circ\text{F}$ . Since no properties <sup>a</sup> for compressed (subcooled) liquid Freon-12 seem to be available, properties for state 1 will be assumed as those of a saturated liquid. Furthermore, since this is an estimate of the change in internal energy caused by the expansion of the pressurized refrigerant, interpolation of table values will be minimized.





$$E = \frac{e}{v_1} V_1 = 247.6 \text{ Btu/ft}^3 \times 9336 \text{ in-lb}_f/\text{Btu} \times \frac{1}{1728} \text{ ft}^3/\text{in}^3 \times 31.24 \text{ in}^3$$

or

$$E = 11,200 \text{ Joules}$$

If the fragment velocity is measured, then the kinetic energy of the fragments would be subtracted to obtain the energy available for driving a blast wave, using eq. (1-5).

For an isentropic expansion of Freon-12 vapor at  $p_1/p_a = 3.45$  and  $\theta_1 = 78^\circ\text{F}$ ,

$$v_1 = 0.90 \text{ ft}^3/\text{lb}_m$$

$$h_1 = 88.42 \text{ Btu/lb}_m$$

$$s_1 = 0.17984 \text{ Btu/lb}_m - ^\circ\text{F}$$

and

$$u_1 = h_1 - p_1 v = 80.2 \text{ Btu/lb}_m$$

At  $P_2 \sim 14.0 \text{ psia}$

$$s_2 = s_1 > s_g \text{ (still in superheated region)}$$

$$v_2 = 2.83 \text{ ft}^3/\text{lb}_m$$

$$h_2 = 78.42 \text{ Btu/lb}_m$$

and

$$u_2 = 71.09 \text{ Btu/lb}_m$$

Therefore,





Also, this transition usually requires some confinement. But detonating fuel-air mixtures are used as weapons [Robinson (1973)], and gaseous fuels mixed with oxygen are used as large blast sources for simulation of nuclear weapons blast [Choromokos (1972)].

Assessment of damage and correlation of the damage with blast yield has been attempted for some large vapor cloud explosions [Tucker (1974), Strehlow and Baker (1975)]. Generally, these estimates show that accidental vapor cloud explosions are almost invariably much less damaging than the planned vapor detonations mentioned above. Blast yields seem to have been, at most, 20% of values estimated on the basis of total heats of combustion of the fuels involved. This is probably so because not all (perhaps very little) of the fuel-air cloud has a mixture ratio lying within the detonable range, because no strong ignition sources capable of starting detonations were present, and because only a deflagration rather than a detonation occurred. This is of small comfort to the victims of vapor cloud explosions, but does indicate that the full potential for damage is probably never realized in an accident. In a way, this conclusion parallels the results of Project PYRO tests for explosions of liquid propellants, which are summarized by Baker, et al (1975). In those experiments, blast yields were seldom greater than a few percent of the maximum potential yield for large-scale experiments.

Because of the great variability in vapor cloud explosions and the uncertainties noted above, estimation of the blast yield of vapor cloud explosions can only be very approximate. We suggest the following procedure:

- 1) Assume a stoichiometric mixture of the fuel in air and calculate the total heat of combustion,  $E_C$ .
- 2) Multiply the heat of combustion by some blast effectiveness factor less than one to obtain estimated blast yield  $E$ . The effectiveness factor can be based on past accident data and should at present be considered as a very crude estimate. Accident data to date indicate that it should probably never be greater than 20%.

Fuels which are gaseous at normal ambient conditions, but have vapor densities\* greater than one, seem the most potentially dangerous candidates for vapor cloud explosions because they remain near the ground surface as they mix with air. Table 1-1 gives a partial listing of some such common fuels, together with detonable limits (when known), flammable limits expressed as volume percents in air, and values of  $E_C$  from Zabetakis (1965). This table also contains properties for the two most common fuels shipped or stored as cryogenics, hydrogen and methane.

\*Vapor density is defined as the ratio of the density of the vapor to that of air at standard temperature and pressure.



Fuels which are gaseous but have low vapor densities ( $< 1$ ) under normal ambient conditions seem potentially much less susceptible to vapor cloud explosions, because they rise rapidly as they mix with air. The two most common such fuels are methane (natural gas) with a vapor density of 0.55 and hydrogen, with a vapor density of 0.07. But both of these fuels are very energetic, and have wide flammability limits, so they cannot be completely excluded as potential sources for vapor cloud explosions.

By listing or mentioning only a limited number of fuels, we, of course, do not mean to exclude only liquid or gaseous fuel as a potential source for vapor cloud explosions. At present, we also cannot give good guidelines for estimating the effectiveness factor for converting maximum chemical energy release to blast yield.



ORIGINAL PAGE IS  
OF POOR QUALITY

TABLE 1-1. SOME FUELS WITH HIGH POTENTIAL FOR  
VAPOR CLOUD EXPLOSIONS

Fuel	Molecular Wt, M	Vapor Density	Boiling Point, °F	Detonability Limits		Flammability Limits		E <sub>c</sub> ' kcal/mol
				Lower, %	Upper, %	Lower, %	Upper, %	
Acetylene	26.04	0.91	gas	10	25	2.5	100	301.5
Ethylene oxide	44.05	1.736	51	6	24	3.0	100	281.1
Ethylene	28.05	0.97	gas	7	21	2.7	36	316.2
Propane	44.09	1.52	gas	--	--	2.1	9.5	488.5
1,3-Butadiene	54.09	1.9	gas	--	--	2	12	576.3
Monomethyl- amine	31.06	1.105	gas	--	--	4.2	20.8	--
Propylene	42.08	1.5	gas	--	--	2	11	460.4
Vinyl chloride	62.50	2.2	7	--	--	3.6	33	--
Butane	58.12	2.01	gas	--	--	1.8	8.4	635.4
Ethane	30.07	1.044	gas	--	--	3.0	12.4	341.3
1-Butene	56.10	1.995	gas	--	--	1.6	10	607.7
Propadiene	40.06	1.38	gas	--	--	2.6	--	--
Hydrogen	2.016	0.07 1.11	gas at B.P (-400.3)	20	65	4.0	75	241
Methane	16.043	0.55 1.52	gas at B.P (-115.8)	6	14	5.0	15	801

## REFERENCES, CHAPTER I

Adamczyk, A. A. and Strehlow, R. A., (1977) "Terminal Energy Distribution of Blast Waves From Bursting Spheres", NASA CR 2903, Grant NSG 3008, September 1977.

ASHRAE Handbook of Fundamentals, (1972) American Society of Heating, Refrigerating and Air Conditioning Engineers, Inc. New York, N.Y., 1972.

Baker, W. E. (1973) Explosions In Air, University of Texas Press, Austin, Texas, 1973.

Baker, W. E., Kulesz, J. J., Ricker, R. E., Bessey, R. L., Westine, P. S., Parr, V. B. and Oldham, G. A., (1975) "Workbook for Predicting Pressure Wave and Fragment Effects of Exploding Propellant Tanks and Gas Storage Vessels," NASA CR-134906, Contract NAS3-19231, Nov 1975 (reprinted September 1977).

Boyer, D. W., Brode, H. L., Glass, I. I. and Hall, J. G., (1958) Blast From a Pressurized Sphere, UTIA Report No. 48, Institute of Aerophysics, University of Toronto, 1958.

Brinkley, S. R., (1969) "Determination of Explosive Yields," AIChE Loss Prevention 3, 1969, pp 79-82.

Brode, H. L., (1959) "Blast Wave From a Spherical Charge," Physics of Fluids 2, 1959, p 217.

Choromokos, J., (1972) "Detonable Gas Explosions - SLEDGE," Proceedings 3rd International Symposium on Military Applications of Blast Simulators, Schwetzingen, Germany, September 1972, pp B4-1 through B4-10.

Esparza, E. D. and Baker, W. E., (1977a) "Measurement of Blast Waves From Bursting Pressurized Frangible Spheres," NASA CR-2843, Grant NSG 3008, May 1977.

Goodwin, R. D., (1974) "The Thermophysical Properties of Methane, from 90 to 500K of Pressures to 700 Bar," NBS Technical Note 653, U.S. Department of Commerce, National Bureau of Standards, April 1974.

Goodwin, R. D., Roder, H. M. and Straty, G. C., (1976) "Thermophysical Properties of Ethane, From 90 to 600K at Pressures to 700 Bar," NBS Technical Note 684, National Bureau of Standards, August 1976.

Parker, R. J., Pope, J. A., Davidson, J. F. and Simpson, W. J., (1974) "The Flixborough Disaster, Report of the Court of Inquiry," Her Majesty's Stationary Office, London, June 1974.



Pittman, J. F., (1976) "Blast and Fragments From Superpressure Vessel Rupture," Report No. NSWC/WOL/TR 75-87, Naval Surface Weapons Center, White Oak, Silver Spring, Md, February 1976.

Pittman, J. F., (1972) " Blast and Fragment Hazards From Bursting High Pressure Tanks," NOLTR72-102, U.S. Naval Ordnance Laboratory, Silver Spring, Md, May 1972.

Robinson, C. A., Jr., (1973) "Special Report: Fuel Air Explosives, Services Ready Joint Development Plan," Aviation Week and Space Technology, February 19, 1973, pp 42-46.

Strehlow, R. A. and Baker, W. E., (1975) "The Characterization and Evaluation of Accidental Explosions," NASA CR-134779, Grant NSG 3008, June 1975.

Tucker, D. M., (1975) "The Explosion and Fire at Nypro (UK) Ltd., Flixborough, on 1 June 1974," Building Research Establishment, Fire Research Station, Borehamwood, Hertfordshire, England, 1975.

Zabetakis, M. G., (1965) "Flammability Characteristics of Combustible Gases and Vapors," Bulletin 627, Bureau of Mines, U. S. Department of the Interior, 1965.





The "starting overpressure" is calculated as follows: The terms

$$\frac{p_1}{p_a}$$

and

$$\frac{\gamma_1 (MW)_a T_1}{\gamma_a (MW)_1 T_a}$$

are computed, where  $p_1$  is pressure,  $\gamma$  is the ratio of specific heats, (MW) is molecular weight, and  $T$  is absolute temperature. The subscript 1 refers to conditions inside the vessel before it bursts, and  $a$  refers to conditions in the surrounding atmosphere. The point

$$\left( \frac{p_1}{p_a}, \frac{\gamma_1 (MW)_a T_1}{\gamma_a (MW)_1 T_a} \right)$$

is located on one of the graphs in Figures 2-2, 2-3, or 2-4, depending on  $\gamma_1$ .  $\bar{P}_s$  is read for the point. The "starting overpressure" is  $\bar{P}_A = 0.21 \bar{P}_s$ . Figure 2-5 is a graph of  $\bar{P}_s$  vs  $\bar{R}$ , where

$$\bar{P}_s = \frac{P_s}{P_a}$$

and

$$\bar{R} = \frac{rp_a^{1/3}}{E^{1/3}}$$

[ $r$  is the distance along the plane of symmetry from the center of the tank, and the energy in the tank is given by eq. (1-1)]. On Figure 2-5, the intersection of the constant  $\bar{P}_s$  line (where  $\bar{P}_s = \bar{P}_A$ ) and Curve A is found. This is the starting point. The nearest curve or curves give the  $\bar{P}_s$  vs  $\bar{R}$  behavior. For the distance of interest, calculate  $\bar{R}$ .  $\bar{P}_s$  is then read from the appropriate curve.

$\bar{I}_s$  is read from Figure 2-6 or 2-7, whichever is more convenient.

$$\bar{I} = \frac{I_s A_a}{p_a^{2/3} E^{1/3}}$$



where  $A_a$  is the speed of sound in the surrounding atmosphere.

$$I_s = \bar{I} \frac{p_a^{2/3} E^{1/3}}{A_a}$$

$P_s$  and  $I_s$  are accurate to about  $\pm 15\%$ . The curves should not be extrapolated.

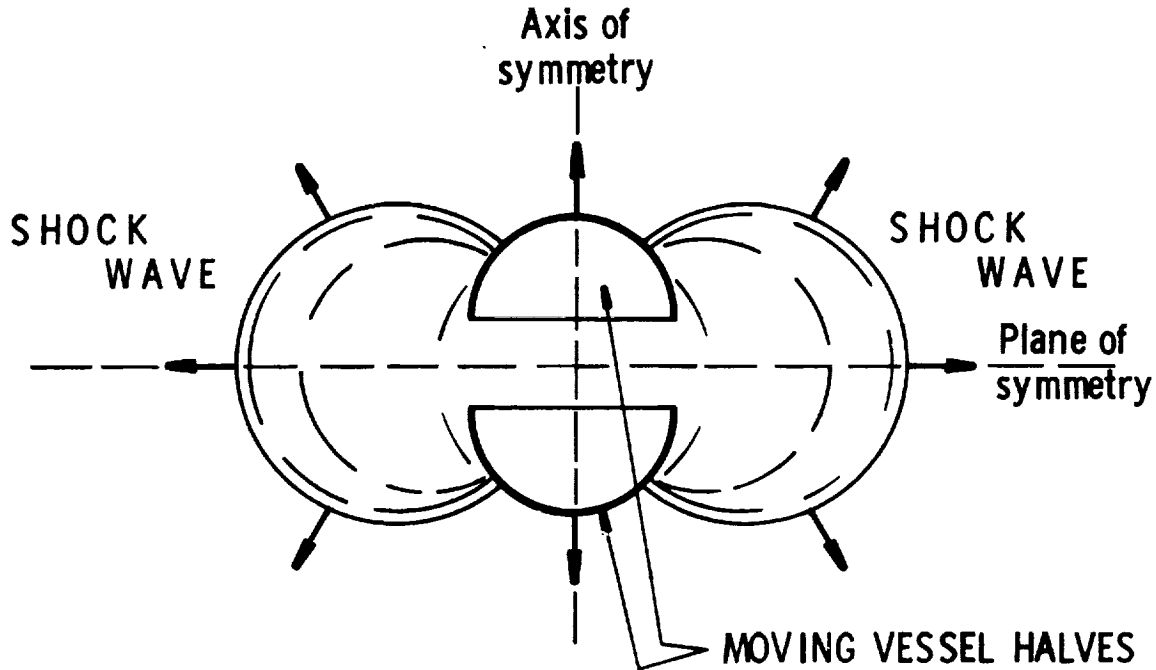


FIGURE 2-1. BURST OF A SPHERICAL PRESSURE VESSEL

The computer analysis on which these curves are based does not extend far enough in time to allow prediction of negative phase characteristics or second shock characteristics.

Example: A spherical vessel containing air ( $\gamma_1 = 1.4$ ) at a pressure of  $10^8 P_a$  (987.2 atm) and a temperature of  $300^\circ F$  bursts at sea level. The inner vessel radius is 0.19m. Find  $P_s$  and  $I_s$  at a distance  $r$  of 1.14m along the plane of symmetry from the center of the vessel.

Solution:

$$\frac{P_1}{P_a} = 987.2$$





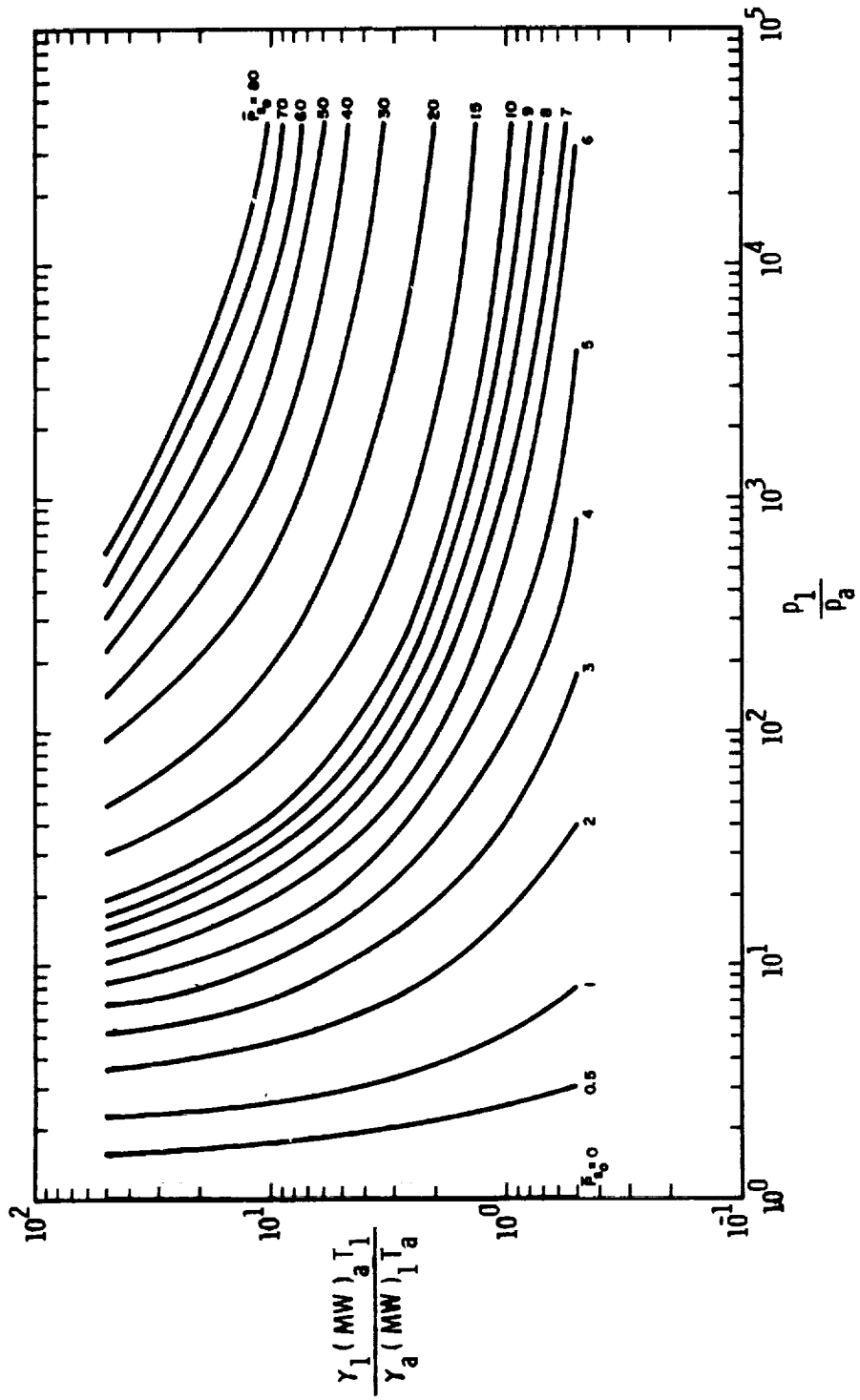


FIGURE 2-3. SCALED STARTING CONDITIONS FOR VARIOUS  $\bar{P}_{s_0}$ ,  $\gamma_1 = 1.667$





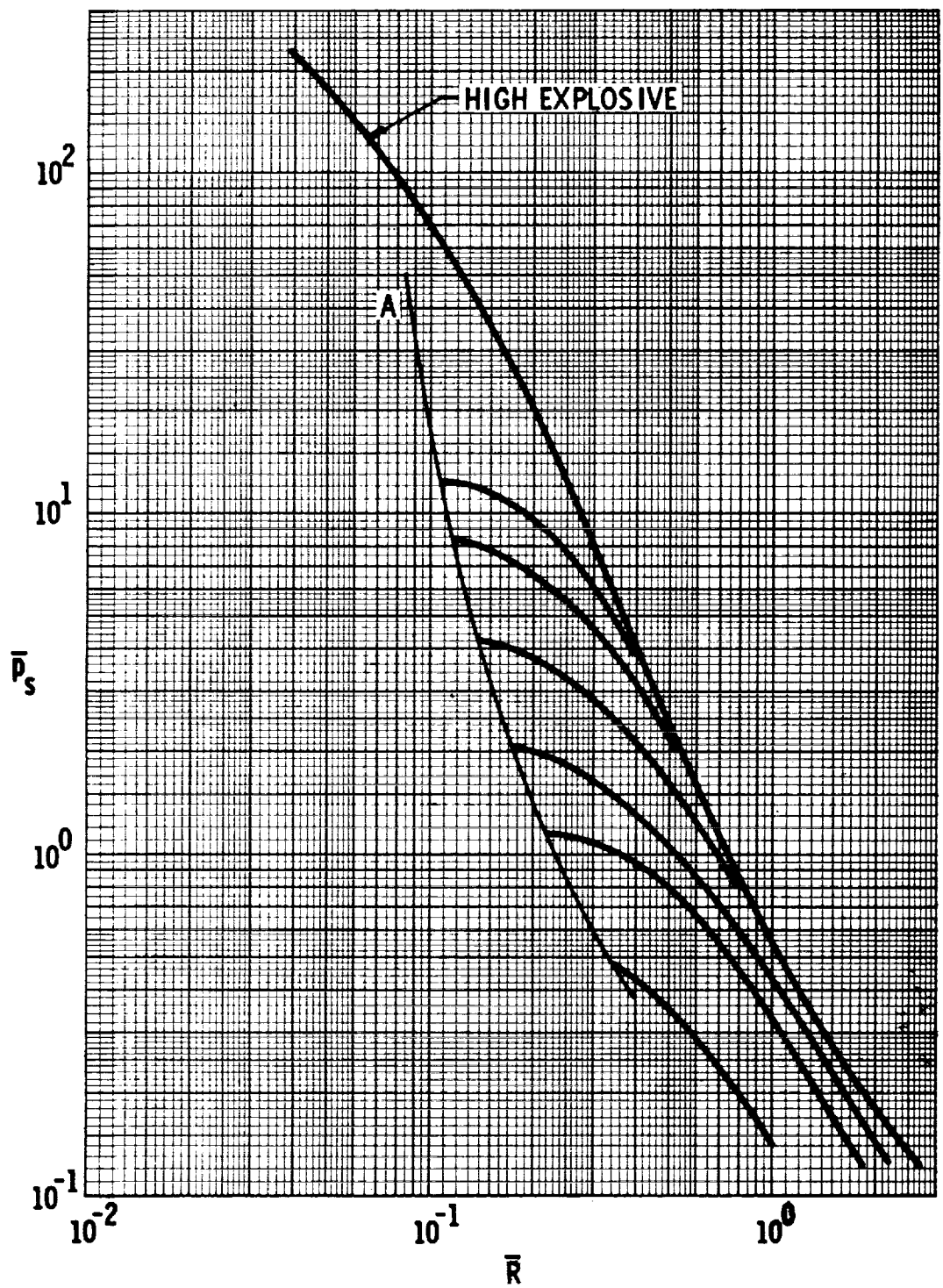


FIGURE 2-5.  $\bar{P}_s$  VS.  $\bar{R}$  FOR OVERPRESSURE CALCULATIONS.  
 DISTANCE ALONG PLANE OF SYMMETRY



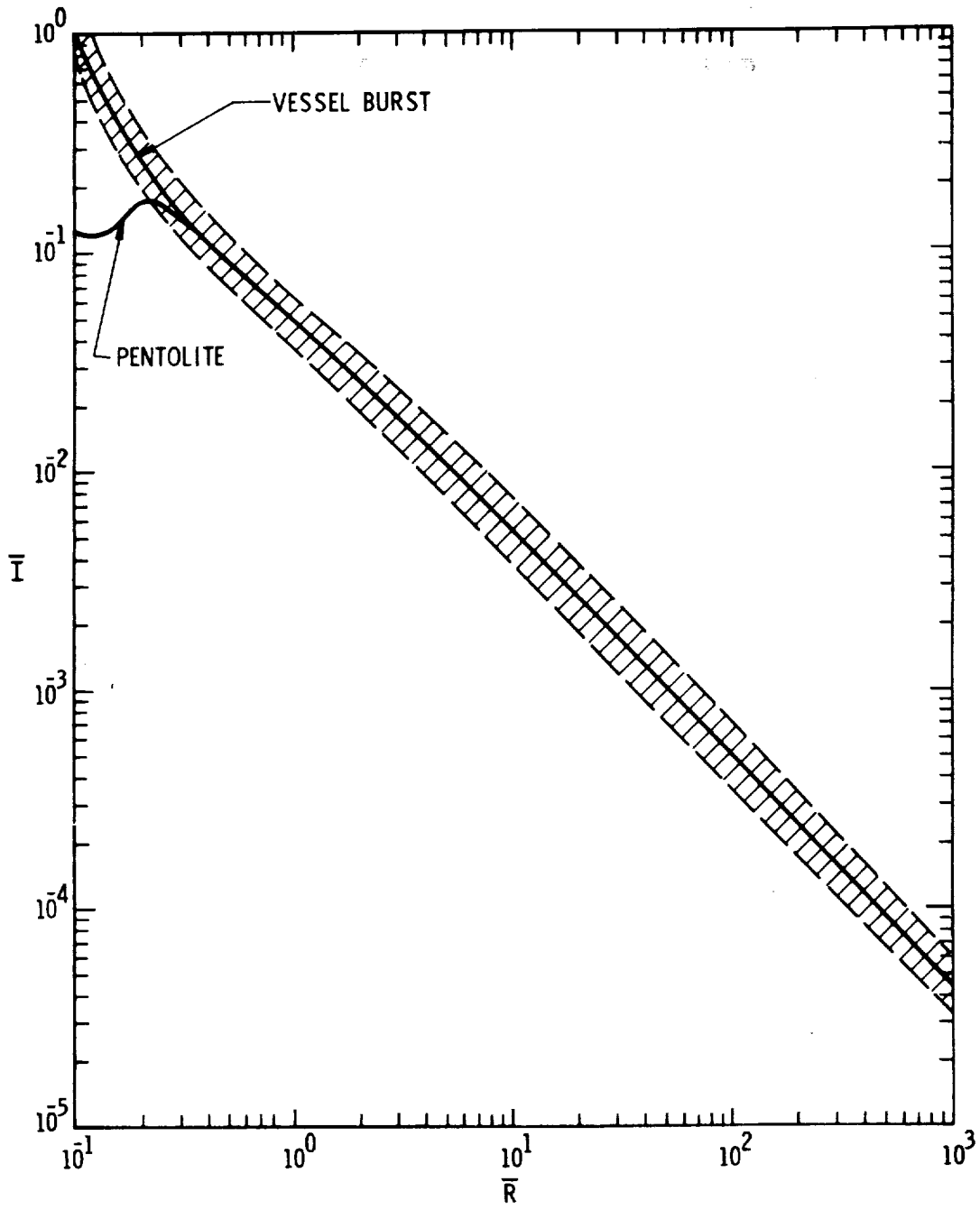


FIGURE 2-6.  $\bar{I}$  VS  $\bar{R}$  FOR PENTOLITE AND GAS VESSEL BURSTS





$$\frac{\gamma_1 (MW)_a T_1}{\gamma_a (MW)_1 T_a} = 1$$

Locating this point on Figure 2-2,  $\bar{P}_{s0} = 11$ .

$$\bar{P}_A = 0.21 \bar{P}_{s0} = 0.21(11) = 2.3$$

Next, find the point on Figure 2-5 where Curve A crosses

$$\bar{P}_s = \bar{P}_A = 2.3.$$

This is near the third curve from the bottom of the page. This gives the  $\bar{P}_s$  vs  $\bar{R}$  behavior.

$$E = V_1 \frac{P_1 - P_a}{\gamma_1 - 1} = \frac{4\pi}{3} (0.19)^3 \frac{10^8 - 1.013 \times 10^5}{1.4 - 1} = 7.8 \times 10^6 \text{ J}$$

$$\bar{R} = \frac{r p_a^{1/3}}{E^{1/3}} = \frac{1.14 \text{ m} (1.013 \times 10^5 \text{ Pa})^{1/3}}{(7.18 \times 10^6)^{1/3}} = 0.27$$

For this value of  $\bar{R}$ ,  $\bar{P}_s = 1.8$ .  $P_s = \bar{P}_s p_a = (1.8) (1.013 \times 10^5 \text{ Pa})$   
 $= 1.8 \times 10^5 \text{ Pa}$

From Figure 2-7,  $\bar{I}_s = 0.16$ . Then  $I_s = \bar{I} \frac{p_a^{2/3} E^{1/3}}{A_a} =$

$$\frac{0.16 (1.013 \times 10^5)^{2/3} (7.18 \times 10^6)^{1/3}}{344 \text{ m/s}} = 1.9 \times 10^3 \text{ Pa}\cdot\text{s}$$

### 2-3 Blast Waves from Bursting Frangible Spheres

Two recent experimental studies form the basis for some additional prediction curves for blast wave properties near bursting pressure spheres. Esparza and Baker, (1977a) and (1977b), report measurements of blasts from bursting frangible pressure spheres containing air and argon (1977a), and the refrigerant Freon 12 as both a compressed liquid and a compressed vapor (1977b).

These measurements, which include side-on pressure-time data over a range of scaled distances, show that compressed gas and vapor sphere explosions can generate waves which are distinctly different from the more familiar waves from condensed explosives.



A typical pressure-time trace is shown in Fig. 2-8. The distinctive characteristics are the pronounced negative phase compared to the first positive phase, and the strong second shock wave. By contrast, waves from condensed explosives show much smaller negative phases and seldom have a discernible second shock.

To report these blast wave properties, we must define more parameters than the usual ones. We have chosen the following ones (see Fig. 2-8).

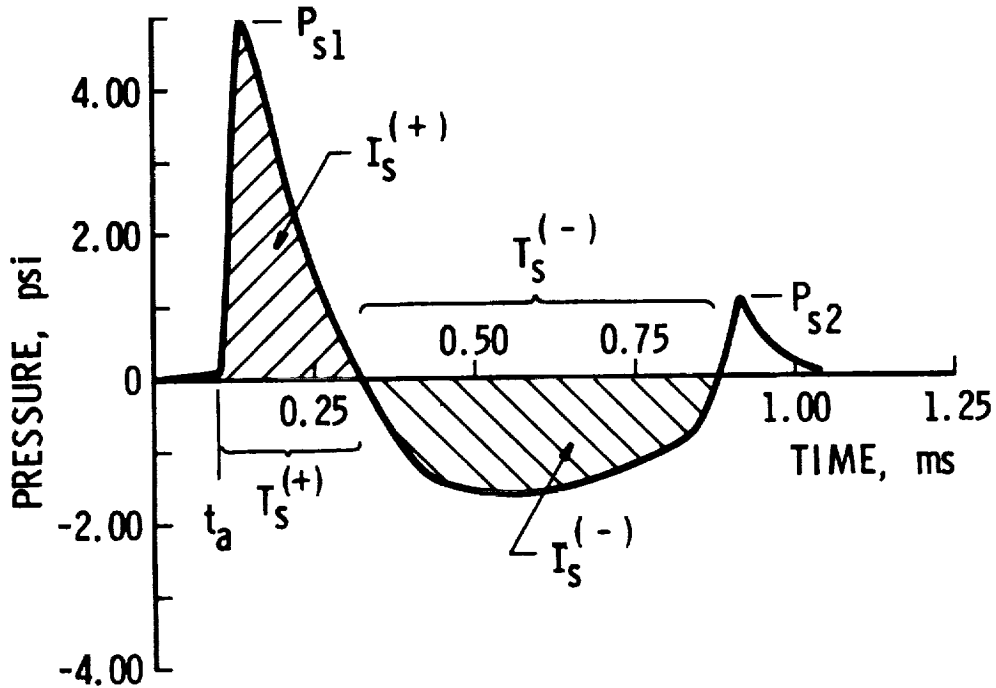


FIGURE 2-8. TYPICAL BLAST PRESSURE HISTORY FOR FRANGIBLE GAS SPHERE BURST

- $P_{s1}$  first shock side-on overpressure
- $I_s^{(+)}$  positive phase impulse for first shock
- $T_s^{(+)}$  duration of positive impulse for first shock
- $I_s^{(-)}$  negative phase impulse for first shock
- $T_s^{(-)}$  duration of negative phase for first shock
- $P_{s2}$  second shock side-on overpressure.

ORIGINAL PAGE IS  
OF POOR QUALITY



Prediction curves for scaled values of these parameters are given here. As in section 2-2, the scaling is given by:

$$\begin{aligned}\bar{P} &= P/p_a \\ \bar{I} &= I A_a p_a^{2/3}/E^{1/3} \\ \bar{T} &= T A_a p_a^{1/3}/E^{1/3} \\ \bar{R} &= R p_a^{1/3}/E^{1/3}\end{aligned}\tag{2-1}$$

and blast yield  $E$  is defined by

$$E = E' - E_k\tag{2-2}$$

where

$$E' = \frac{V_1(p_1 - p_a)}{(\gamma_1 - 1)}\tag{2-3}$$

for perfect gases and

$$E' = \frac{V_1}{v_1} (u_1 - u_2)\tag{2-4}$$

for wet vapors or gases near the thermodynamic "vapor dome."\*

Figures 2-9 through 2-16 are derived from Esparza and Baker (1977a) for compressed gases. Blast wave characteristics were found to be only weakly dependent on specific heat ratio  $\gamma_1$  for gas in the vessels and on initial pressure ratio ( $p_1/p_a$ ).

The latter parameter was varied over the range  $9.9 \leq (p_1/p_a) \leq 42.0$  in the tests. Because of the weak dependence on these two parameters, all data are combined for various initial pressure ratios and ratios of specific heat. The figures show the range of all test data within the cross-hatched areas, and a "best fit" solid curve through the data. We suggest that the best fit curve be used for estimation, but one can use the upper limit curves to indicate uncertainties in the data.

Figures 2-17 through 2-22 are curves for compressed vapor for Freon-12 refrigerant, similar to the previous figures for compressed gases, from Esparza and Baker (1977b). That reference

\*Chapter 1 gives methods for calculating the internal energy change ( $u_1 - u_2$ ).



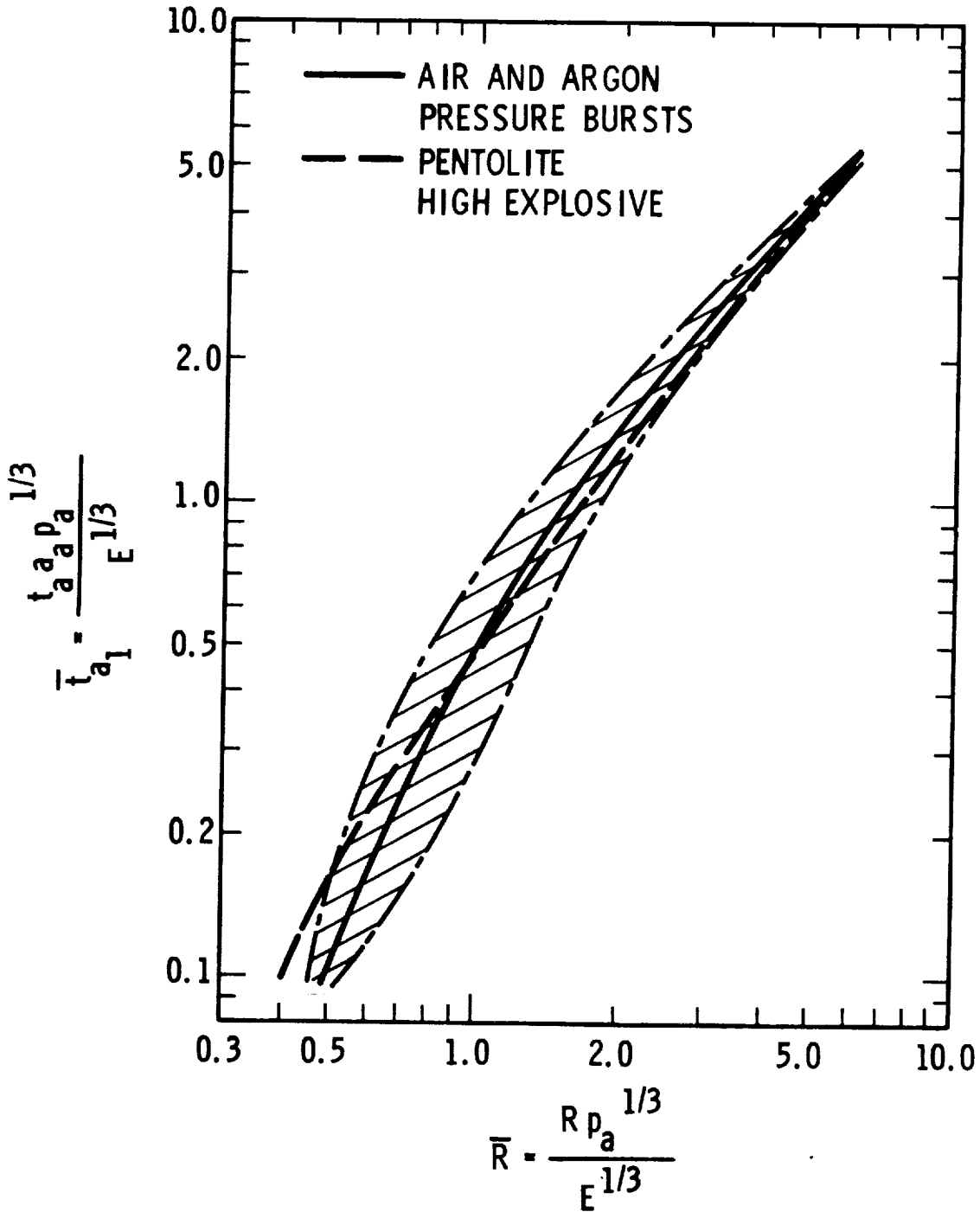


FIGURE 2-9. SCALED TIME OF ARRIVAL OF FIRST SHOCK WAVE FROM BURSTING GAS SPHERES



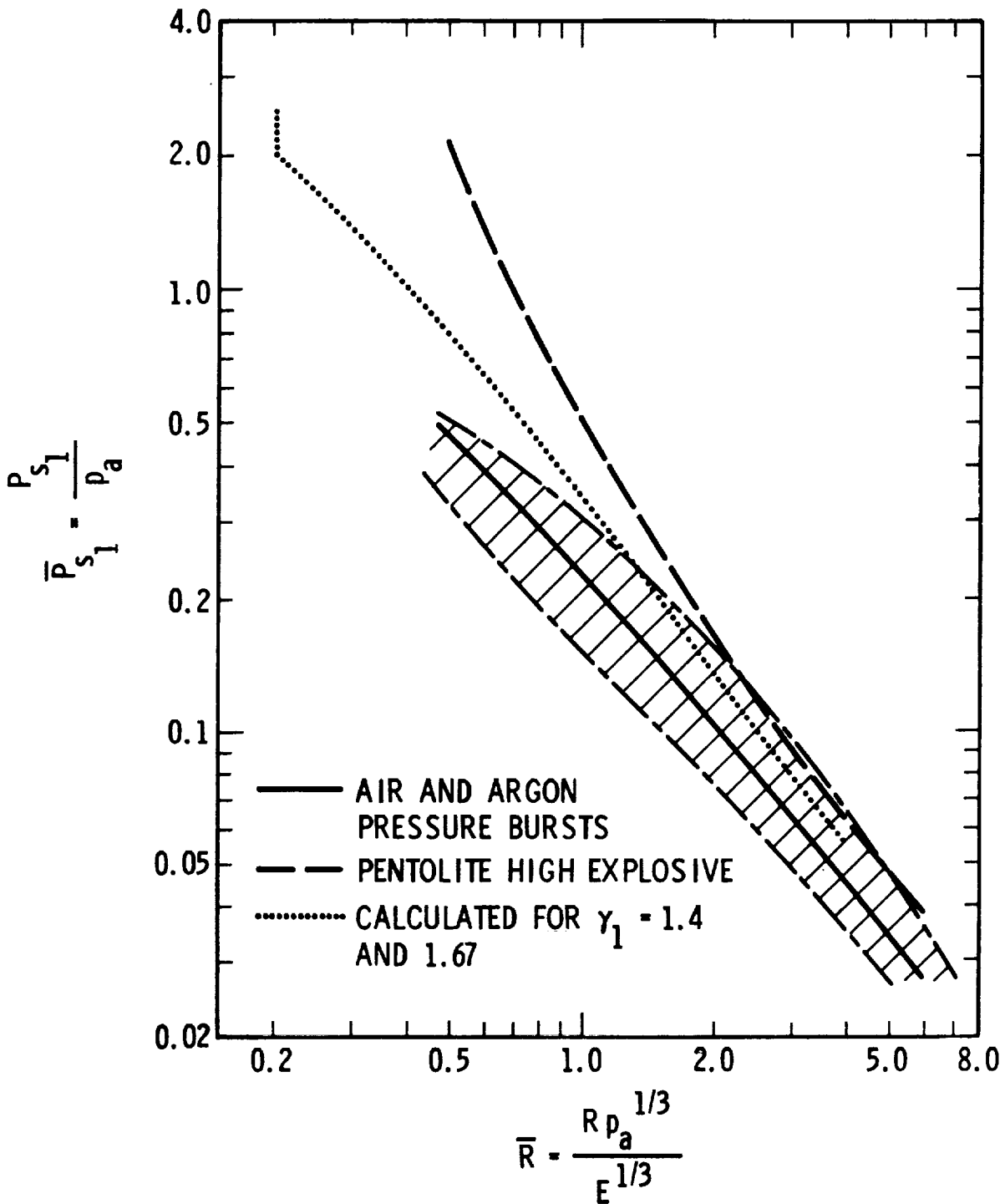


FIGURE 2-10. SCALED SIDE-ON PEAK OVERPRESSURE FOR FIRST SHOCK FROM BURSTING GAS SPHERES





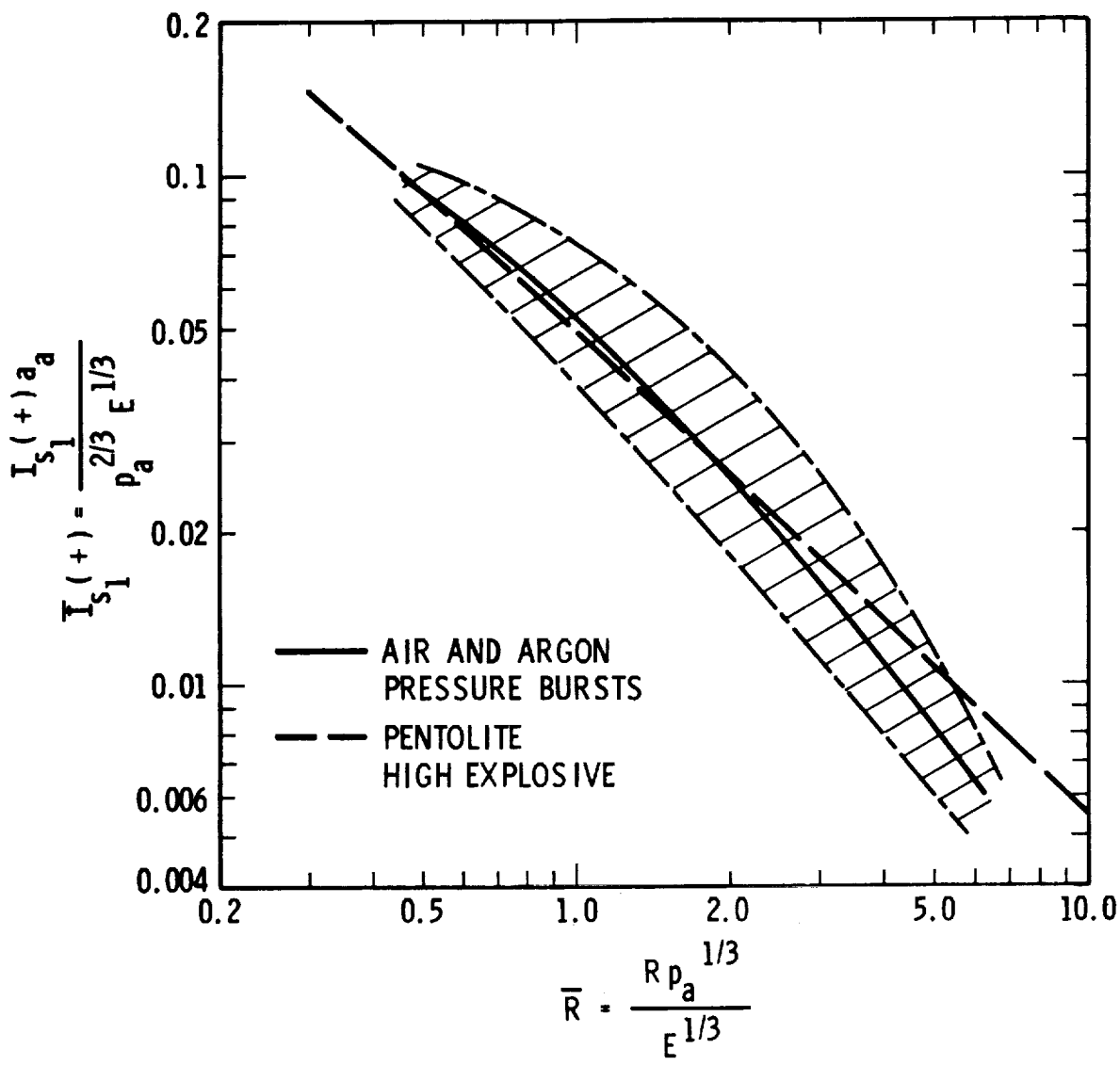


FIGURE 2-12. SCALED SIDE-ON POSITIVE IMPULSE FROM BURSTING GAS SPHERES







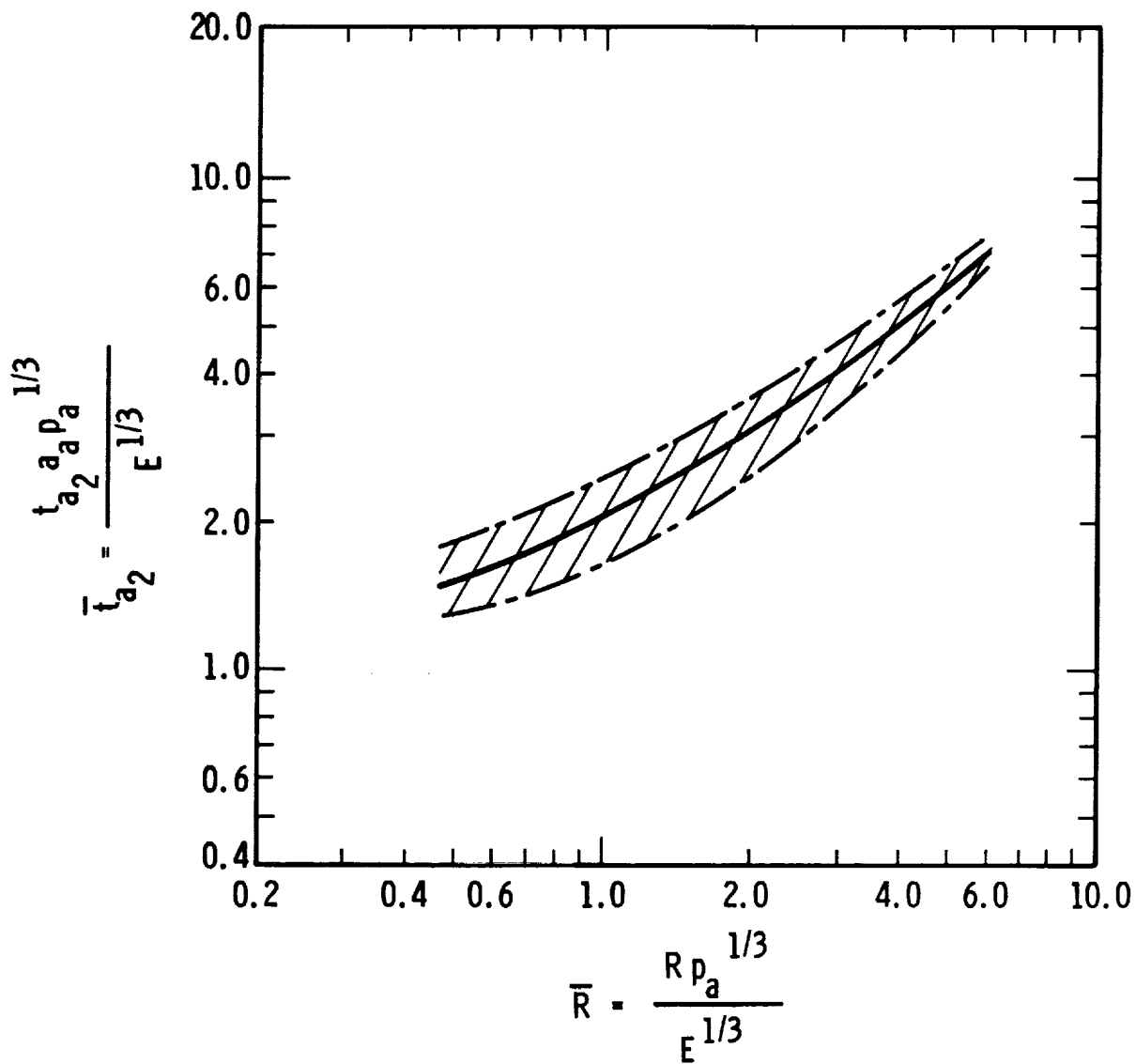


FIGURE 2-15. SCALED TIME OF ARRIVAL OF SECOND SHOCK WAVE FROM BURSTING GAS SPHERES



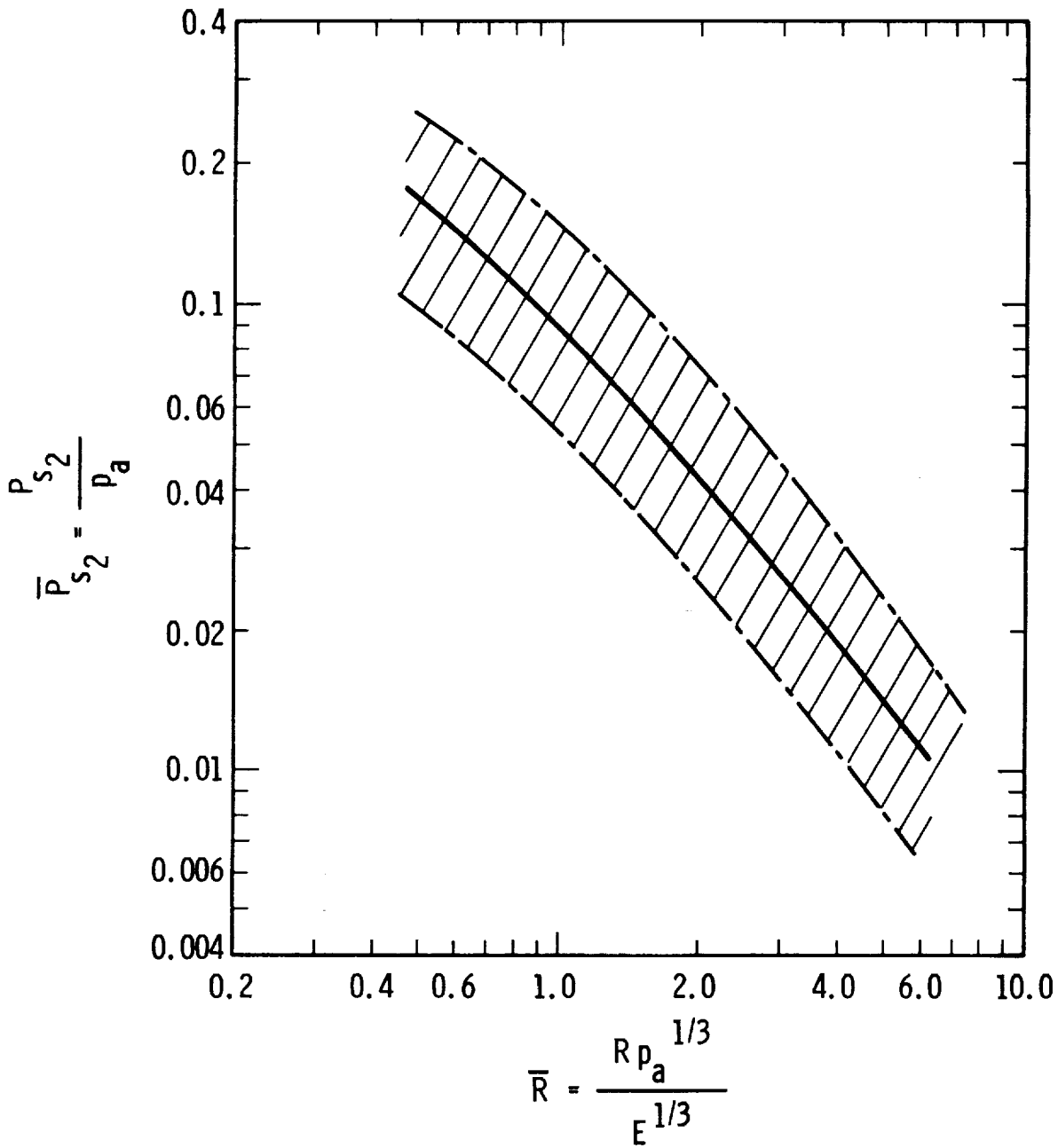


FIGURE 2-16. SCALED SIDE-ON PEAK OVERPRESSURE OF SECOND SHOCK FOR BURSTING GAS SPHERES



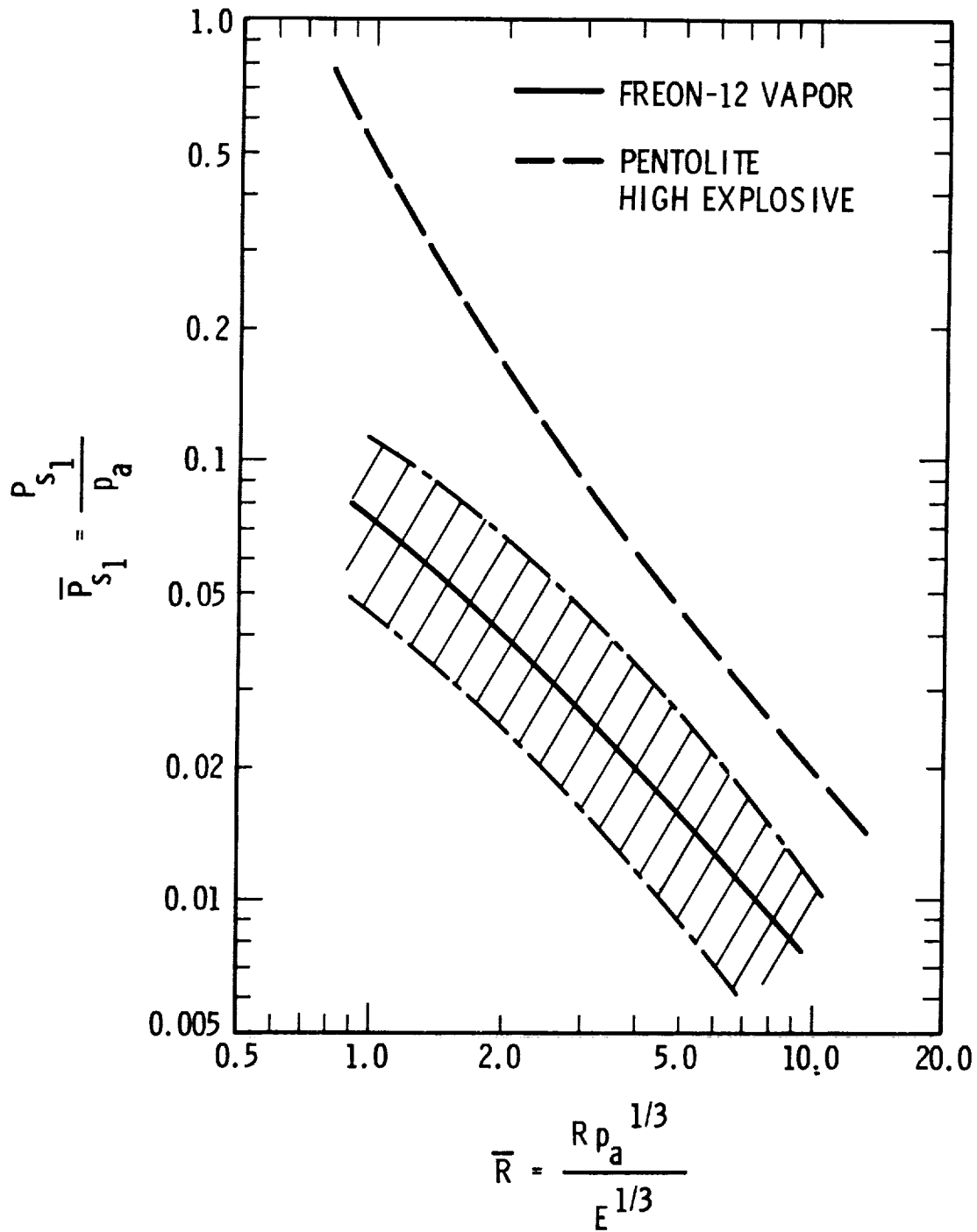


FIGURE 2-17. SCALED SIDE-ON PEAK OVERPRESSURE FOR BURSTING FREON-12 VAPOR SPHERE AT ROOM TEMPERATURE





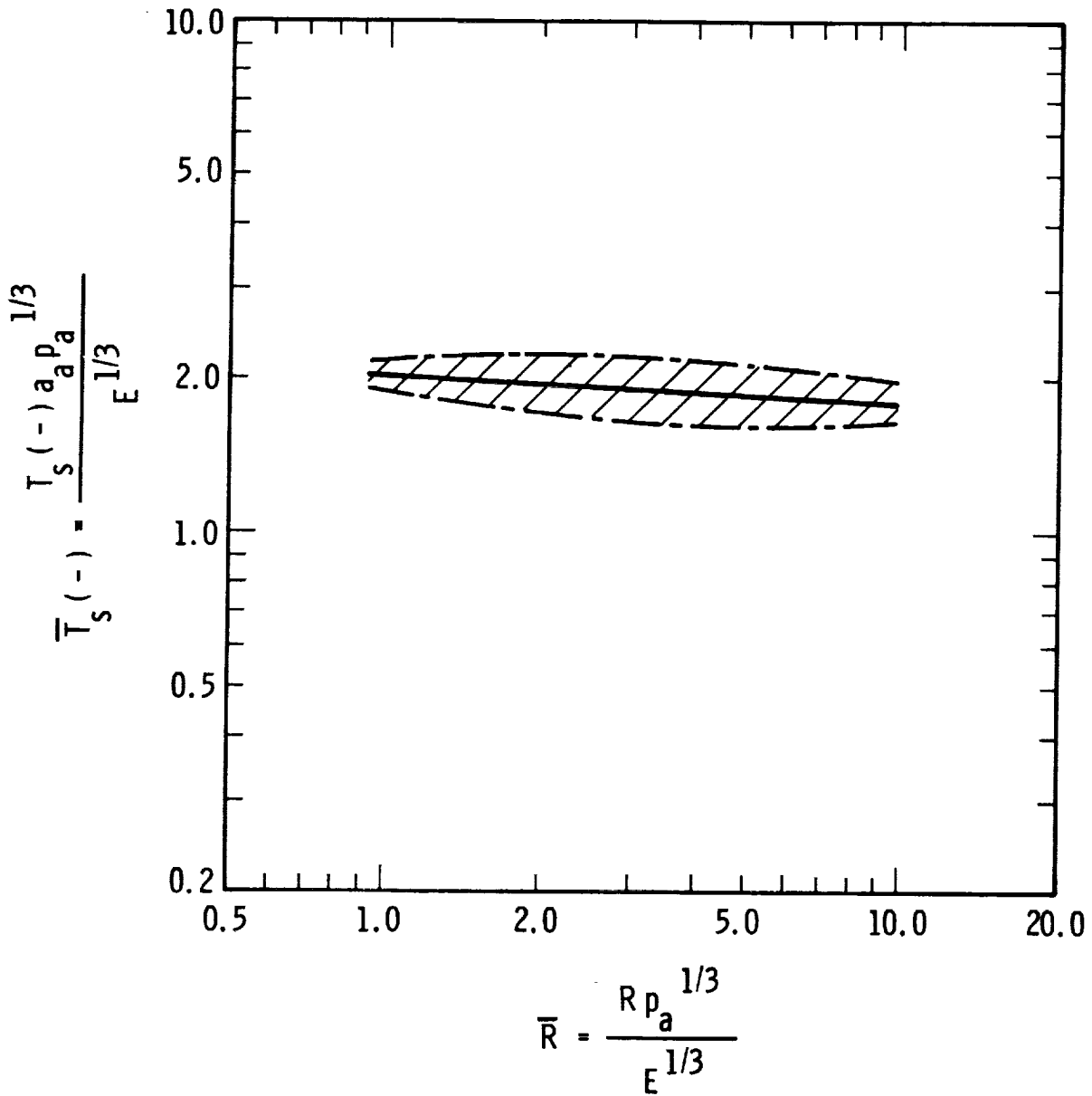


FIGURE 2-19. SCALED DURATION OF NEGATIVE PHASE OF BLAST WAVE FROM BURSTING FREON-12 VAPOR SPHERE





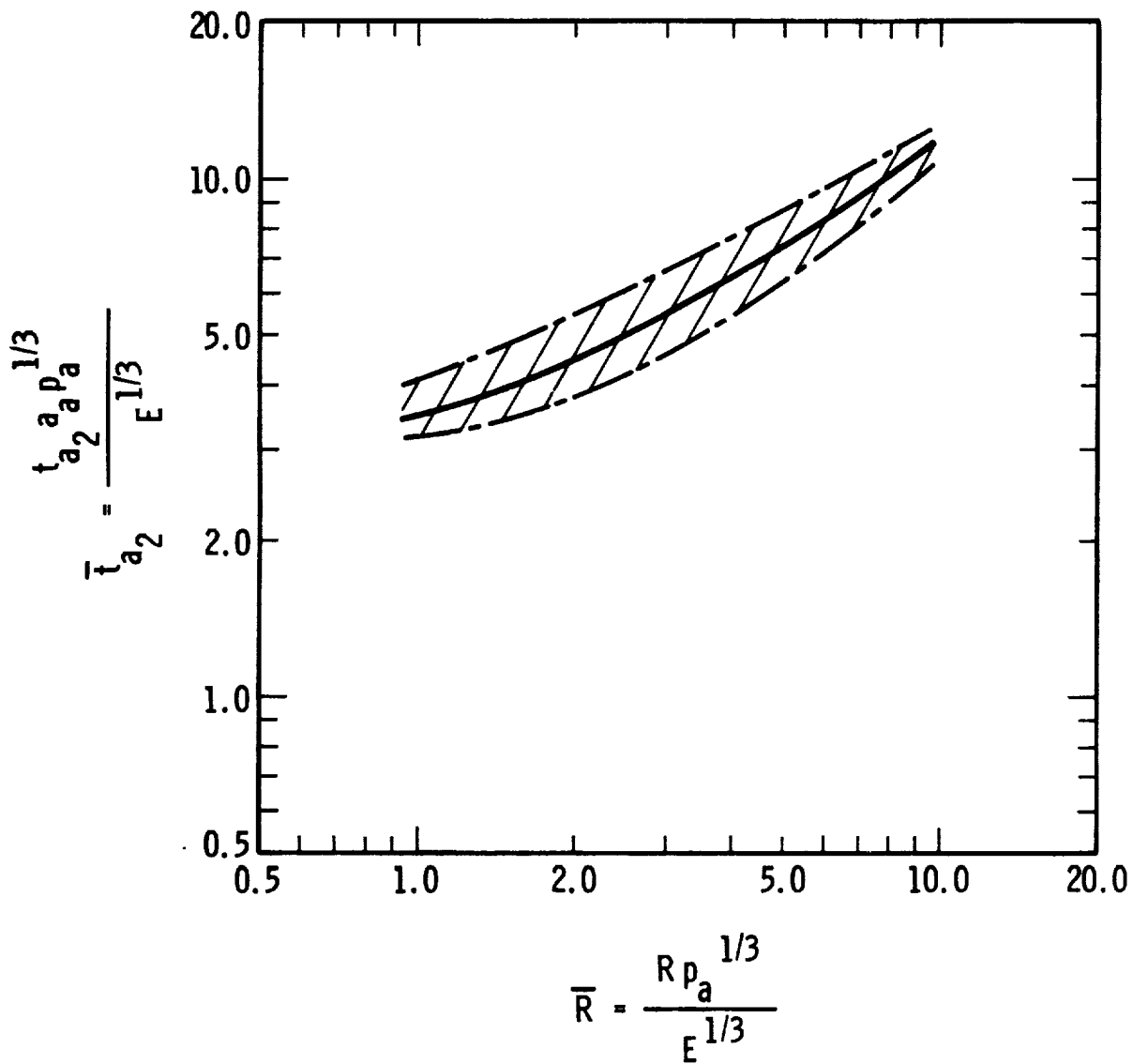


FIGURE 2-21. SCALED TIME OF ARRIVAL OF SECOND SHOCK WAVE FROM BURSTING FREON-12 VAPOR SPHERE





shows that blast waves from sudden release of compressed liquid Freon-12 were almost always so weak that they were essentially sound waves, and therefore had negligible damaging potential. No data were taken for the intermediate cases of wet vapor, which should have intermediate explosion properties between saturated liquid and saturated vapor.

Some data exist for blast waves generated by bursts of heated, ductile pressure vessels containing steam as a flash-evaporating fluid [Baker, et al (1978)] which show that such bursts can indeed be quite energetic blast sources. Strong vessels containing varying amounts of water which were heated to steam and burst at pressures of about 32 MPa generated strong blast waves, with specific source energies as great as  $2.31 \times 10^8$  J/m<sup>3</sup> on a volume basis or  $4.04 \times 10^5$  J/kg of fluid on a mass basis. The latter figure, when compared to the specific energy for TNT of  $4.19 \times 10^6$  J/kg, gives a "TNT equivalent" of 0.097 kg TNT/kg H<sub>2</sub>O. But, the data are too sparse to generate prediction curves.



REFERENCES, CHAPTER II

Baker, W. E., Kulesz, J. J., Ricker, R. E., Bessey, R. L., Westine, P. S., Parr, V. B. and Oldham, G. A., (1975) "Workbook For Predicting Pressure Wave and Fragment Effects of Exploding Propellant Tanks and Gas Storage Vessels," NASA CR-134906, Contract NAS3-19231, November 1975 (reprinted September 1977).

Baker, W. E., Esparza, E. D., Hokanson, J. C., Funnell, J. E., Moseley, P. K. and Deffenbaugh, D. M., "Initial Feasibility Study of Water Vessels for Arresting Lava Flow," AMSAA Contractor Report to be published.

Esparza, E. D. and Baker, W. E., (1977a) "Measurements of Blast Waves From Bursting Pressurized Frangible Spheres," NASA CR-2843, Grant NSG 3008, May 1977.

Esparza, E. D. and Baker, W. E., (1977b) "Measurements of Blast Waves From Bursting Frangible Spheres Pressurized with Flash-Evaporating Vapor or Liquid," NASA CR-2811, National Aeronautics and Space Administration, Washington, D. C., November 1977.



## CHAPTER III

### EFFECTS OF PRESSURE WAVES

#### 3-1 General

It should be clear from the discussions in earlier chapters that the pressure (blast) waves from accidental explosions in ground systems can differ significantly from "classical" blast waves from condensed explosives. But, the basic methods presented by Baker, et al (1975) for predicting effects of pressure waves are independent of the exact character of the explosion source, and are primarily related to blast wave properties such as peak side-on overpressure  $P_s$  and positive impulse  $i_s$ , or peak reflected overpressure  $P_r$  and the corresponding reflected impulse  $i_r$ .

Because of the correlation of the blast effects prediction methods in Baker, et al (1975) with blast wave properties, all of the graphs and equations in Chapter III of that reference are equally applicable for the ground burst accidents which are the topic of this workbook. Topics covered in Baker, et al (1975) are:

- 1) Thresholds for glass breakage.
- 2) Empirical blast damage estimates for residential buildings.
- 3) Toppling or overturning of vehicles and other objects.
- 4) Damage thresholds for beam structural elements.
- 5) Damage predictions for brittle and ductile rectangular plate elements.
- 6) Damage thresholds for rectangular membranes.
- 7) Blast injury estimates for humans.

We will not duplicate any of those prediction methods here, but will instead give supplementary prediction curves based on further damage prediction analyses by our staff.

#### 3-2 Additional Beam Response Predictions

Methods were given in Baker, et al (1975) for prediction of damage thresholds for beams with various boundary conditions. The techniques used to obtain that set of prediction curves were based on assumed rigid-plastic beam behavior, and energy balance methods. Other prediction curves can be obtained by assuming elastic-plastic beam behavior, or purely elastic behavior. The curves are given here, and the procedures used in developing them are given in



Appendix B.

Figure 3-1 is a nondimensionalized pressure-impulse (P-i) diagram for determining the maximum strain and deflection in beams loaded by a blast wave. The blast wave is characterized by its peak applied pressure P and impulse i. These pressures and impulses are either side-on or reflected ones dependent upon the orientation of the building relative to the enveloping wave. In this graphical solution, we assume that the loading is uniform over the entire span of length  $\ell$ . The beam has a loaded width b, a mass density  $\rho$ , a cross-sectional area A, a total depth H, an elastic modulus E, a yield point  $\sigma_y$ , a second moment of area I, and a plastic (not elastic) section modulus Z.

Different boundary conditions can be evaluated by inserting the appropriate nondimensional numbers, i.e., the appropriate  $\Psi$  coefficients from the table in Figure 3-1. Simply-supported, clamped-clamped, clamped-pinned, and cantilever beams are all included in this graphical solution. No strain energy is absorbed in extensional or shear behavior. This solution is entirely a bending one. Any self-consistent set of units can be used because this solution is nondimensional.

As an illustration of how Figure 3-1 may be applied, consider a 12H5 as a joist in a flat roof.\* The joist will have 4-ft centers and be a simply-supported beam with a 20-ft span. The weight of the concrete and insulation being supported by this joist is assumed to equal 30.2 lb/ft<sup>2</sup>. The joist is made of steel with a weight density of 0.283 lb/in<sup>3</sup>, an elastic modulus of  $30 \times 10^6$  psi, and a yield stress of 33,000 psi. The AISC handbook gives a weight per length of 7.1 lb/ft, a maximum moment based on a 30,000-psi yield of 222 in-kips, and a depth of 12.0 inches. These properties indicate that the second moment of area equals  $Mh/2\sigma$ , or 44.4 in<sup>4</sup>, and that the elastic section modulus is  $2I/h$ , or 7.4 in<sup>3</sup>. We will assume that the plastic section modulus Z equals the elastic section modulus in a beam with this shape. In a simply-supported beam, the  $\Psi_p$  number equals 10.0,  $\Psi_i$  equals 0.913, and  $\Psi_c$  equals 1.25.

Next the nondimensional quantities

$$\frac{Pb\ell^2}{\Psi_p \sigma_y Z}$$

and

\*English units are used in this and some subsequent examples because all of the handbook properties of structural steel members are given in these units, and they are the common units used by structural designers.



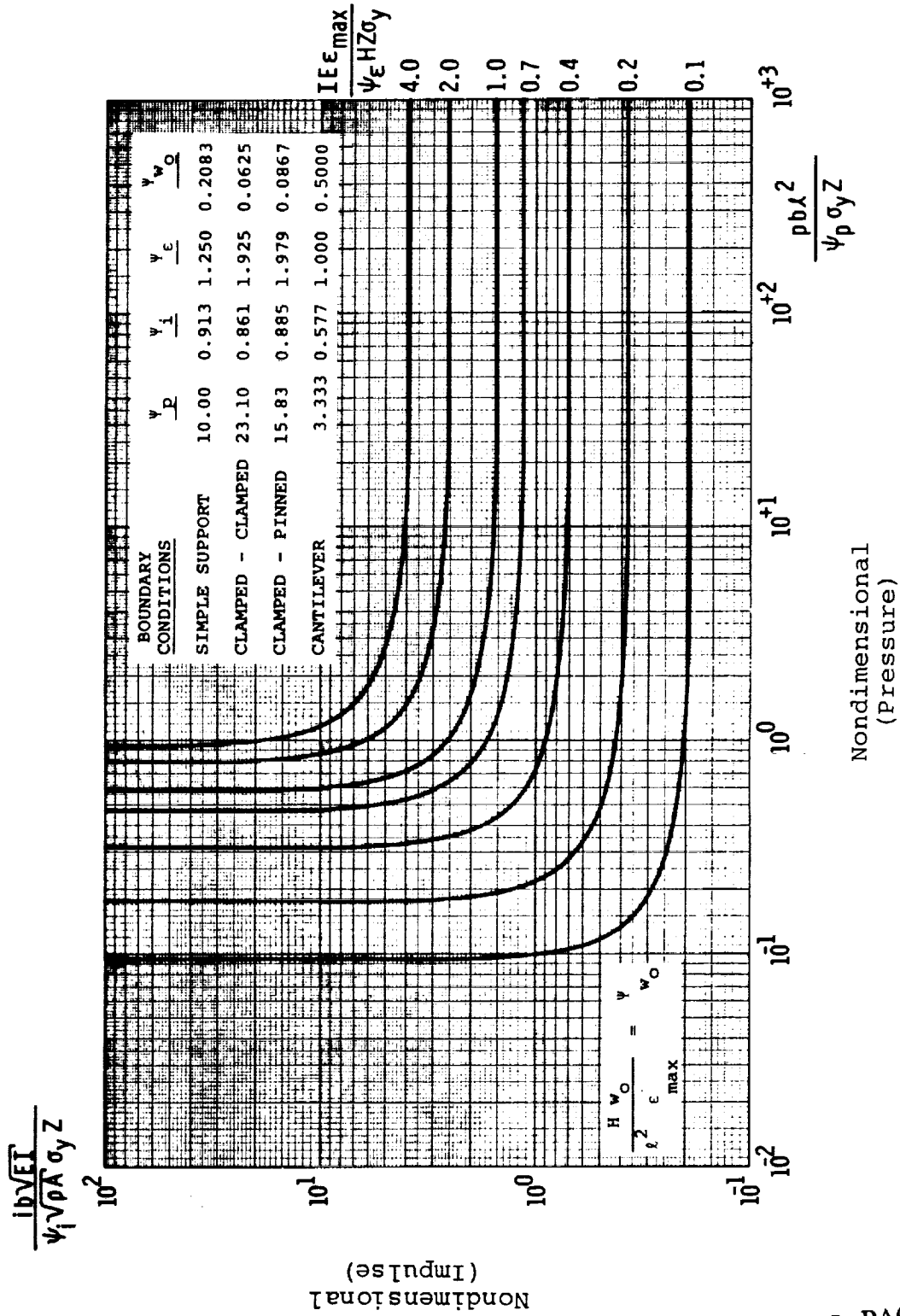


FIGURE 3-1. ELASTIC-PLASTIC SOLUTION FOR BLAST LOADED BEAMS

ORIGINAL PAGE IS OF POOR QUALITY



Figure 3-2 is a corresponding bending beam solution for elastic response only. The major added benefit derived from Figure 3-2 is that it can be used to estimate the shear forces at the supports. For a Bernoulli-Euler beam, a plastically responding beam has no shear force at the instant of maximum deformation, as

$$\frac{dM}{dx} = 0.$$

Obviously, a maximum shear is reached earlier in the response which is not handled by an energy solution. An energy solution only handles end states; it never yields a transient solution. For an elastic solution, a maximum shear force  $V$  is reached when the beam is in its maximum elastically deformed position. Provided the response is elastic, Figure 3-2 essentially yields the same solution as an elastically responding beam from the more generalized Figure 3-1 solution.

We will illustrate the use of Figure 3-2 with the same 12H5 roof joint exposed to the same 1.42 psi and 0.0145 psi-sec pressure-impulse blast loading as in the previous example. The elastic scaled pressure and impulse quantities which must be calculated are

$$\frac{PbH\ell^2}{\alpha_p EI} \text{ and } \frac{ibH}{\alpha_i \sqrt{\rho EIA}}.$$

Once again multiply and divide the scaled impulse by  $g^{1/2}$  to form

$$\frac{ibH \sqrt{g}}{\alpha_i \sqrt{(\rho g A) EI}}$$

which takes advantage of the weight per unit length quantity  $(\rho g A)$ . Substituting as before,  $P = 1.42$  psi,  $b = 48$  in.,  $H = 12$  in.,  $\ell = 240$  in.,  $\alpha_p = 8.00$ ,  $E = 30 \times 10^{10}$  psi, and  $I = 44.4$  in<sup>4</sup> gives  $4.42 \times 10^{-3}$  for the scaled pressure quantity

$$\frac{PbH\ell^2}{\alpha_p EI}.$$

Substituting  $i = 0.0145$  psi-sec,  $b = 48$  in.,  $H = 12$  in.,  $g = 386$  in/sec<sup>2</sup>,  $\alpha_i = 1.461$ ,  $(\rho g A) = 10.66$  lb/in,  $E = 30 \times 10^{10}$ , and  $I = 44.4$  in<sup>4</sup> gives  $9.43 \times 10^{-4}$  for the scaled impulse quantity

$$\frac{ibHg^{1/2}}{\alpha_i \sqrt{\rho Ag} EI}.$$



ORIGINAL PAGE IS  
OF POOR QUALITY

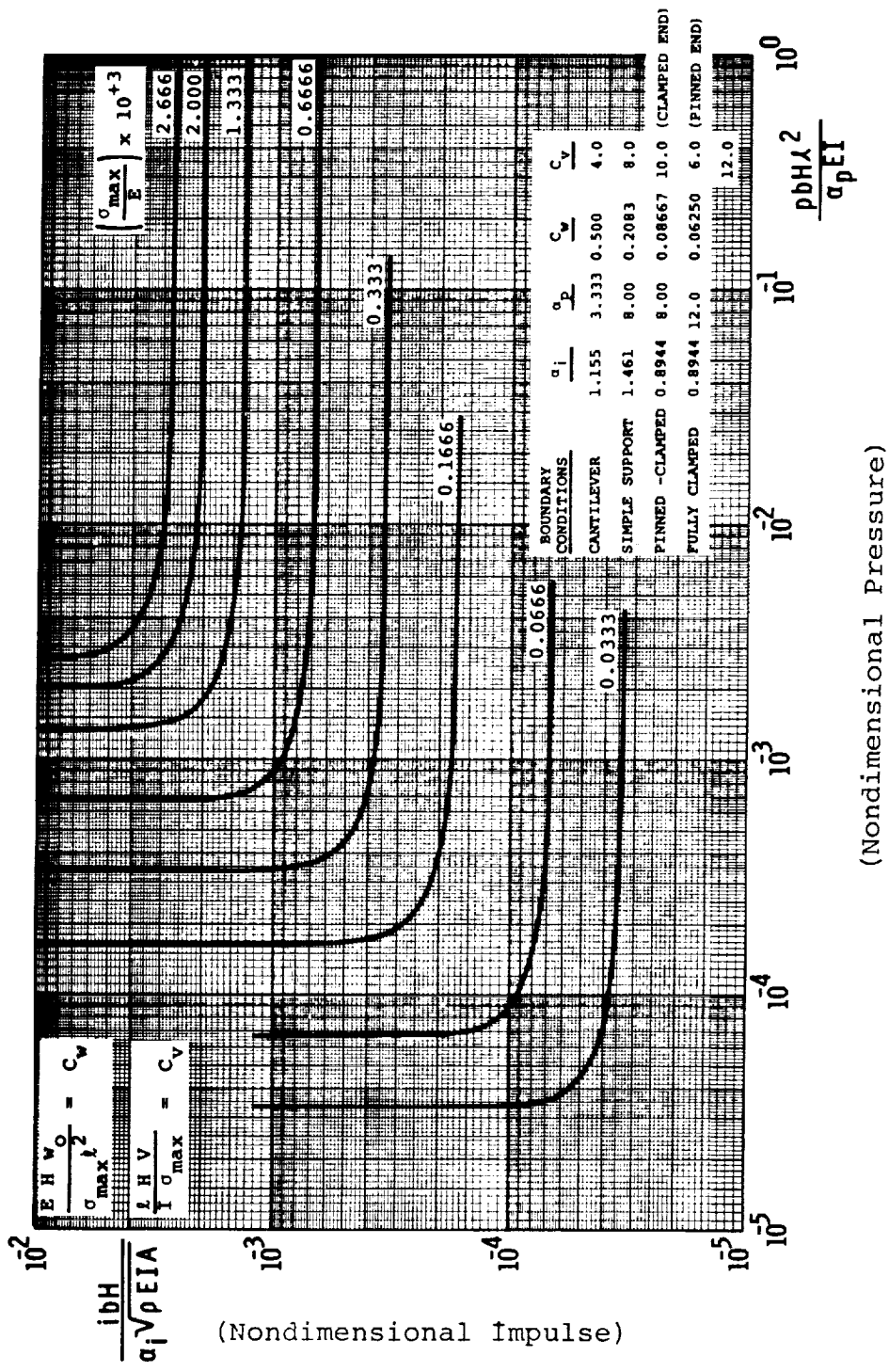


FIGURE 3-2. STRESSES, SHEARS, AND DEFLECTIONS IN BLAST LOADED ELASTIC BEAMS

The coefficients differ in Figures 3-1 and 3-2; however, the appropriate values are provided in tabular inserts. Entering Figure 3-2 for this specific combination of scaled pressure and scaled impulse gives a scaled stress

$$\left( \frac{\sigma_{\max}}{E} \times 10^{+3} \right)$$

of approximately 1.0 after extrapolating. After substituting for E; this calculation indicates that the maximum stress caused by the air blast wave is approximately 30,000 psi. This answer is identical, within the limits of graphical accuracy, to the 27,200 psi stress found using Figure 3-1. In addition, the shear force at the support caused by this dynamic load can also be determined. The equations in the upper left hand corner of Figure 3-2 permit the maximum elastic deformation  $w_o$  and the shear force at the supports to be determined after  $\sigma_{\max}$  has been computed. The coefficients  $C_w$  and  $C_v$ , also found in the table accompanying Figure 3-2, depend upon the boundary conditions. For a simply-supported beam,  $C_v = 8.0$ . Substituting  $C_v = 8.0$ ,  $\sigma_{\max} = 30,000$  psi,  $I = 44.4 \text{ in}^4$ ,  $\ell = 240 \text{ in.}$ , and  $H = 12 \text{ in.}$  gives 3,700 lbs for the maximum elastic shear force caused by the blast load.

Whenever a member undergoes large deformations relative to its thickness, the principal mode of energy dissipation is extensional rather than bending. Figure 3-3 presents an elastic-plastic, one-dimensional, extensional solution. An extensional solution assumes that the ends are constrained from moving together so that in-plane forces can be developed. The results presented in Figure 3-3 are very similar to the previously presented bending solution in that contours of constant scaled strain are presented on a plot of scaled applied impulse and pressure. All loads are assumed to be uniformly distributed over the member being loaded. After the strain has been determined, the maximum deformation, the slope at the boundaries, and the magnitude of the anchoring force can all be determined using Figure 3-3.

The symbols in Figure 3-3 are very similar to those used previously. The one new symbol is A, the cross-sectional area of the member. Other symbols include the applied reflected or side-on overpressure P, the applied reflected or side-on impulse i, the loaded width b, the total span  $\ell$ , the mass density  $\rho$ , the elastic modulus E, the yield point  $\sigma_y$ , the maximum strain  $\epsilon_{\max}$ , the maximum deformation  $w_o$ , and the maximum slope

$$\left( \frac{dy}{dx} \right)_{\max}$$



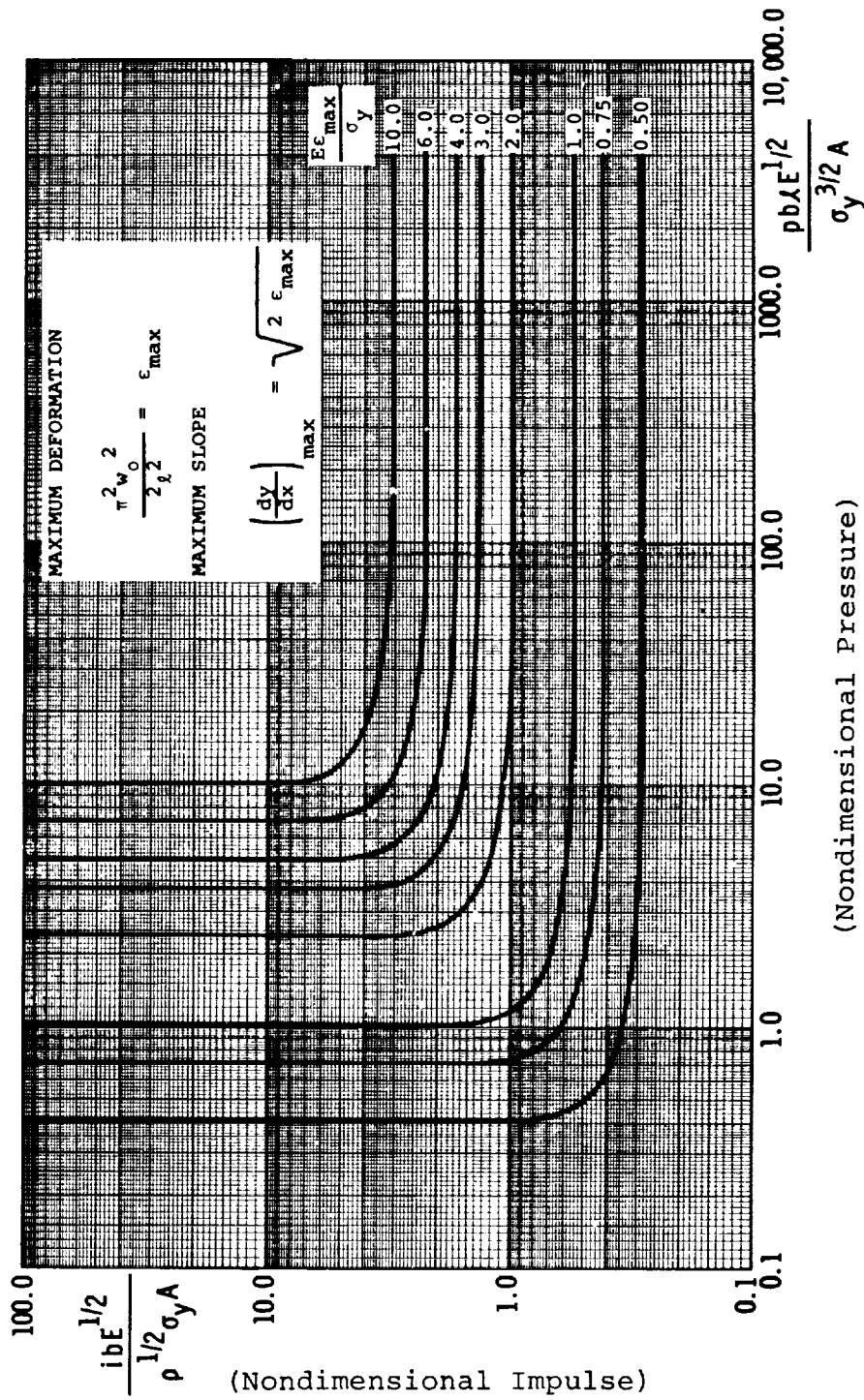


FIGURE 3-3. ELASTIC-PLASTIC STRING SOLUTION

Any self-consistent set of units can be used, as all scaled quantities are nondimensional.

We will illustrate the use of Figure 3-3 by evaluating wall siding. Let us assume normally reflected pressure of 3.0 psi, and a normally reflected impulse of 30.0 psi-ms. Most siding is corrugated so one direction is much stiffer than its orthogonal counterpart. This observation means we can use a strip theory for estimating the response. If we have a steel siding with a yield point of 33,000 psi, a cross-sectional area per inch of width of 0.0625 in<sup>2</sup>/in, a weight per inch width and per inch length of 0.0236 lb/in<sup>2</sup>, and a span of 156 in., then the scaled pressure can be presented in the format

$$\frac{P \ell E^{1/2}}{\sigma_Y^{3/2} (A/b)}$$

which equals

$$\frac{(3.00)(156)(30 \times 10^{+6})^{1/2}}{(33,000)^{3/2}(0.0625)}, \text{ or } 6.84.$$

The scaled impulse should be multiplied and divided to  $g^{1/2}$  to form

$$\frac{i E^{1/2} g^{1/2}}{(\rho g \frac{A}{b})^{1/2} \sigma_Y (\frac{A}{b})^{1/2}},$$

which equals

$$\frac{(0.030)(30 \times 10^{+6})^{1/2}(386)^{1/2}}{(0.0236)^{1/2}(33,000)(0.0625)^{1/2}}, \text{ or } 2.55.$$

Entering Figure 3-3 for these values of scaled pressure and impulse gives a scaled strain

$$\frac{E \epsilon_{\max}}{\sigma_Y}$$

of approximately 4.0. Because

$$\frac{\sigma_Y}{E}$$





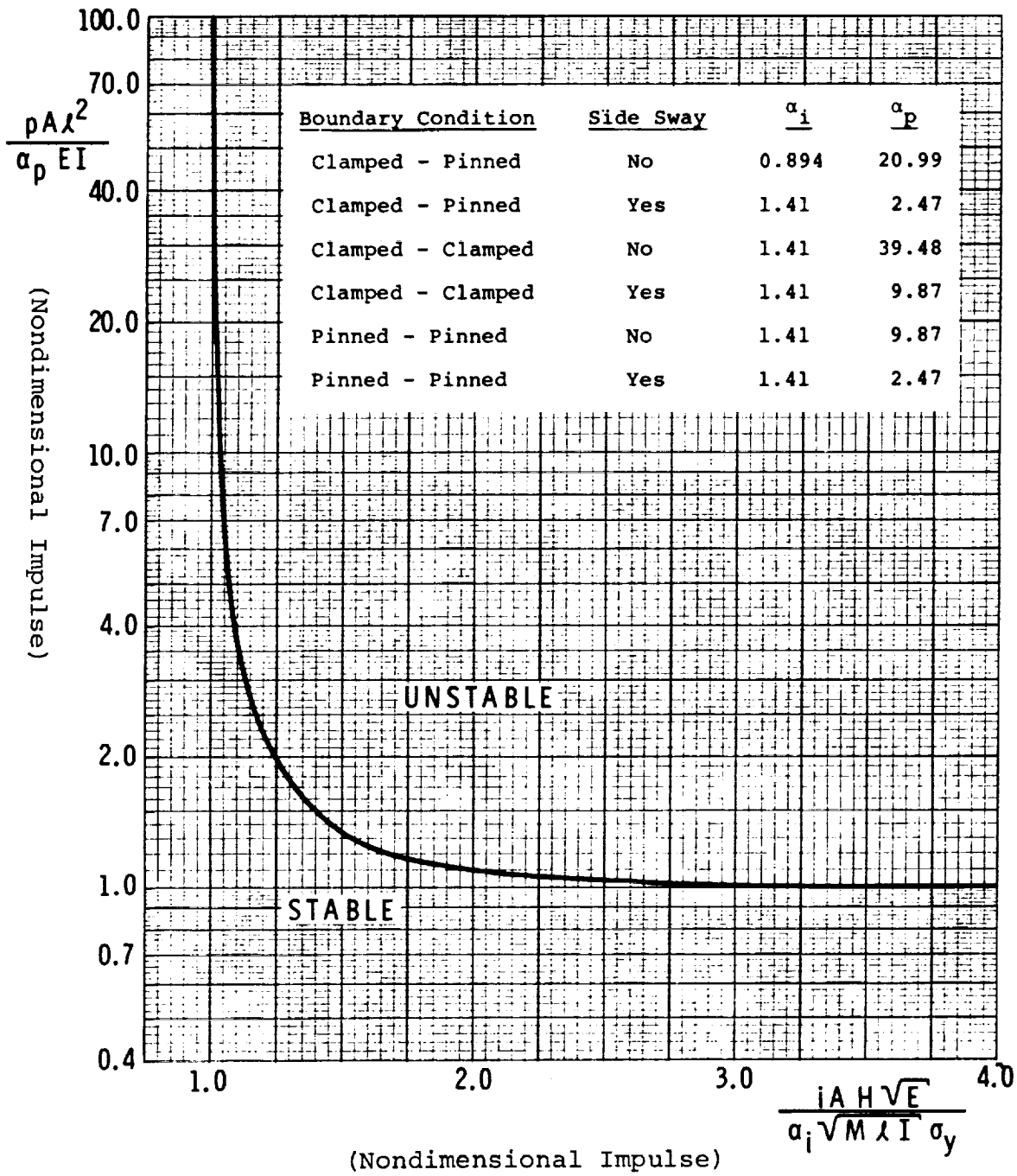


FIGURE 3-4. BUCKLING FOR DYNAMIC AXIAL LOADS

ORIGINAL PAGE IS  
OF POOR QUALITY



$$\frac{PA\lambda^2}{\alpha_p EI}$$

gives

$$\frac{(1.42)(288 \times 240)(150)^2}{(9.87)(30 \times 10^6)(93.0)},$$

or 0.0802. The scaled impulse parameter

$$\frac{iAH \sqrt{E}}{\alpha_i \sqrt{M\lambda I} \sigma_y}$$

gives

$$\frac{(0.0145)(288 \times 240)(10)(30 \times 10^6)^{1/2}}{1.41 \sqrt{\frac{0.02285 \times 288 \times 240}{386}} (150)(93)(33,000)},$$

or 1.56. Because this combination of loads plots below the scaled pressure asymptote of 1.0, the column should be stable.



REFERENCES, CHAPTER III

AISC Handbook, (1961) "Steel Construction," American Institute of Steel Construction, 5th Edition, New York, New York, 1961.

Baker, W. E., Kulesz, J. J., Ricker, R. E., Bessey, R. L., Westine, P. S., Parr, V. B. and Oldham, G. A., (1975) "Workbook for Predicting Pressure Wave and Fragment Effects of Exploding Propellant Tanks and Gas Storage Vessels," NASA CR-134906, Contract NASA-19231 November 1975 (reprinted September 1977).



## CHAPTER IV

### CHARACTERISTICS OF FRAGMENTS

#### 4-1 General

In Baker, et al (1975), there was extensive coverage of such characteristics of fragments from flight-weight vehicles as initial velocities, size and mass distributions, fragment trajectories, and the distances or ranges the fragments travelled. The data and prediction methods given in that reference were based on accident reports and tests with liquid propellant explosions and lightweight gas vessel bursts, development and exercise of a variety of special-purpose computer programs, and statistical analysis of test and accident data.

Accidental explosions in ground systems tend to produce very different types of fragments or missiles than do similar explosions in flight-weight systems. The most striking difference lies in the number of fragments generated, with the number usually being much less for the ground systems than for flight systems. This difference is primarily a function of the differences in storage or pressure vessel materials and construction. Relatively thick-walled vessels, made of ductile steels, dominate in ground storage and transport systems. These vessels often split, or fragment into only two pieces, after failure. Accidental explosions which generate more than a dozen vessel fragments are quite uncommon. For storage or transport vessels containing flash-evaporating liquids such as propane (LPG), a common failure mode is an asymmetric burst of a long cylindrical vessel, with the major part remaining intact and "rocketing" as the fluid exhausts and flashes. Accident reports of such failures show that the vessel can travel great distances, and of course cause a major hazard where they impact.

In this chapter, we present the results of studies on the characteristics of fragments from ground vessel explosions, and highlight the differences from fragmentation of flight-weight vehicles. As before, a survey and statistical analysis of accident data is included; several new computer programs were developed and exercised; and prediction curves on methods generated for various characteristics of the relatively large and massive fragments generated in accidental explosions in ground systems are presented.



## 4-2 Analytical Predictions of Fragment Velocity Distributions

### Estimates of Initial Velocities of Fragments from Bursting Spheres and Cylinders

#### Equal Fragments

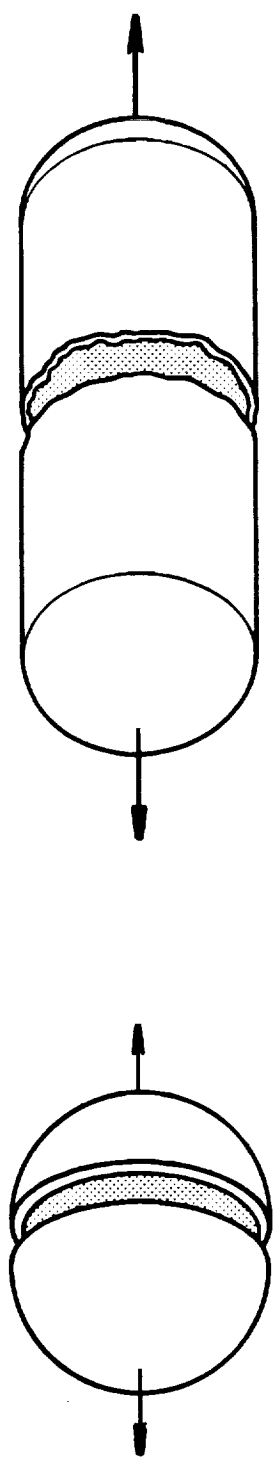
The method developed by Taylor and Price (1971) and modified by Baker, et al (1975) for calculating velocities of fragments from bursting spherical and cylindrical pressure vessels was used to provide velocities of various fragments which could be plotted in some form of prediction curve. The model analyses for reducing and analyzing the data and the results of these analyses are explained in Appendix C. The development of the necessary equations, the numerical iteration method used to simultaneously solve the differential equations and the computer programs can be found in Appendix IV A and Appendix IV C of Baker, et al (1975) (see microfiche). The only assumptions included here are those needed to determine fragment velocities.

The basic assumptions are:

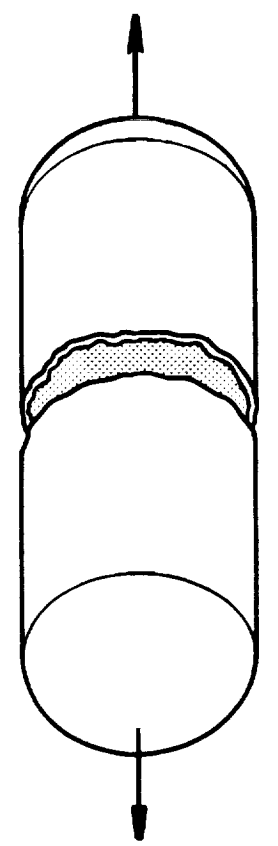
- 1) The vessel with gas under pressure bursts into equal fragments. If there are only two fragments, and the vessel is cylindrical, the vessel bursts perpendicular to its axis of symmetry. If there are more than two fragments, and the vessel is cylindrical, strip fragments (end caps are ignored) are formed and expand radially about the axis of symmetry (see Figure 4-1).
- 2) The cylindrical containment vessel has hemispherical end caps. (These are ignored when the vessel bursts into multiple fragments.)
- 3) The thickness of the containment vessel is uniform.
- 4) Vessels have a length-to-diameter (L/D) ratio of 10.0 for cylinders or 1.0 for spheres.
- 5) Contained gases are either hydrogen (H<sub>2</sub>), air, argon (Ar), helium (He) or carbon dioxide (CO<sub>2</sub>).

Figure 4-2 contains plots of the velocity term versus the pressure term for two fragments, ten fragments and one hundred fragments from spherical or cylindrical vessels. Three separate regions have been bounded to account for scatter:  
(1) cylindrical vessels bursting into multiple fragments;  
(2) spherical vessels bursting in half or multiple fragments and  
(3) cylindrical vessels bursting into two fragments. Estimates of the initial velocities of cylinders and spheres can be extracted from the nondimensional terms read directly from the appropriate bounded regions on the graph. The two nondimensional

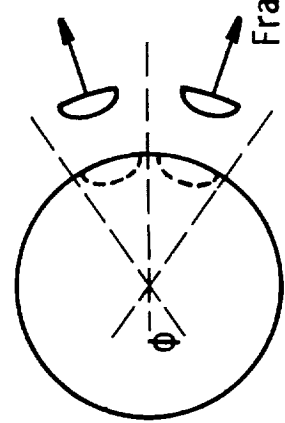




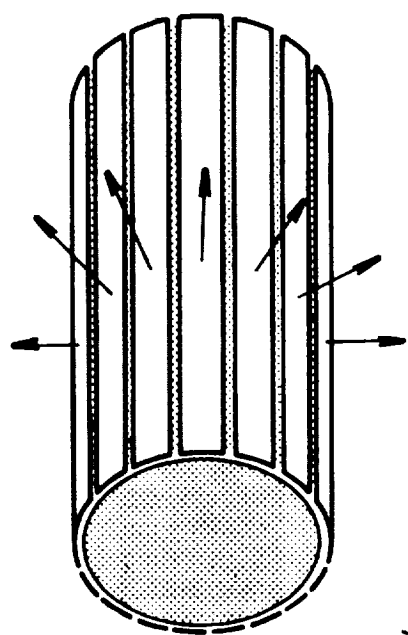
(a) Spheres bursting into two equal fragments



(b) Cylinder bursting into two equal fragments



(c) Sphere bursting into n equal fragments



(d) Cylinder bursting into n equal strip fragments

FIGURE 4-1. ASSUMED FRAGMENTATION PATTERNS

terms in Figure 4-2 are:

- 1) Nondimensional pressure term

$$= \frac{(P-p_a)V_o}{M_c \gamma R_m T_o} = \frac{(P-p_a)V_o}{M_c a_{gas}^2} =$$

$$\frac{\text{(pressure - atm. pressure) (Volume)}}{\text{(Mass of container) (sound speed of the gas)}^2}$$

- 2) Nondimensional velocity term

$$= \frac{u}{K\sqrt{\gamma R_m T_o}} = \frac{u}{Ka_{gas}} = \frac{\text{(velocity)}}{\text{(constant) (sound speed of the gas)}}$$

where K equals 1.0 for equal fragments.

The technique for predicting initial fragment velocities for spherical or cylindrical pressure vessels bursting into equal fragments requires knowledge of the internal pressure P, internal volume  $V_o$ , mass of the container  $M_c$ , ratio of specific heats  $\gamma$ , ideal gas constant adjusted for the gas  $R_m$ , and the temperature of the gas  $T_o$ , at burst. Table 4-1 contains the corresponding  $\gamma$ 's and  $R_m$ 's for the gases for which this analysis is appropriate.

In summary, in order to estimate the initial velocity of fragments from pressurized spheres and cylinders which burst into equal fragments, one should use the following procedures:

- Step 1. Calculate the nondimensional pressure term

$$\frac{(P-p_o)V_o}{M_c \gamma R_m T_o}$$

- Step 2. Locate the corresponding value of the nondimensional velocity term  $\frac{u}{K\sqrt{\gamma R_m T_o}}$  and solve for

$$\frac{u}{K\sqrt{\gamma R_m T_o}}$$

velocity u (Note: K = 1.0 for equal fragments)

Note: Axes of Figure 4-2 are nondimensional terms and merely require that one use a self-consistent set of units.



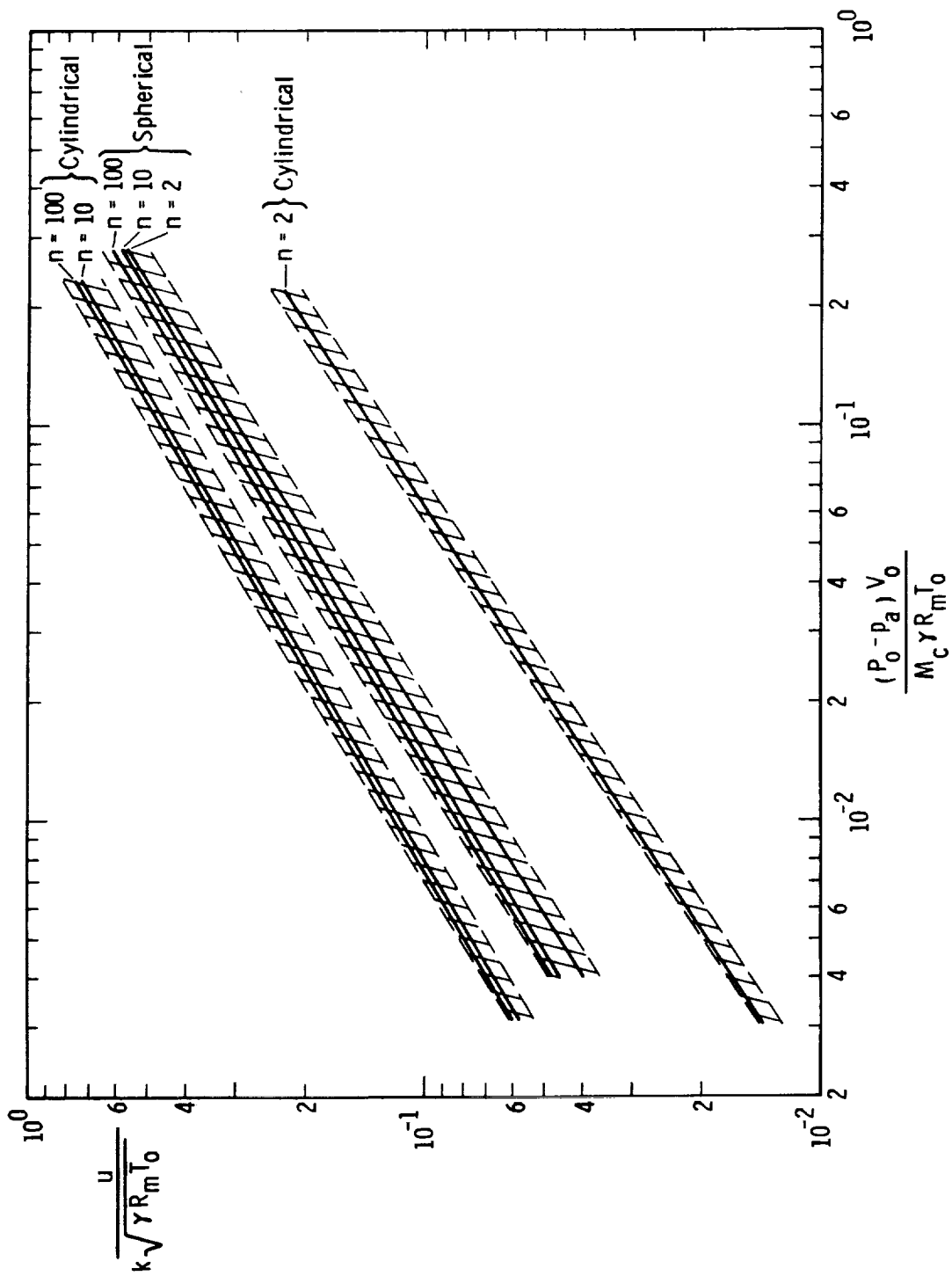


FIGURE 4-2. SCALED FRAGMENT VELOCITY VS. SCALED PRESSURE



TABLE 4-1. SUMMARY OF RATIOS OF SPECIFIC HEAT AND IDEAL GAS CONSTANTS FOR DIFFERENT GASES

Gas	Ratio of Specific Heats $\gamma$	Ideal Gas Constant $R_m$	
		$\left(\frac{m^2}{sec^2 \cdot ^\circ K}\right)$	$\left(\frac{in^2}{sec^2 \cdot ^\circ R}\right)$
Hydrogen	1.4	4124	$3.551 \times 10^6$
Air	1.4	287.0	$2.471 \times 10^5$
Argon	1.67	208.1	$1.792 \times 10^5$
Helium	1.67	2078	$1.789 \times 10^6$
Carbon Dioxide	1.225	188.9	$1.627 \times 10^5$

Example 1:

Determine the initial velocity of a fragment from a pressurized sphere containing hydrogen gas which bursts in half. The following properties may be assumed:

$$P = 10 \times 10^6 \text{ Pa (1464.7 psi)}$$

$$V_o = 0.03m^3 \text{ (1830 in}^3\text{)}$$

$$M_c = 17.13Kg \text{ (37.76 lbs)}$$

$$T_o = 300^\circ K$$

From Table 4-1  $\gamma = 1.4$

$$R_m = 4124 \frac{m^2}{sec^2 \cdot ^\circ K} \quad (3.551 \times 10^6 \frac{in^2}{sec^2 \cdot ^\circ R})$$

Step 1. Nondimensional pressure term =

$$\frac{(P-p_o)V_o}{M_c \gamma R_m T_o} = \frac{(10 \times 10^6) (0.03)}{(17.13) (1.4) (4124) (300)} = 0.01011$$

Step 2. Since the sphere bursts in half,  $K = 1.0$ . From Figure 4-2  $\frac{u}{K\sqrt{\gamma R_m T_o}} = .071$  and solving for  $u$  re-

$$K\sqrt{\gamma R_m T_o}$$

sults in an initial velocity of 93.44 m/sec (306.6 ft/sec).



Program SPHERE [See Chapter IV, Baker, et al (1975) (microfiche)] results show the initial velocity to be 94.92 m/sec (311.4 ft/sec).

$$\text{Percent Error} = \frac{94.92-93.44}{94.92} \times 100 = 1.6\%$$

Example 2:

Determine the initial velocity of a fragment from a pressurized cylindrical vessel containing argon which bursts into 50 equal fragments. Assume the following properties:

$$P = 1.5 \times 10^6 \text{ Pa (217.7 psi)}$$

$$V_o = 0.03 \text{ m}^3 \text{ (1830 in}^3\text{)}$$

$$M_c = 3.21 \text{ Kg (7.07 lbs)}$$

$$T_o = 700^\circ\text{K}$$

From Table 4-1  $\gamma = 1.67$

$$R_m = 208.1 \frac{\text{m}^2}{\text{sec}^2 \cdot ^\circ\text{K}} \left( 1.792 \times 10^5 \frac{\text{in}^2}{\text{sec}^2 \cdot ^\circ\text{R}} \right)$$

Step 1. Nondimensional pressure term =

$$\frac{(P-p_o)V_o}{M_c \gamma R_m T_o} = \frac{(1.4 \times 10^6) (0.03)}{(3.21) (1.67) (208.1) (700)} = 0.0538$$

Step 2. Since the cylinder bursts into 50 equal fragments,  $K = 1.0$ . From Figure 4-2,  $\frac{u}{K\sqrt{\gamma R_m T_o}} = 0.3$  and solving

for  $u$  results in an initial velocity of 148 m/sec (485 ft/sec).

Program SPHERE results show the initial velocity to be 149.2 m/s (489.4 ft/sec).

$$\text{Percent error} = \frac{149.2-148}{149.2} \times 100 = 0.80\%$$



## Cylinders with Length-to-Diameter Ratio of 10.0 Bursting into two Unequal Fragments

The Taylor and Price (1971) method modified by Baker, et al (1975) for calculating velocities of fragments from bursting spherical and cylindrical gas vessels has been expanded to provide initial velocities of unequal fragments from cylindrical vessels. The development of the necessary equations and the subsequent computer program UNQL are explained in depth in Appendix D. The assumptions essential to the velocity calculations follow:

- 1) The vessel with gas under pressure breaks into two unequal fragments along a plane perpendicular to the cylindrical axis, and the two container fragments are driven in opposite directions (see Figure 4-3).
- 2) The containment vessel is cylindrical and has hemispherical end caps.
- 3) The thickness of the containment vessel is uniform.
- 4) Vessels have a length-to-diameter (L/D) ratio of 10.0.
- 5) Contained gases are either hydrogen (H<sub>2</sub>), air, argon (Ar), helium (He) or carbon dioxide (CO<sub>2</sub>).

The technique for predicting initial fragment velocities for fragments from a cylinder (L/D = 10.0) which breaks into two unequal fragments perpendicular to its axis of symmetry is identical to that for equal fragments except for the value of the constant K. The value of K depends on the ratio of the fragment mass to the total mass of the cylinder as shown in Figure 4-4. To estimate the initial velocity of a fragment from a pressurized cylinder (L/D = 10.0) which bursts into unequal fragments, one should use the following procedures:

Step 1. Calculate the nondimensional pressure term =

$$\frac{(P-p_o)V_o}{M_c \gamma R_m T_o}$$

Step 2. Locate the corresponding value of the nondimensional velocity term  $\frac{u}{K\sqrt{\gamma R_m T_o}}$  in the region bounded for

$$n = 2 \text{ (cylindrical vessels).}$$

Step 3. Determine the value of K from Figure 4-4.

Step 4. Solve for velocity u.



ORIGINAL PAGE IS  
OF POOR QUALITY

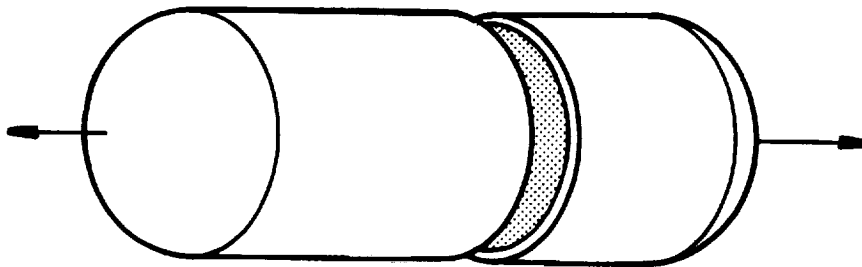


FIGURE 4-3. ASSUMED BREAKUP INTO TWO UNEQUAL FRAGMENTS

U U

Note: Axes of Figure 4-2 are nondimensional terms and merely require that one use a self-consistent set of units.

Example 1:

Determine the initial velocity of a fragment from a pressurized cylindrical vessel containing carbon dioxide which bursts into two unequal fragments. Assume the following properties:

$$\begin{aligned}
 P &= 69 \times 10^6 \text{ Pa (10,010 psi)} \\
 V_o &= 30.0 \text{ m}^3 \text{ (1.83} \times 10^6 \text{ in}^3\text{)} \\
 M_c &= 1.92 \times 10^5 \text{ kg (4.23} \times 10^5 \text{ lbs)} \\
 T_o &= 500^\circ\text{K}
 \end{aligned}$$

From Table 4-1,  $\gamma = 1.225$

$$R_m = 188.9 \frac{\text{m}^2}{\text{sec}^2 \cdot ^\circ\text{K}} \left( 1.627 \times 10^5 \frac{\text{in}^2}{\text{sec}^2 \cdot ^\circ\text{R}} \right)$$

Fraction of the total mass for fragment under consideration = 0.75.

Step 1. Nondimensional pressure term =

$$\frac{(P-p_o)V_o}{M_c \gamma R_m T_o} = \frac{(68.9 \times 10^6) (30.0)}{(1.92 \times 10^5) (1.225) (188.9) (500)} = 0.093$$

Step 2. The corresponding value of  $\frac{u}{K\sqrt{\gamma R_m T_o}} = 0.13$ .

Step 3. From Figure 4-4,  $K = 0.61$ .

Step 4. Solving for  $u$  gives an initial velocity of 27 m/s (88 ft/sec).

Program UNQL results (Appendix D) show the initial velocity to be 26.5 m/s (86.9 ft/sec).

$$\text{Percent error} = \frac{27-26.5}{26.5} \times 100 = 1.9\%$$







4-3 Analytic Predictions of Fragment Trajectories, Ranges and Impact Conditions

Predicting Ranges of Free-Flying Fragments

The range of a flying fragment from a bursting container is dependent on the lift and drag forces acting on the fragment. Two types of fragment cases were studied in this analysis: (1) fragments whose geometry is such that both the lift and drag forces act on them during flight, i.e., disc-shaped fragments and long, thin fragments; and (2) fragments whose geometry is such that only the drag forces act and there is no lift. A method of predicting the distance traveled by a fragment was developed and computerized (Code FRISB) by Baker, et al (1975) and this section expands on their efforts.

A set of generalized curves (Figure 4-5) was developed for use in estimating the maximum fragment range. These curves were developed by performing a model analysis to generate dimensionless parameters which describe the general problem (Appendix E), next using the computer code FRISB to determine ranges for selected cases, and then plotting the results to form the curves. It should be noted that, in generating these curves, several initial trajectory angles were used in the analysis to obtain the maximum range for the respective fragments. For ease in understanding the use of these curves, the example which follows is presented. The procedure for determining fragment range is:

- Step 1. Calculate the lift/drag ratio =  $\frac{C_L A_L}{C_D A_D}$  for the fragment.
- Step 2. Calculate the velocity term =  $\frac{\rho_0 C_D A_D V^2}{Mg}$  for the fragment.
- Step 3. Select the curve on the graph for the appropriate lift/drag ratio; locate the velocity term on the horizontal axis; find the corresponding range term,  $\frac{\rho_0 C_D A_D R}{M}$  and determine the range, R.

Note that, for lift to drag ratios  $\frac{C_L A_L}{C_D A_D}$  that are not on the curve, a linear interpolation procedure can be used to determine the range from the curve. Interpolation in the steep areas of the curve can cause considerable error and it is recommended that, for these cases, the computer code FRISB be exercised.

FRISB example: Assume  $\rho_0$  = density of air =  $1.293 \frac{kg}{m^3}$

$g$  = gravity constant =  $9.807 \text{ m/s}^2$



Example 1, for lifting fragments:

Determine the maximum range of a long rectangular fragment assuming the following properties:  $V_i = 100$  m/s (328 ft/sec), Mass = 30.827 kg (67.96 lb<sub>m</sub>), Projected area = 0.03018m<sup>2</sup> (0.3249 ft<sup>2</sup>), Cylinder length = 1.58m (5.18 ft), Thickness of fragment = 0.0191m (0.0627 ft), Planform or lift area = 0.20623m<sup>2</sup> (2.2198 ft<sup>2</sup>), Drag coefficient = 2.05, lift coefficient = 0.3, and the initial trajectory of the fragment at  $t = 0$  was  $\alpha_i = 20^\circ$ .

Step 1. Determine the lift/drag ratio for the fragment =

$$\frac{C_{L A_L}}{C_{D A_D}} = \frac{(0.3) (0.20623)}{(2.05) (0.03018)} = 1.0$$

Step 2. Determine the value of the velocity term =

$$\frac{\rho_o C_{D A_D} V^2}{Mg} = \frac{(1.293) (2.05) (0.03018) (100)^2}{(30.827) (9.807)} = 2.65$$

Step 3. From Figure 4-5  $\frac{\rho_o C_{D A_D} R}{M} = 1.65$  and solving for R results in a range of 635.8 meters (2086 ft).

Program FRISB results show the maximum range to be 633.43m (2078 ft).

$$\text{Percent error} = \frac{635.8 - 633.43}{633.43} \times 100 = 0.37\%$$

Predicting Ranges of Rocketing Fragments

In an accident involving propellant (propane, butane, etc.) storage systems, large fragments (greater than one-fourth of the vessel), which travel long distances, are sometimes generated. These large fragments are typically sections of the tank which break free intact and initially contain some entrapped propellant. These large fragments exhibit a rocketing behavior (see Appendix E) which results from the changing of all or part of the liquid propellant into a gas when the external pressure is released during the fracturing of the vessel (flash evaporation). The gas escapes from the opening in the vessel in a manner similar to gas exiting a rocket motor and propels the somewhat stabilized fragment to great distances.

The physics of this process is explained in greater detail in Appendix F. This appendix also contains a computer program for predicting the range and impact velocity of the rocketing



fragment. As explained in the model analysis in Appendix G, this phenomenon is not readily adaptable to consolidated prediction curves and requires some further development effort in this area. Therefore, for the present, in order to predict the distance traveled by "thrusting" fragments, one must either run the computer program in Appendix F or acquire the values from Table 4-2, (see Appendix G, p. 7) if the storage tanks and fragments being examined have characteristics similar to the vessels and fragments contained in the table. Table 4-2 was generated for comparison to some accident reports. Calculated values for fragment ranges were in good agreement with actual values, considering limitations in available information. In general, rocketing fragments from accidents of this type have low launch angles (5-10 degrees). To determine range, or impact velocity, of rocketing fragments (see Table 4-2 and/or Appendix F), one needs to know the pressure of the fluid at rupture, the volume of the container, the volume partially enclosed by the fragment, the volume of the liquid before rupture, the volume of the vapor before rupture, the exit area for the propellant contained in the fragment, the mass of the fragment, and the launch angle of the fragment.

#### 4-4 Statistical Analysis of Fragments

##### Statistical Analysis of Accidental Explosions

###### Introduction

Data were gathered on twenty-five events. A detailed description of these events, in terms of the explosive source and the containment vessel, is given in Table H-1 in Appendix H. Table H-2 in Appendix H gives available fragment information (mass, range, trajectory elevation and shape) for each event.

Due to the limited amount of data on most of the events, it was desirable to group the data from like events in order to yield an adequate base for meaningful statistical analysis. From Tables H-1 and H-2, the six groups of like events shown in Table 4-3 were obtained. Statistical analyses were performed on data from each of the groups to yield (as the data permitted) estimates of fragment range distribution, fragment mass distribution and fragment mean velocity as a function of the ratio of explosion energy to vessel weight. Other relationships were also investigated and the results are given in the following paragraphs.

###### Fragment Range Distribution

As shown in Appendix H-2, the fragment range for each of the groups of events follows a log normal distribution. That is, the logarithms of the fragment ranges follow a normal or



TABLE 4-2. PREDICTED RANGES FOR ROCKETING FRAGMENTS

EXAMPLE NUMBER	SOURCE OF ACTUAL DATA	INITIAL PRESSURE (P <sub>a</sub> )	VOLUME OF CONTAINER (m <sup>3</sup> )	VOLUME OF FRAGMENT ENCLOSURE (m <sup>3</sup> )	VOLUME OF LIQUID BEFORE RUPTURE (m <sup>3</sup> )	VOLUME OF VAPOR BEFORE RUPTURE (m <sup>3</sup> )	EXIT AREA (m <sup>2</sup> )	MASS OF FRAGMENT (kg)	LAUNCH ANGLE (degrees)	CALCULATED IMPACT VELOCITY (m/s)	CALCULATED RANGE (m)	ACTUAL RANGE (m)	PERCENT DIFFERENCE IN RANGE (%)	BEST ESTIMATE FOR LAUNCH ANGLE (degrees)
1	NTSR- HAR- 76-4 4/29/75	701,197	38.02	28.23	33.10	4.916	3.75	3885	5	194	426	314	36	5
2	NTSR- HAR- 73-4 9/21/72	1,034,214	37.85	30.32	27.29	10.56	3.41	5083	5	189	471	398	18	5
3	NTSR- HAR- 73-4 9/21/72	1,034,214	37.85	1.28	27.29	10.56	3.41	652	5	94	154	165	-6.7	5
4a	Propane Tank Explosion in San Antonio	1,378,951	1.8927	0.5513	1.586	0.3067	2.336	171	5	159	450	123	266	5-10
4b	Propane Tank Explosion in San Antonio	1,378,951	1.8927	0.5513	1.586	0.3067	2.336	171	10	154	846	123	-588	5-10
4c	Propane Tank Explosion in San Antonio	1,378,951	1.8927	0.2002	1.586	0.3067	0.6567	171	5	72	90	123	-27	5-10
4d	Propane Tank Explosion in San Antonio	1,378,951	1.8927	0.2002	1.586	0.3067	0.6567	171	10	71	179	123	46	5-10

ORIGINAL PAGE IS  
OF POOR QUALITY

TABLE 4-3. GROUPS OF LIKE EVENTS TAKEN FROM TABLES H-1 and H-2

Event Group Number	Event	Explosion Source		Vessel		
		Material	Energy Range, J	Shape	Mass, kg	Number Of Fragments
1	1, 2, 3, 18	Propane, anhydrous ammonia	1.487X10 <sup>5</sup> to 5.95X10 <sup>5</sup>	RR Tank Car	25,542 to 83,900	14
2	6, 7, 8, 9, 10, 13, 14, 15, 19	LPG	3814 to 3921.3	RR Tank Car	25,464	28
3	17	Air	5.198X10 <sup>11</sup>	Cylinder Pipe and Spheres	145,842	35
4	20, 24	LPG, Propylene	549.6	Semi Trailer (cylindrical)	6,343 to 7,840	31
5	21, 22, 23	Argon	2.438X10 <sup>9</sup> to 1.133X10 <sup>10</sup>	Sphere	46.26 to 187.33	14
6	25	Propane	24.78	Cylinder	511.7	11

Gaussian distribution. Figure 4-6 presents the fragment range distributions for groups 1 and 2, and Figure 4-7 presents the fragment range distributions for groups 3, 4, 5 and 6.

Figures 4-6 and 4-7 can be used to estimate the percentage of fragments which will have a range,  $R_i$ , equal to or less than a particular range.

For example, if we wished to estimate the percentage of fragments which would have a range equal to or less than 600 m for an explosion involving a rail tank car filled with propane (group 1), we would refer to Figure 4-6, and on the range axis (abscissa) at 600 m go upward to the intersection of the group 1 line. Then, at the intersection point read the percentage value from the ordinate, which is 96%. Conversely, if we wanted to know what range 90% of the fragments would not exceed, we would enter the chart on the 90% line, go over to the intersection of the group 1 line and read downward to the range axis the value of 380 m.

#### Fragment Mass Distribution

Pertinent fragment mass information was available on three event groups (2, 3 and 6). As shown in Appendix H-3, the fragment mass for each of the three groups follows a log normal distribution. Figure 4-8 presents the fragment mass distributions for groups 2 and 3, and Figure 4-9 presents the fragment mass distribution for group 6.

These charts can be used in the same manner as Figures 4-6 and 4-7 are used for fragment range.

#### Mean Fragment Mass as a Function of Normalized Yield

In events 21, 22 and 23, spherical containers were pressurized until rupture. The spheres were constructed of steel with an approximate ultimate stress ( $\sigma_u$ ) of 834 MPa. The spheres were the same volume for all three events. The wall thickness of the spheres was the same within events, but was different across events.

Pertinent data and calculated parameters for each of the spheres are given in Table 4-4, where  $\bar{W}$  is the geometric mean fragment mass for each event,  $W(T)$  is the sphere weight for each event,  $\bar{P}$  is the average burst pressure for each event, and  $E_0$  is the energy of detonation of 1 gram of TNT or 4190J.

Figure 4-10 is a plot of the normalized yield ( $\bar{P}\bar{V}/E_0$ ) versus mean fragment mass ( $\bar{W}$ ) for the three events. One could estimate the mean (geometric) fragment mass for any decided ratio of  $\bar{P}\bar{V}/E_0$  from 693 to 2347.



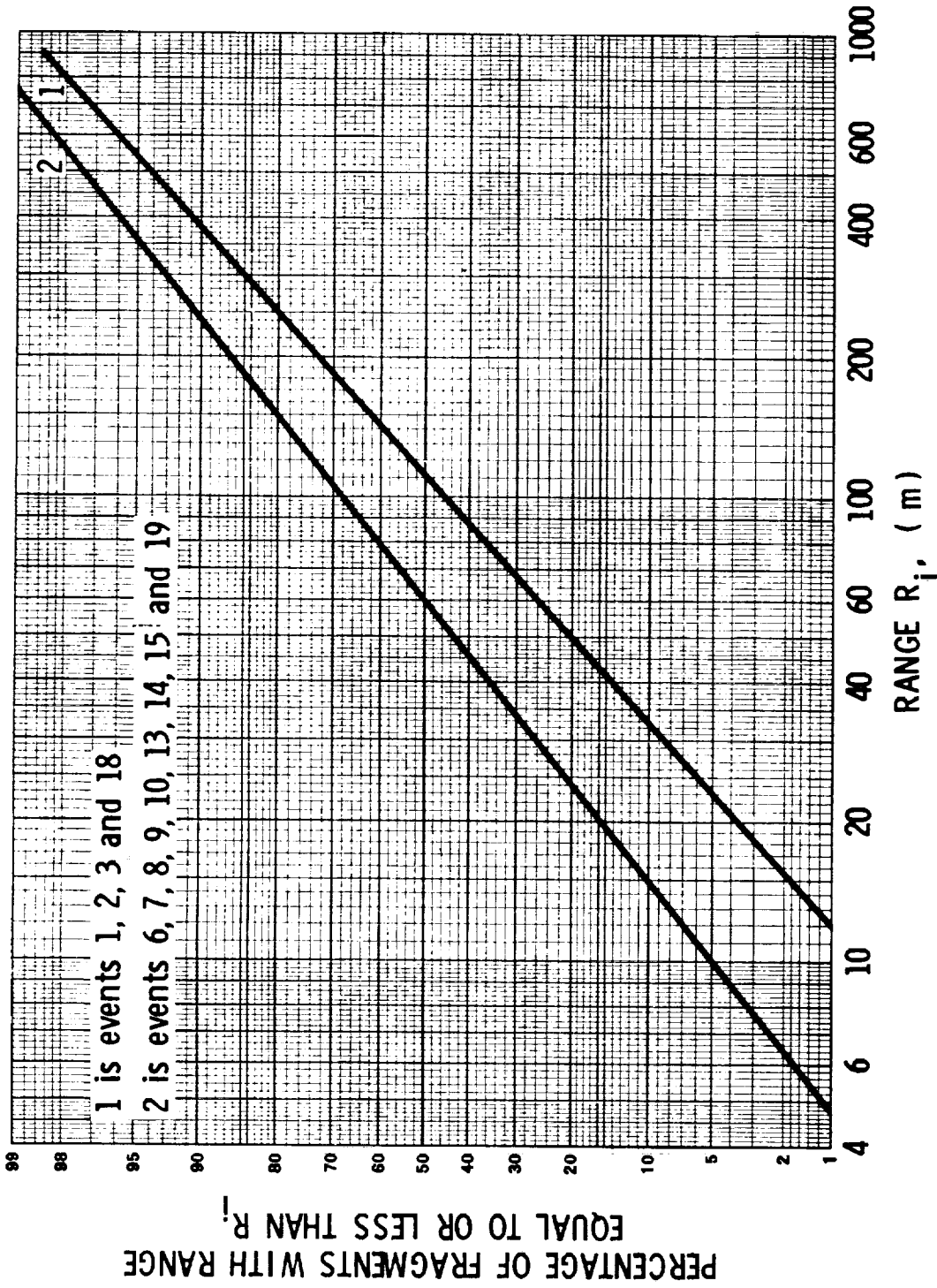


FIGURE 4-6. FRAGMENT RANGE DISTRIBUTION FOR EVENT GROUPS 1 AND 2.

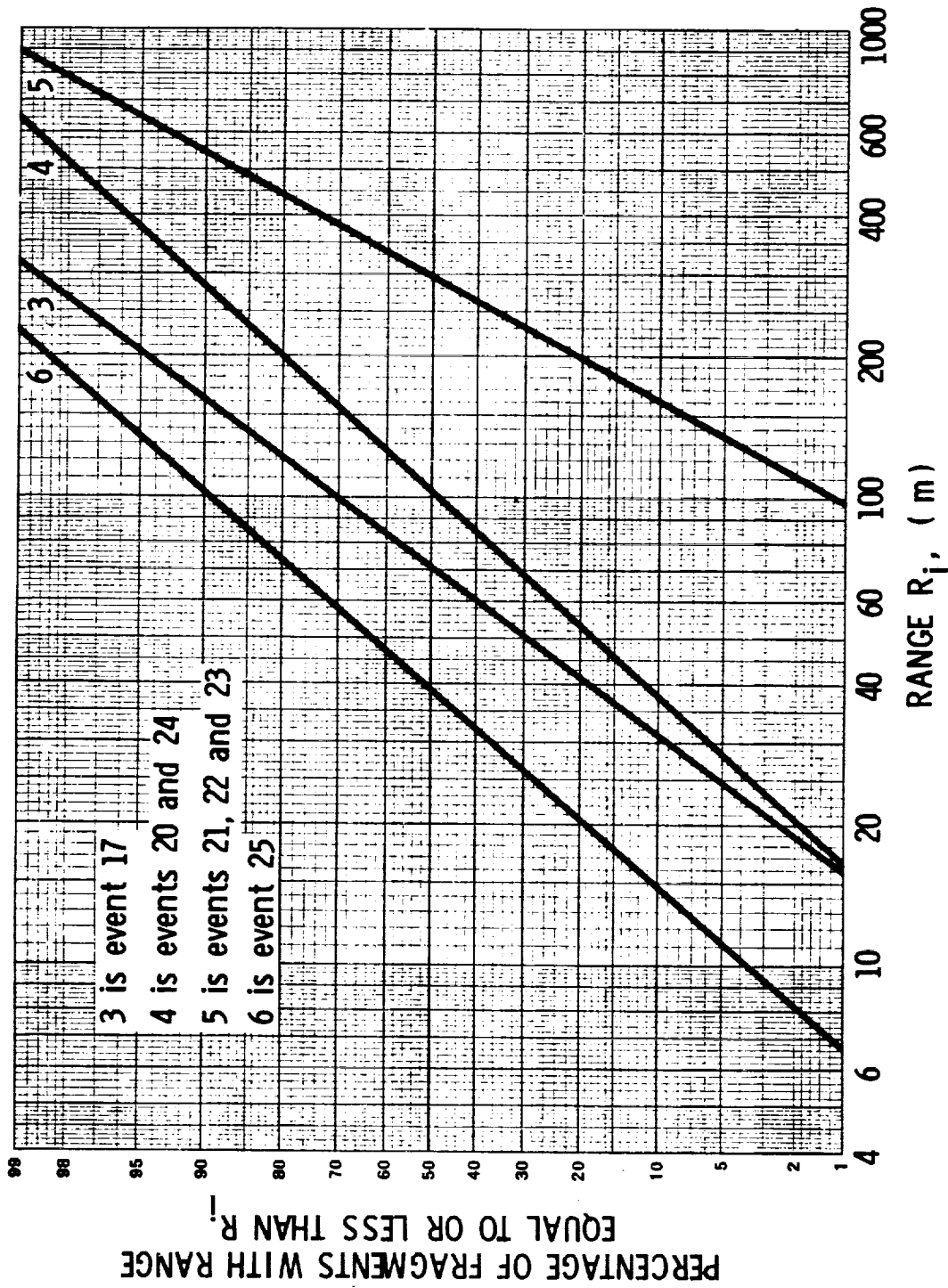


FIGURE 4-7. FRAGMENT RANGE DISTRIBUTION FOR EVENT GROUPS 3, 4, 5 AND 6

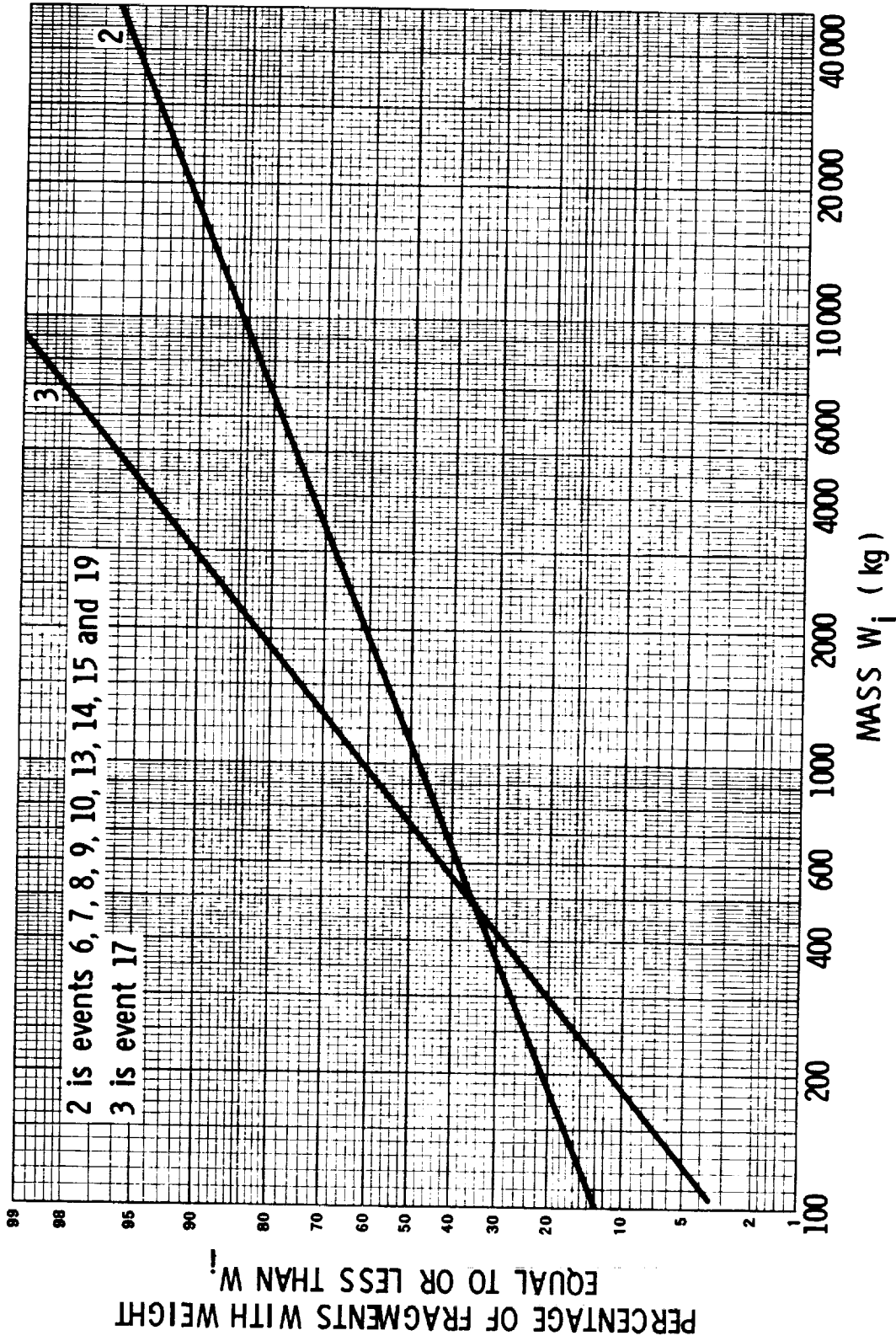


FIGURE 4-8. FRAGMENT MASS DISTRIBUTION FOR EVENT GROUPS 2 AND 3

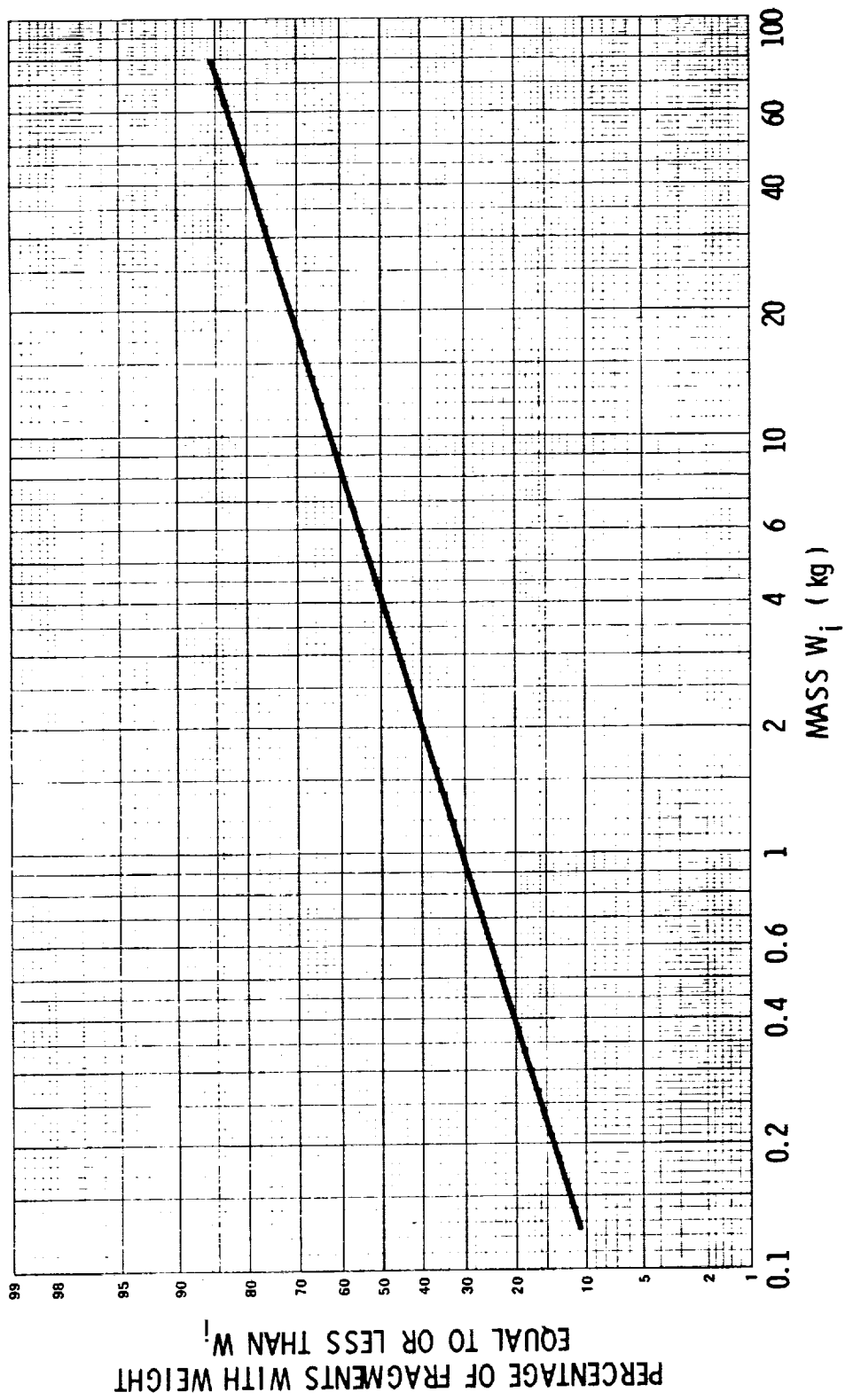


FIGURE 4-9. FRAGMENT MASS DISTRIBUTION FOR EVENT GROUP 6 (EVENT 25)

The correlation coefficient,  $r$ , for the regression equation shown on Figure 4-10 was 0.9999, which indicates a high degree of correlation between  $\bar{P}V/E_0$  and  $\bar{W}$ .

Correlation Between Fragment Range and Fragment Mass Within Event Groups

Only three event groups (2, 3 and 6) contained sufficient fragment range and mass data for correlation analysis. Various curve fitting techniques were employed to determine if a predictable relationship existed between fragment range and mass as indicated by the data on the three events. Appendix H-4 contains a description of the techniques and the results.

Figure 4-11 depicts the relationship of the fragment range to fragment mass for Group 2. The correlation coefficient is 0.79.

Figure 4-12 shows the relationship of the fragment range to fragment mass for Group 6. The correlation coefficient is 0.68.

Correlation of Fragment Range to the Ratio of Mean Fragment Weight to Vessel Weight for Cylindrical Tanks

Five events contained sufficient information for this type of analysis. Data for each of the events are contained in Appendix H-5. Figure 4-13 is a plot of the mean (arithmetic) fragment weight versus the ratio of mean fragment weight to the vessel weight for the events.

From Figure 4-13, one could estimate the mean fragment range for any decided ratio of mean fragment weight to vessel weight for the types of tanks in the events.

Correlation of Fragment Velocity to the Ratio of Energy to Vessel Weight

Only in event group 5 were there reports of mean velocity for fragments. Figure 4-14 is a plot of the relationship between the mean fragment velocity and the ratio of the energy to vessel weight. The velocities were chosen as the maximum velocity reported within an event for events 21, 22 and 23 (see Table 4-4). The correlation coefficient for the regression equation is 0.93.

One could use Figure 4-14 to predict the average velocity for fragments from bursting steel spheres over a range of an energy to vessel weight ratio of  $4.5 \times 10^7$  to  $6.05 \times 10^7$ . However, the analytic predictions for fragment velocity presented earlier in this chapter are more useful because they cover a much wider range of bursting vessel conditions.

TABLE 4-4. PARAMETERS OF BURSTING SPHERES

Event	Shot No.	Fragment Mass, Kg	Fragment Average Velocity, (m/s)	Burst Pressure, Pa	Volume, V (m <sup>3</sup> )	Vessel Weight WT, (kg)	Energy, J	Average (1) Fragment Weight, W, kg	(2) $\frac{E_V}{E_0}$
21	1	22.49 23.77	96.9	1.044X10 <sup>8</sup>	.0283	46.26	2.438X10 <sup>9</sup>	23.14	693.43
	2	22.36 23.90	98.6	1.030X10 <sup>8</sup>	.0283	46.46			
22	6	23.18 23.18		1.006X10 <sup>8</sup>	.0283	46.26			
	3	69.18 66.90	107.59	2.372X10 <sup>8</sup>	.0283	136.08	6.078X10 <sup>9</sup>	55.69	1541.6
23	7	48.99 42.41	83.52	2.193X10 <sup>8</sup>	.0283	136.08			
	4	117.03 70.03	65.84	3.475X10 <sup>8</sup>	.0283	187.33	1.133X10 <sup>10</sup>	89.75	2347.1
	5	122.92 64.41	71.63	3.475X10 <sup>8</sup>	.0283	187.33			

(1) Geometric mean fragment mass

(2)  $\bar{P}$  = Average burst pressure $E_0$  = Energy of detonation of 1 g TNTORIGINAL PAGE IS  
OF POOR QUALITY

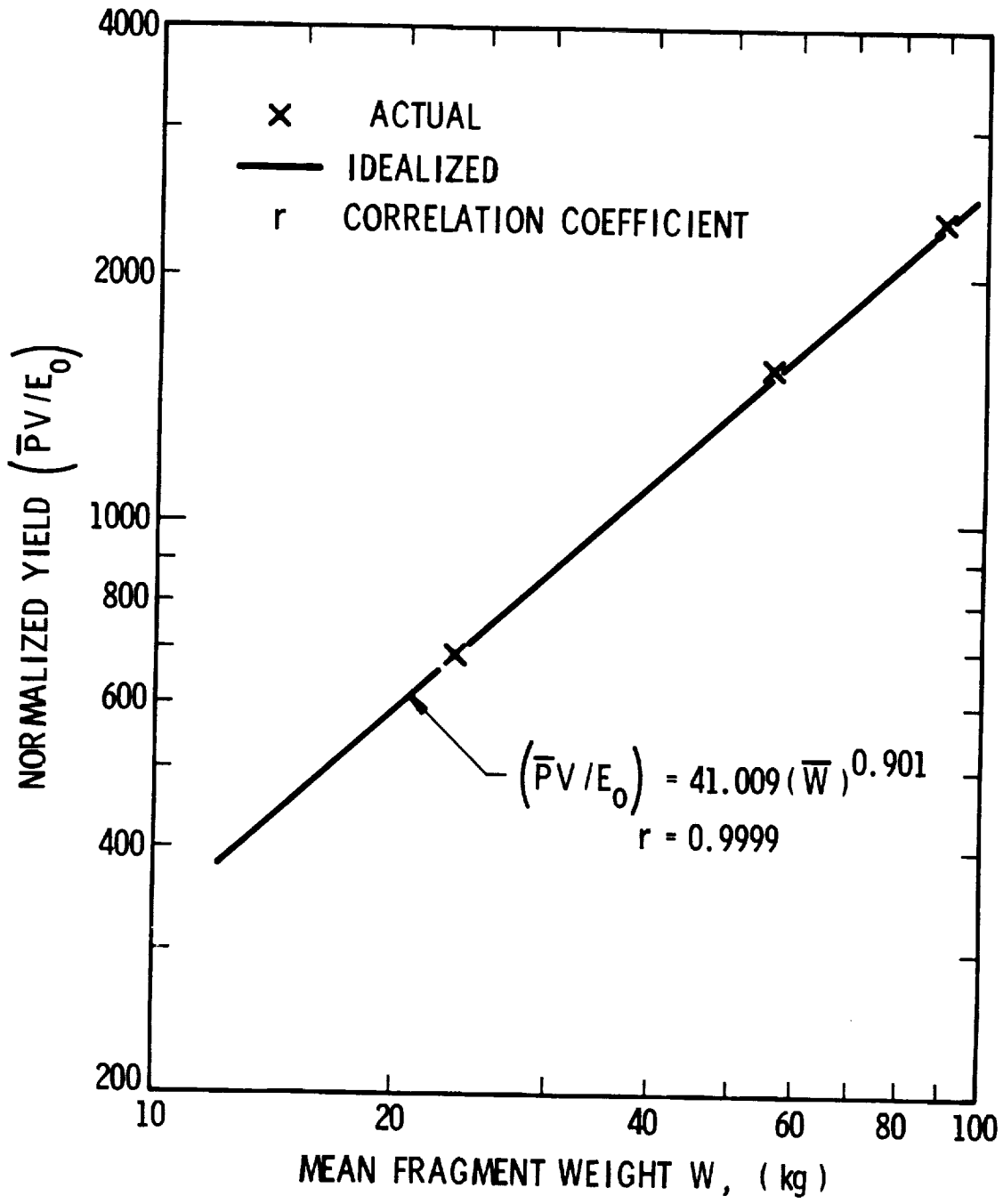


FIGURE 4-10. NORMALIZED YIELD VERSUS MEAN FRAGMENT WEIGHT FOR BURSTING SPHERES



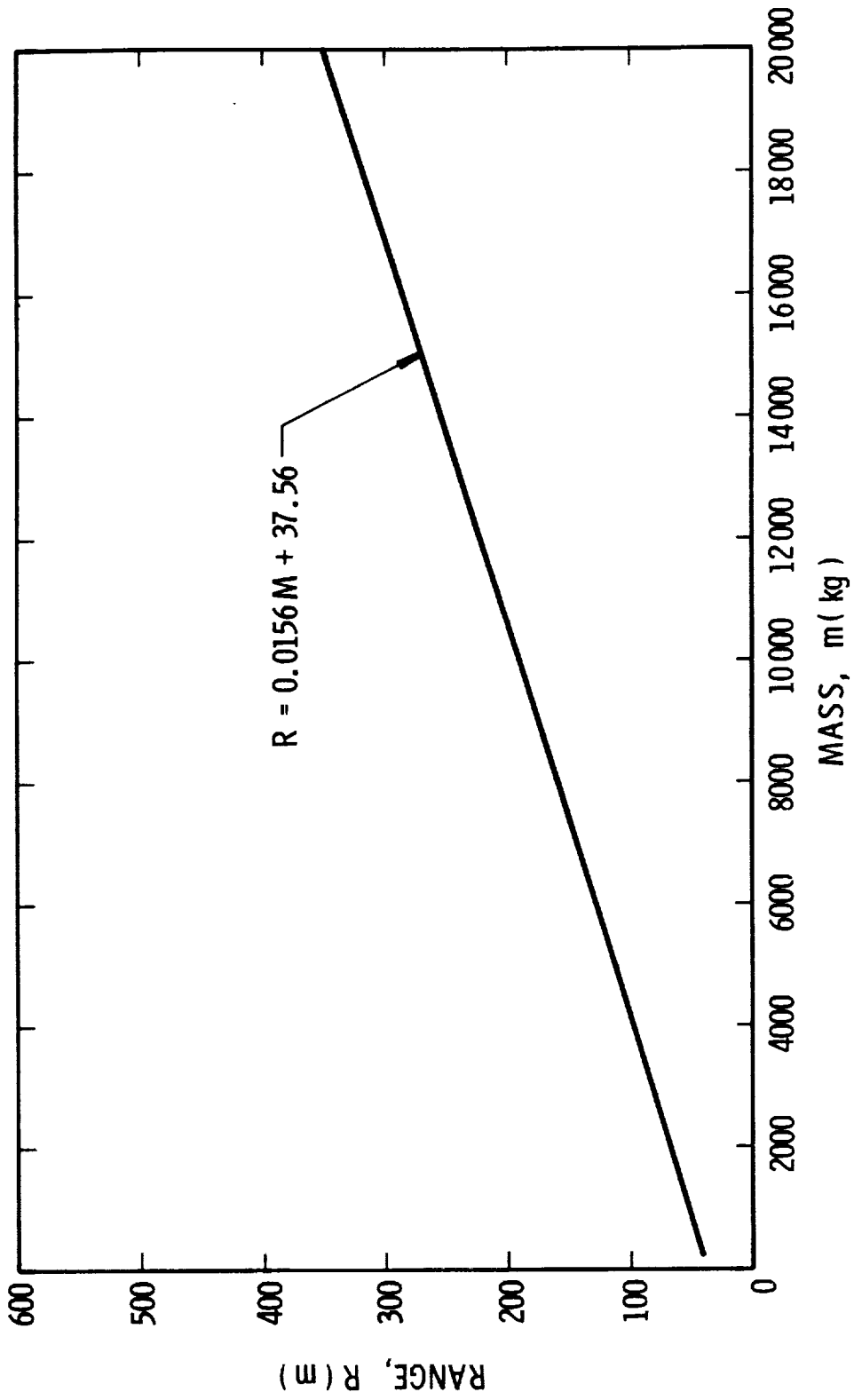


FIGURE 4-11. FRAGMENT RANGE VERSUS FRAGMENT MASS FOR EVENT GROUP 2

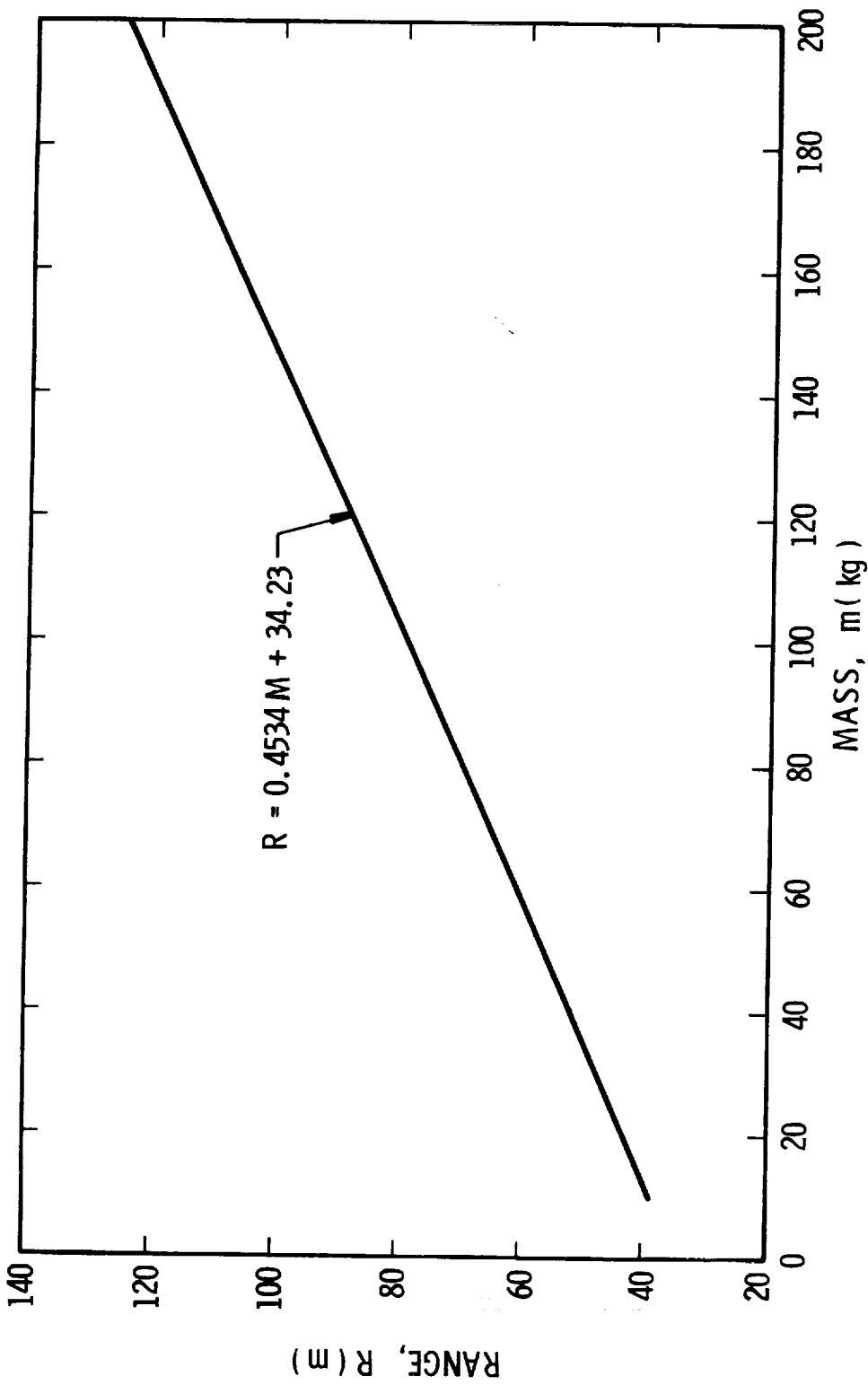


FIGURE 4-12. FRAGMENT RANGE VERSUS FRAGMENT MASS FOR EVENT GROUP 6

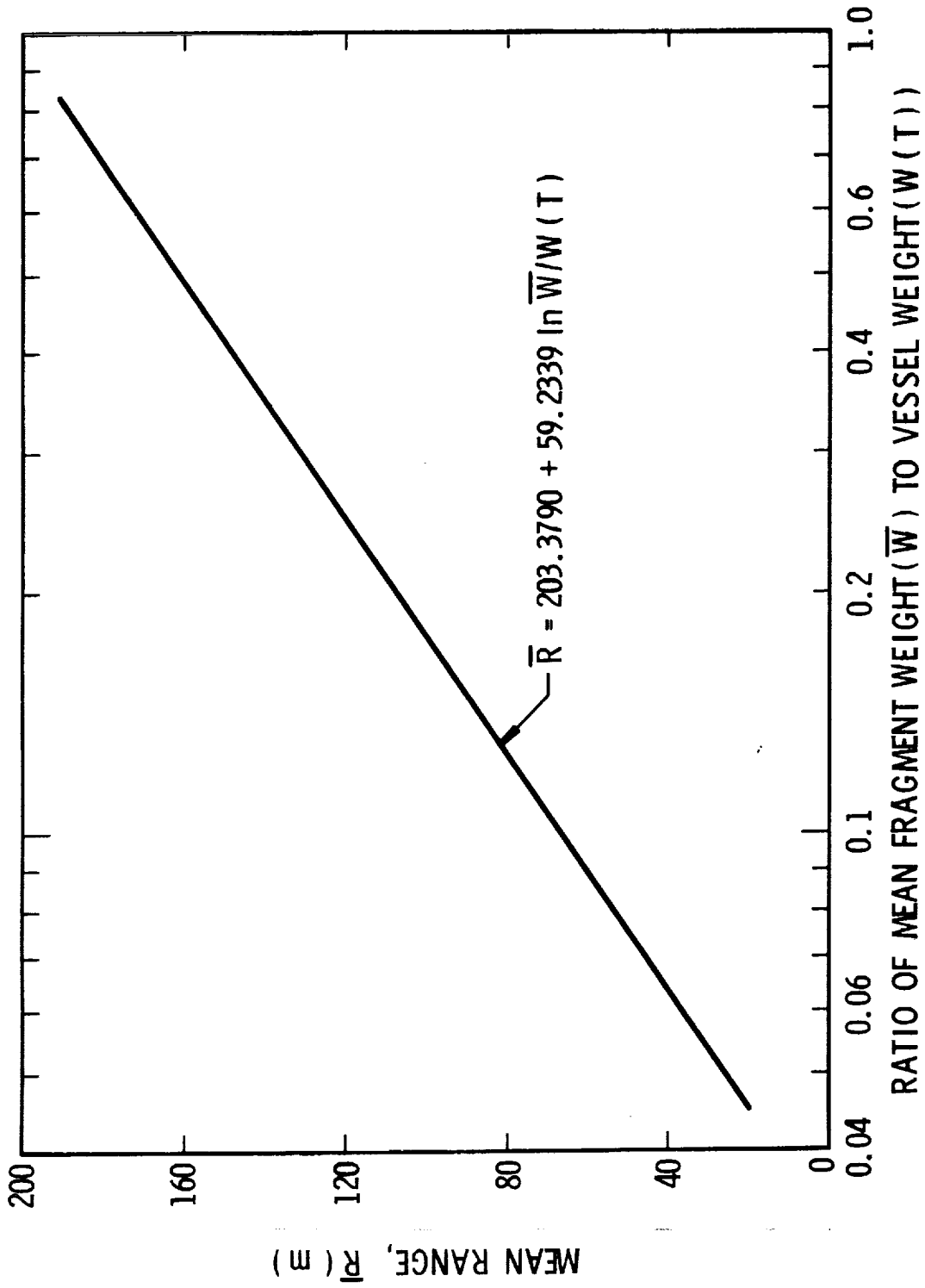


FIGURE 4-13. RANGE VERSUS THE RATIO OF MEAN FRAGMENT WEIGHT TO TANK WEIGHT FOR CYLINDRICAL VESSELS

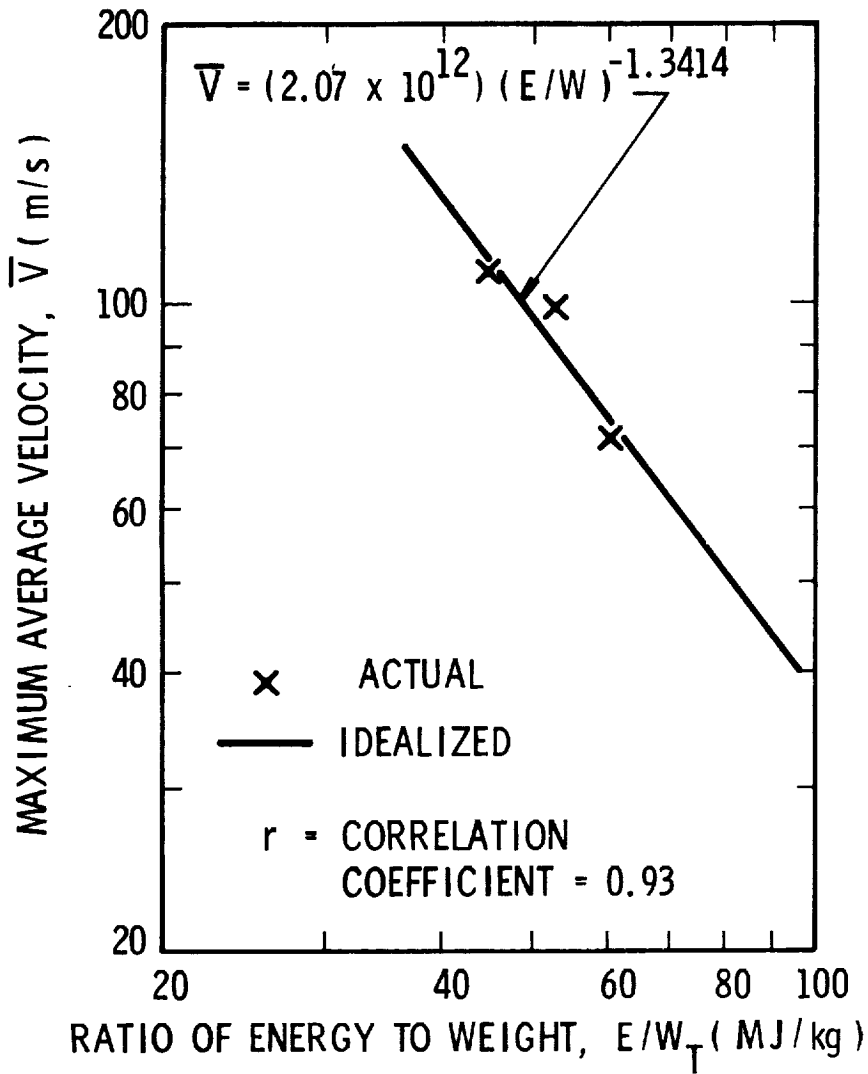


FIGURE 4-14. MAXIMUM MEAN VELOCITY VERSUS RATIO OF ENERGY TO VESSEL WEIGHT FOR BURSTING SPHERES



LIST OF REFERENCES

1. Baker, W. E., Kulesz, J. J., Ricker, R. E., Bessey, R. L., Westine, P. S., Parr, V. B. and Oldham, G. A. (1975), "Workbook for Predicting Pressure Wave and Fragment Effects of Exploding Propellant Tanks and Gas Storage Vessels", NASA CR-134906, Contract NASA-19231, November 1975 (reprinted September 1977).
2. Taylor, D. B. and Price, C. F. (1971), "Velocities of Fragments From Bursting Gas Reservoirs", ASME Transactions, Journal of Engineering for Industry, November 1971.



C-2

CHAPTER V

EFFECTS OF FRAGMENTS AND RELATED TOPICS

5-1 General

In Chapter V of Baker, et al (1975), some methods were given for prediction of effects of impact of typical fragments from accidental explosions involving flight-weight hardware. For the even more massive fragments typical of explosions in ground systems, the voluminous literature on terminal effects of military fragments and projectiles is of very little use. But, since the earlier workbook was prepared, some data and prediction methods have been developed related to impact effects of tornado-borne missiles. Generally, this class of missile lies within the range of masses and velocities shown in Chapter IV for fragments from explosions in ground systems. Wooden poles and planks, pipes, pieces of steel reinforcing bar, and more massive bodies such as compact cars and entire storage tanks have been picked up and hurled at damaging velocities by tornadoes. Much of this work is summarized in Peterson (1976), and has its impetus in tornado-proof design requirements for nuclear plants.

Similarly, new nuclear plants must now be designed to be proof against other accidents including crash of aircraft on the containment structures, and external vapor-cloud explosions. Some preliminary design methods have evolved for massive, non-penetrating missile impacts to meet the aircraft crash design requirements. Typical of recent literature references to this problem are Drittler and Gruner (1976 a and b) Hammel (1976), and Degen, et al (1976). But in spite of these recent additions to the literature, we feel that impact effects of quite massive, but crushable, missiles are not well enough known to be reduced to design graphs in this workbook.

In Baker, et al (1975), methods were given to predict velocities of fragments and objects located near accidental explosions (appurtenances). In preparing this workbook, we were asked to consider modifying these procedures to account for the two-dimensional character of some accident blast waves. Although we have generated some graphs for the prediction of two-dimensional blast wave properties in Chapter II, these are not extensive enough to allow modification of the previous procedures. We suggest that at present the reader simply use the procedures in the previous workbook.

In certain fixed ground installations having a high potential for accidental explosion, or limited real estate, barricades may be built in an attempt to attenuate blast waves and to reduce fragment hazards. The barricades may be earth berms, retaining



walls backed by earth fill, or built-up walls of reinforced concrete, timber, or steel construction. Unless structures to be protected are located very close to the barricades, they are almost totally ineffective in attenuating blast waves. The waves simply diffract over the barricades and reform. Barricades are, however, quite effective in arresting fragments and may be worth constructing for that purpose alone. We will give some prediction graphs for blast attenuation for barricades of several forms located close to protected structures. No data or proven prediction methods exist for effects of barricades on non-ideal blast waves, so the predictions will be limited to attenuations for condensed high explosives.

## 5-2 Penetration Effects of Massive Missiles

Some prediction methods of penetrating effects of massive missiles can be added to the methods in Baker, et al (1975). The "targets" for these missiles are primarily reinforced concrete or steel plate panels or walls.

### Concrete Panels

Concrete containment walls are very likely to be struck by fragments generated by an accidental explosion. Unfortunately, analytical prediction of penetration phenomena is in many ways more difficult for concrete than for homogeneous materials. This is due to the inhomogeneity of the panels and to the different construction techniques in use today--prestressing and post-tensioning, for example. In addition, since concrete targets are so expensive to fabricate, the amount of extant test data is limited.

Figure 5-1 shows schematically three different mechanisms of missile impact damage. At low velocities, the missile strikes the panel and rebounds without causing any local damage. As the velocity increases, pieces of concrete are spalled (ejected) off of the front or impacted face of the target. This spalling forms a spall crater that extends over a substantially greater area than the cross-sectional area of the striking missile. As the velocity continues to increase, the missile will penetrate the target to depths beyond the depth of the spall crater, forming a cylindrical penetration hole with a diameter only slightly greater than the missile diameter. As the penetration depth increases, the missile will stick to the concrete target rather than rebounding. At this stage the impact meets the criterion of a "plastic" impact. However, even at lesser penetration depths the impact can be approximately treated as a plastic impact when determining the energy absorbed by the impacted target. Further increases in velocity produce cracking of the concrete on the back surface followed by scabbing (ejection) of concrete from this rear surface. The zone of scabbing will generally be much wider, but not as deep as the front face spall crater. One scabbing begins, the



depth of penetration will increase rapidly. For low barrier thickness to missile diameter ratios (less than 5), the pieces of scabbed concrete can be large in size and have substantial velocities. As the missile velocity increases further, perforation of the target will occur as the penetration hole extends through to the scabbing crater. Still higher velocities will cause the missile to exit from the rear face of the target.

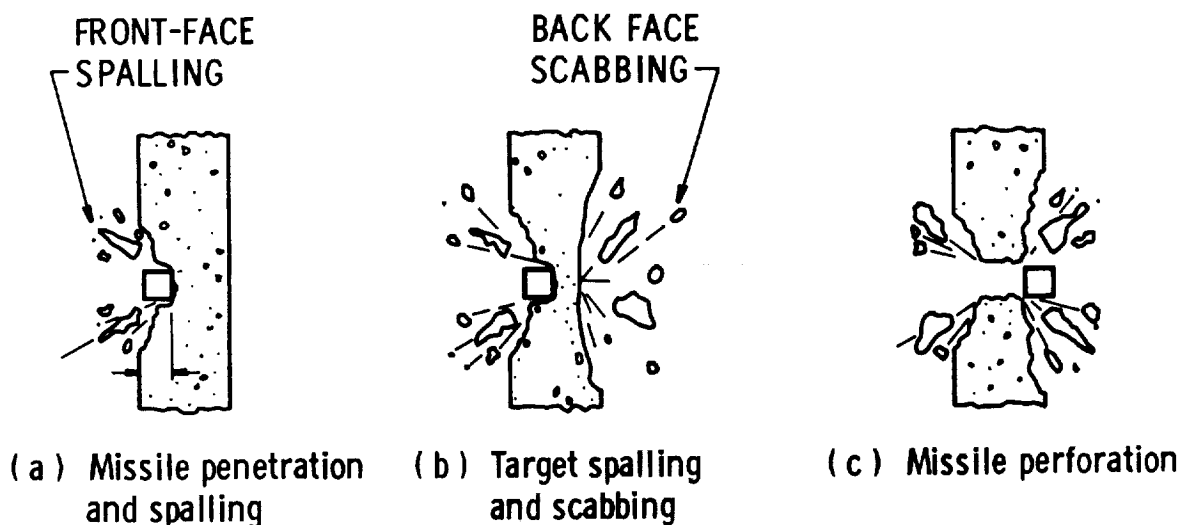


Figure 5-1. Missile Impact Damage [Kennedy (1976)]

Upon plastic impact, portions of the total kinetic energy of the impacting missile are converted to strain energy associated with deformability of the missile, and energy losses associated with target penetration. The remainder of the energy is absorbed or inputted to the impact target. This absorbed energy results in overall target response that includes flexural deformation of the target barrier and deformation of its supporting structure.

Currently depth of penetration, perforation and scabbing thickness are being predicted using one of several empirical formulas. These equations are based on experiments conducted prior to 1946 for concrete slabs perforated by projectiles and bombs. The most commonly used formulas are the modified Petry, Army Corps of Engineers, modified NRDC, the Amman and Whitney, and the BRL. [These formulas and their limitations and limits of applicability are summarized by Kennedy (1976)]. All of these formulas were derived for a nondeformable projectile (often made from armor-piercing steel) impacting normal to the target face.

In 1946 the National Defense Research Committee proposed a theory of penetration for a short, nondeforming projectile pene-

ORIGINAL PAGE IS  
OF POOR QUALITY



trating a massive concrete target which offered a good approximation of the experimental results. This theory of penetration enables one to not only calculate the total depth of penetration, but also to calculate the impact force-time history and penetration-depth time history. Based upon this theory of penetration, the National Defense Research Committee (NDRC) proposed that the penetration depth  $x$  be obtained from

$$G_{(x/d)} = KNd^{0.20} D (V_S/304.7)^{1.80} \quad (5-1)$$

where

$$G_{(x/d)} = \begin{cases} (x/2d)^2, & \text{for } x/d \leq 2.0 \\ [(x/d) - 1], & \text{for } x/d \geq 2.0 \end{cases} \quad (5-2)$$

and

- K = Concrete penetrability factor (measures the resistance of concrete to penetration) ( $m^{2.8}/kg$ ).
- N = Projectile nose shape factor: 0.72 for flat nose shapes, 0.84 for blunt bodies, 1.0 for average bullet nose, and 1.14 for very sharp nose.
- d = Projectile diameter (m). The equations presented herein are based entirely on cylindrical projectiles. For arbitrary shaped fragments, d is the diameter of an equivalent cylindrical projectile with the same contact surface area as the actual missile.
- D =  $M/d^3$  = caliber density of the projectile ( $kg/m^3$ )
- $V_S$  = Missile striking velocity (m/s).
- x = Total penetration depth (m); the depth a missile will penetrate into an infinitely thick target. This neglects all rear face boundary effects and therefore applies only when target thickness is sufficient to prevent scabbing at the rear face.

The primary advantage of this formula is that, since it is based on a theory of penetration, it can be extrapolated beyond the range of available test data with greater confidence than is true with the other equations. Unfortunately, because of the reduction of interest in projectile penetration of concrete after 1946, the NRDC effort was aborted before the factor K was completely defined.

According to the NDRC report, K should lie between 2 and 5 (in English units), depending upon the concrete strength, to fit the available test data. Based upon both theoretical and experi-



mental considerations, it was suggested in 1966 that the concrete penetrability factor  $K$  is proportional to the reciprocal of the ultimate concrete tensile strength, which in turn was taken to be proportional to the square root of the ultimate concrete compressive strength  $f'_c$ . By fitting this relationship to the experimental data available for the larger missile diameters, the following relationship for  $K$  was obtained:

$$K = 1.134 / (f'_c)^{1/2} \quad (\text{m}^{2.8} / \text{kg}) \quad (5-3)$$

The combination of Equations 5-2 and 5-3 is defined herein as the modified NDRC formula for penetration.

For slab thickness to projectile diameter ratios greater than three, Equation 5-1 can be used in conjunction with Equations 5-4 and 5-5 for predicting perforation and scabbing thicknesses.

$$e/d = 1.32 + 1.24 (x/d), \quad \text{for } (3 \leq e/d \leq 18) \quad (5-4)$$

$$s/d = 2.12 + 1.36 (x/d), \quad \text{for } (3 \leq s/d \leq 18) \quad (5-5)$$

where

$e$  = perforation thickness (m); the maximum thickness of concrete which will be completely penetrated by missile at a given velocity.

and

$s$  = scabbing thickness (m); thickness of a target required to prevent scabbing of material from the backface for a missile with a given velocity.

However, for many impact problems, the slab thickness to projectile diameter is substantially less than three. Beth (1945) gives a curved-fit extrapolation of these equations for slab thickness to projectile diameter ratios less than three so that the equation would pass through the origin. Parabolic fits which both pass through the origin and have the same slope as Equations 5-4 and 5-5 at a slab thickness to projectile diameter ratio of three have been proposed [Kennedy (1976)]. This parabolic fit leads to

$$\frac{e}{d} = 3.19 \left(\frac{x}{d}\right) - 0.718 \left(\frac{x}{d}\right)^2, \quad \text{for } x/d \leq 1.35, \quad (5-6)$$

$$\frac{s}{d} = 7.91 \left(\frac{x}{d}\right) - 5.06 \left(\frac{x}{d}\right)^2, \quad \text{for } x/d \leq 0.65, \quad (5-7)$$



whereas for larger  $x/d$  ratios, Equations 5-4 and 5-5 are to be used. These modifications, when used together with Equations 5-2 and 5-3, are known as the modified NDRC formulae for perforation and scabbing. Their primary advantage over the other formulae is that they can be extrapolated to slab thickness to projectile diameter ratios less than three without leading to unreasonable results.

All of the formulas for concrete penetration are based on a limited range of parameter variation. Unless otherwise noted, these formulas are valid only for the following ranges:

$$\begin{aligned}
 t/d &\geq 3 \\
 d &\leq 0.4 \text{ m} \\
 5.5 \times 10^3 \text{ kg/m}^3 &\leq D \leq 2.20 \times 10^4 \text{ kg/m}^3 \\
 500 \text{ m/s} &\leq V \leq 3000 \text{ m/s} \\
 3 &\leq e/d \leq 18 \\
 3 &\leq s/d \leq 18
 \end{aligned}
 \tag{5-8}$$

For long rods impacting concrete panels, recent model and full-scale testing of simulated tornado-borne missiles also gives prediction methods for scabbing thresholds for reinforced concrete panels. Sources for the basic data are discussed, and the curves generated, by Baker, Hokanson, et al (1976).

Figure 5-2 gives scabbing thresholds for steel pipes impacting normally on lightly reinforced concrete panels, with rebar percentages  $< 1\%$ . In this figure,  $KE$  is impact kinetic energy,  $h$  is concrete panel thickness,  $d$  is pipe outside diameter, and  $t_w$  is pipe wall thickness. Length-to-diameter ratios are variable, but all are greater than 5:1. Each curve gives the scabbing threshold for a particular wall thickness ratio.

Curves for scabbing caused by normal impact of solid rods, of material strong compared to the concrete, are given in Figure 5-3. The thresholds are quite different for slabs which are reinforced heavily enough for the rebar spacing to be significantly closer than the rod diameter (heavy reinforcing) and for spacing open enough that a rod can pass through without striking a rebar (light reinforcing). Rods were of  $l/d$  ratios ranging from 1.75-40. A number of long wooden missiles were also fired against reinforced concrete panels, but these missiles were invariably defeated by the panels, with negligible damage to the panels themselves.



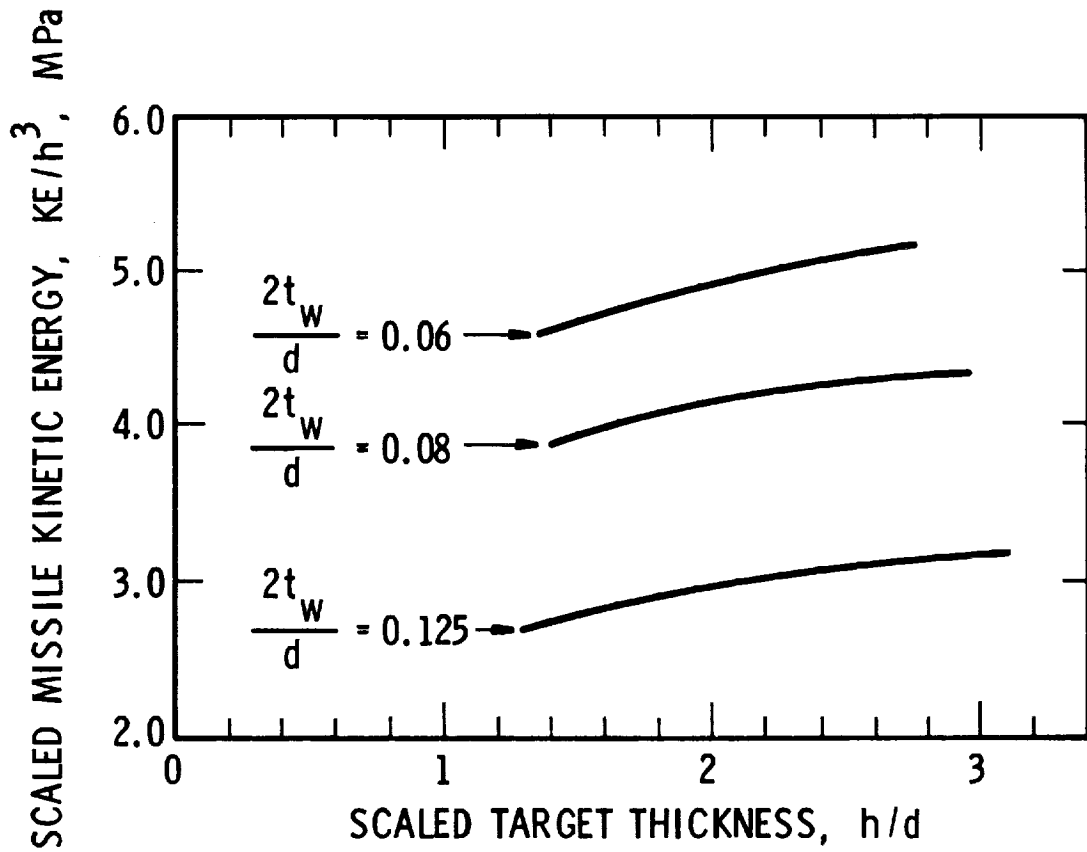


FIGURE 5-2. SCABBING THRESHOLD FOR MILD STEEL PIPES IMPACTING REINFORCED CONCRETE PANELS



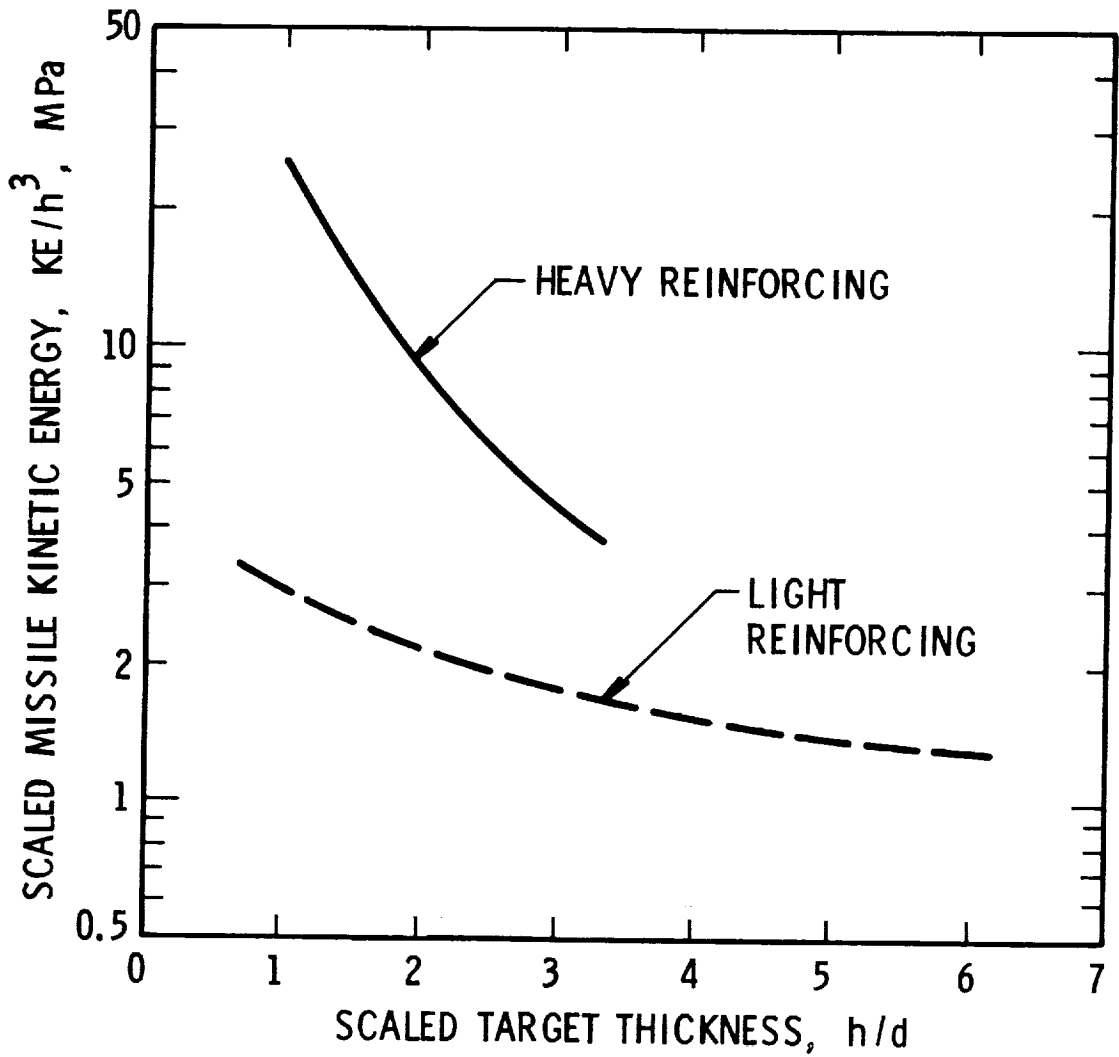


FIGURE 5-3. SCABBING THRESHOLDS FOR SOLID ROD MISSILES IMPACTING REINFORCED CONCRETE PANELS





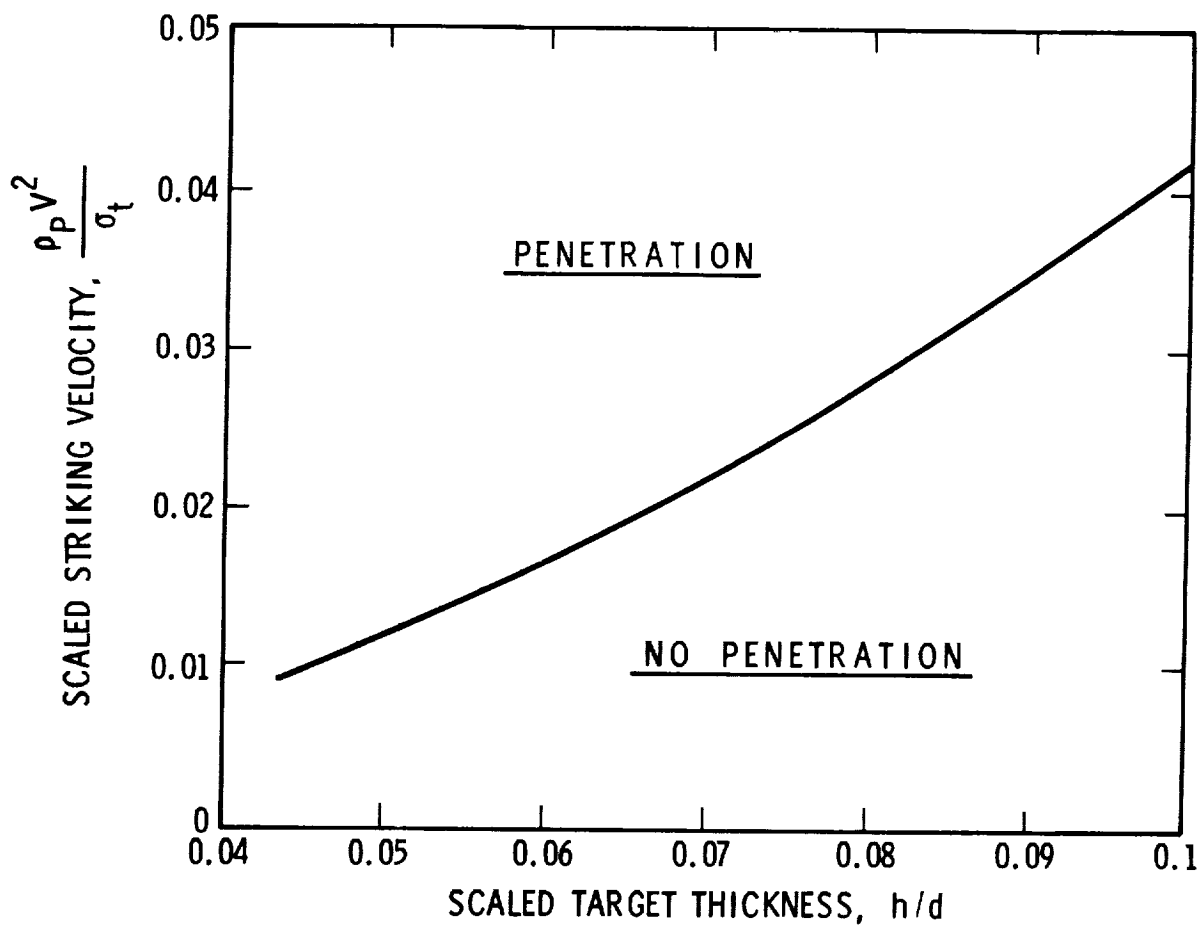


FIGURE 5-4. PREDICTION OF PENETRATION THRESHOLD FOR STEEL PANELS IMPACTED BY WOODEN PROJECTILES WITH  $\ell/d = 31.1$



Step 4. Substitute in Equation (5-1) and calculate G.

$$G = 2.224 \times 10^{-4} \times 0.72 \times 0.075^{0.2} \times 1.896 \times 10^4 \left( \frac{600}{304.7} \right)^{1.8}$$

$$G = \underline{\underline{6.124}}$$

Step 5. Use Equation (5-2) to calculate penetration x. Assume that  $(x/2d) > 2.0$ . Then,  $(x/d) = 1 + G = 1 + 6.124 = 7.124$ .

$$x = 7.124 d = 7.124 \times 75 = \underline{\underline{534 \text{ mm}}} = \underline{\underline{0.534 \text{ m}}}$$

Step 6. Use Equation (5-4) to calculate e.

$$e = 75 \left[ 1.32 + 1.24 \times \frac{534}{75} \right] = \underline{\underline{762 \text{ mm}}} = \underline{\underline{0.762 \text{ m}}}$$

Step 7. Use Equation (5-5) to calculate s.

$$s = 75 \left[ 2.12 + 1.36 \times \frac{534}{75} \right] = \underline{\underline{886 \text{ mm}}} = \underline{\underline{0.886 \text{ m}}}$$

#### Example 2:

A steel rod of diameter  $d = 25 \text{ mm}$  with a mass  $M = 10 \text{ kg}$  impacts a heavily reinforced concrete wall which has a thickness  $h = 100 \text{ mm}$  with an impact velocity  $v = 60 \text{ m/s}$ . Will the wall scab?

Step 1. Calculate impact kinetic energy.

$$KE = \left( \frac{1}{2} \right) MV^2 = \frac{1}{2} \times 10 \times 60^2 = 18 \text{ kJ}$$

Step 2. Calculate scaled kinetic energy.

$$\frac{KE}{h^3} = \frac{18 \times 10^3}{0.1^3} = 18 \text{ MPa}$$

and scaled target thickness

$$\frac{h}{d} = \frac{100}{25} = 4$$

Step 3. Enter Figure 5-3, and plot intercept from Step 2. This lies well above the threshold curve for heavy reinforcing, so scabbing should occur.



Example 3:

A long steel pipe with  $d = 75$  mm,  $t_w = 3.0$  mm impacts a 100 mm reinforced concrete panel at 20 m/s. It has a mass of 10 kg. Will it cause scabbing?

Step 1. Calculate impact kinetic energy.

$$KE = \frac{1}{2} \times 10 \times 20^2 = 2 \text{ kJ}$$

Step 2. Calculate scaled kinetic energy, and scaled target thickness, scaled wall thickness

$$\frac{KE}{h^3} = \frac{2 \times 10^3}{0.1^3} = 2 \text{ MPa}$$

$$\frac{h}{d} = \frac{75}{100} = 0.750$$

$$\frac{2t_w}{d} = \frac{2 \times 3}{75} = 0.08$$

Step 3. Enter Figure 5-2. In this case, our intercept lies along the bottom line and somewhat to the left of the curves. We wish to compare to the middle curve, for which scaled wall thickness is 0.08. We cannot say unequivocally whether scabbing will or will not occur, because we are beyond the range of the fitted curves.

Example 4:

A wooden post is hurled against a steel curtain wall at 100 m/s. The post has a diameter  $d = 150$  mm, a length  $\ell = 4.5$  m, and a density  $\rho_p = 650$  kg/m<sup>3</sup>. The steel curtain wall is 6 mm thick and has a yield strength  $\sigma_t = 240$  MPa. Will the post penetrate?

Step 1. Calculate scaled quantities to enter Equation (5-9).

$$\frac{h}{d} = \frac{6}{150} = 0.04$$

$$\frac{\ell}{d} = \frac{4500}{150} = 30$$



Step 2. Calculate scaled striking velocity from Equation (5-9) for incipient penetration.

$$\frac{\rho_p V_s^2}{\sigma_t} = \frac{1.751 \times 0.040}{30} + \frac{144.2 \times 0.04^2}{30}$$

$$\frac{\rho_p V_s^2}{\sigma_t} = \underline{\underline{1.00 \times 10^{-2}}}$$

Step 3. Calculate scaled striking velocity from input parameters, and compare to threshold value.

$$\frac{\rho_p V_s^2}{\sigma_t} = \frac{650 \times 100^2}{240 \times 10^6} = \underline{\underline{2.71 \times 10^{-2}}}$$

This value is more than double the threshold for penetration, so the wood post goes through the steel curtain wall like a knife through hot butter.

### 5-3 Effects of Barricades on Blast Waves

Barricades are constructed either near potential explosion sources or near structures and facilities located in the vicinity of potential explosion sources. As noted earlier, they are intended as protective devices to arrest fragments or attenuate blast waves.

The two most common types of barricades are earthworks (mounds), and earthworks behind retaining walls (single-revetted barricades). The definitions of these types of barricades, taken from Department of Defense explosive safety regulations, follow:

Mound. An elevation of earth having a crest at least 3 feet wide, with the earth at the natural slope on each side and with such elevation that any straight line drawn from the top of the side wall of a magazine or operating building or the top of a stack containing explosives to any part of a magazine, operating building or stack to be protected will pass through the mound. The toe of the mound shall be located as near the magazine, operating building, or stack as practicable.

Single-Revettted Barricade. A mound which has been modified by a retaining wall, preferably of concrete, of such slope and thickness as to hold firmly in place the 3-foot width of earth required for the top, with



the earth at the natural angle on one side. All other requirements of a mound shall be applicable to the single-revetted barricades.

Most of the useful data on attenuation of blast effects behind barricades appear in a single reference, Wenzel and Bessey (1969). Scaled tests for both mound and single-revetted barricades, with spherical Pentolite explosion sources generating the blast waves, were conducted for the explosion sources near the barricades (near field) and near the protected structure (far field). Specific configurations tested are shown in Figure 5-5. All explosive spheres were located at scaled height  $\bar{H} = 0.036$  above an armor plate reflecting surface to eliminate cratering effects, at the scaled distances  $\bar{R}$  shown in Figure 5-5.\* The barricade dimensions were scaled to represent full-size barricades with heights  $h$  of about 3 m and 6 m.

The principal conclusions reached by Wenzel and Bessey (1969) as a result of their tests were:

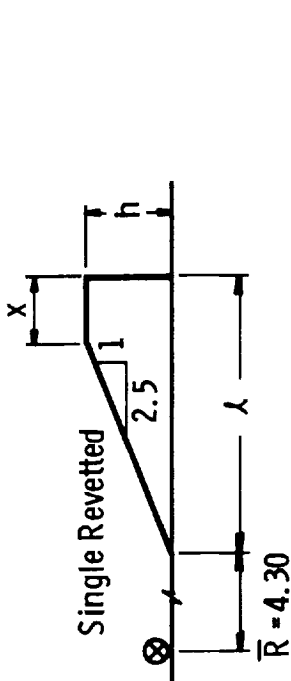
- 1) Barricades do reduce the peak pressures and impulses immediately behind the barricades.
- 2) Single-revetted barricades are more efficient in reducing peak pressures and impulses than mound barricades.
- 3) Values of peak pressure and impulse are greatly influenced by the gage height relative to the ground, the location of the barricade, and the barricade dimensions and configurations.
- 4) In the near field case for single-revetted barricade configurations, a significant reduction of pressure and impulse was observed out to scaled distances of  $\bar{R} = 1$ . Beyond that distance, the peak pressures tend to approach those of the free field case very rapidly, and the impulses also tend to approach those of the free field case but not as rapidly as the peak pressures. The times of arrival in specific locations are greater than those of the free field case up to scaled distances of  $\bar{R} = 1.6$ . At scaled distances greater than  $\bar{R} = 1.6$  they approach rapidly those of the free field case.

---

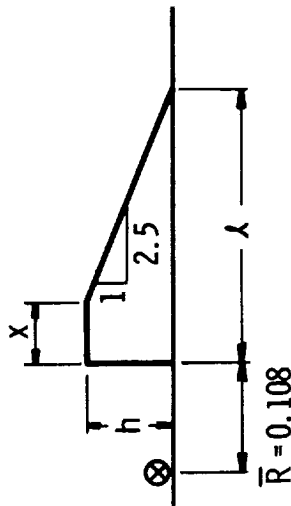
\* Definitions for scaled distance are given in Chapter II.



Barricade in far field



Barricade in near field



⊗ - Location of energy source

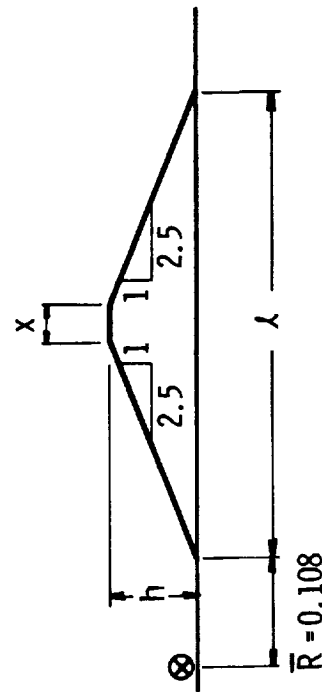
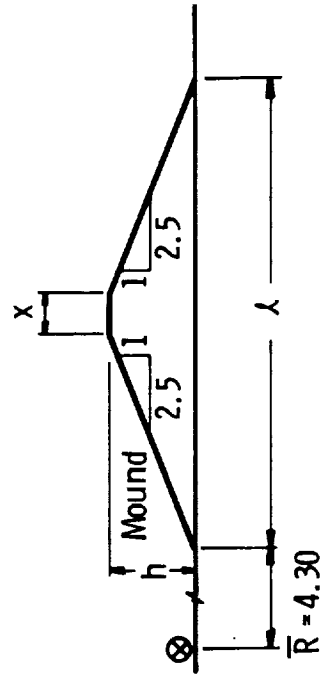


FIGURE 5-5. BARRICADE CONFIGURATIONS STUDIED BY WENZEL & BESSEY (1969)

- 5) In the near field case, mound configuration, the peak pressures and impulses are not greatly reduced, and actually are increased over the free field case at a scaled gage height of  $\bar{H}_g = 0.02$  and a scaled distance of  $\bar{R} = 0.43$ . However, the pressure and impulse observed at the scaled gage height of  $\bar{H}_g = 0.05$  at  $\bar{R} = 0.32$  are both less than the free field values. There was a considerable decrease in pressure and impulse for the gage located at  $\bar{R} = 4.84$  and scaled height of  $\bar{H}_g = 0.016$ , respectively. The times of arrival were the same as those observed in the free field case for all scaled distances and scaled heights.
- 6) For the far field case, single-revetted barricade configuration, the peak pressures and impulses were significantly reduced immediately behind the barricade; however, their individual values varied as a function of gage height. The times of shock arrival were the same as those observed in the free field case for all stations measured.
- 7) For the far field case, mound configuration, the same observations as those made for the single-revetted case can be made here except that the effect of the barricades is considerably less than for the single-revetted configurations.

The blast attenuation caused by mound barricades, although measurable in the experiments cited above, is small enough to be essentially negligible, for the purposes of this workbook. Similarly, the attenuation for single-revetted barricades in the far-field case is so localized and directional that no general predictions can be made. But, for the single-revetted barricades in the near field, we can give scaled curves for blast wave properties which are attenuated from surface burst explosion waves without barricades. Figure 5-6 shows variation of scaled side-on overpressure  $\bar{P}_s$  with scaled distance  $\bar{R}$  for this configuration, for surface burst explosive charges without barricade and with single-revetted barricade. Similarly Figure 5-7 gives variation of scaled side-on pressures  $\bar{I}_s$  versus  $\bar{R}$  for this situation.

These curves should only be used to predict blast attenuations over the ranges of scaled distances shown, i.e.,  $0.35 < \bar{R} < 9.0$ . They should also be applied with caution for blast sources other than condensed explosives because there are no extant data for effects of barricades on the non-ideal blast waves from accidental explosions. Data scatter for the peak overpressure curves is about  $\pm 5\%$ , and for the impulse curves, about  $\pm 10\%$ .







### Example Problem

A single-revetted barricade is located close to a propellant storage source with potential blast energy  $E = 1000\text{MJ}$ , calculated by methods given in Chapter I. If the source explodes, what are the incident blast wave parameters at a distance of 100 m? The site is located near sea level, with  $p_0 = 1.01 \times 10^5 \text{ Pa}$  and  $a_0 = 340 \text{ m/s}$ .

Step 1. Calculate scaled distance  $\bar{R}$ . It is defined as (see Chapter II).

$$\bar{R} = R p_0^{1/3} / E^{1/3}$$
$$\bar{R} = \frac{100 \times (1.01 \times 10^5)^{1/3}}{(10^9)^{1/3}} = \underline{\underline{4.66}}$$

Step 2. Enter Figures 5-6 and 5-7 to obtain scaled overpressure and impulse. From dashed curves,

$$\bar{P}_s = 0.070, \bar{I}_s = 0.0087$$

Step 3. "Unscale" to obtain blast parameters.

$$P_s = \bar{P}_s \times p_0 = 0.070 \times 1.01 \times 10^5 = \underline{\underline{7.07 \text{ kPa}}}$$
$$I_s = \frac{\bar{I}_s \times p_0^{2/3} \times E^{1/3}}{a_0} = \frac{0.0087 \times (1.01 \times 10^5)^{2/3} \times (10^9)^{1/3}}{340}$$
$$I_s = \underline{\underline{55.5 \text{ Pa}\cdot\text{s}}}$$



REFERENCES, CHAPTER V

1. Baker, W. E., Hokanson, J. C. and Cervantes, R. A., (1976) "Model Tests of Industrial Missiles", Final Report, SwRI Project No. 02-9153-001, Southwest Research Institute, San Antonio, Texas, May 1976.
2. Baker, W. E., Kulesz, J. J., Ricker, R. E., Bessey, R. L., Westine, P. S., Parr, V. B., and Oldham, G. A., (1975) "Workbook for Predicting Pressure Wave and Fragment Effects of Exploding Propellant Tanks and Gas Storage Vessels", NASA CR-134906, Contract NAS3-19231, November 1975 (reprinted 1977).
3. Beth, R. A. , (1945) "Concrete Penetration", OSRD-4856, National Defense Research Committee Report, A-319, March 1945.
4. Degen, P., Furrer, H., and Jemielewski, J., (1976) "Structural Analysis and Design of a Nuclear Power Plant Building for Aircraft Crash Effects", Nuclear Engineering and Design, 37, 1976, pp. 249-268.
5. Drittler, K. and Gruner, P., (1976a) "Calculations of the Total Force Acting Upon a Rigid Wall by Projectiles", Nuclear Engineering and Design, 37, 1976, pp. 231-244.
6. Drittler, K. and Gruner, P., (1976b) "The Force Resulting from Impact of Fast-Flying Military Aircraft Upon a Rigid Wall", Nuclear Engineering and Design, 37, 1976, pp. 245-248.
7. Hammel, J., (1976) "Aircraft Impact on a Spherical Shell", Nuclear Engineering and Design, 37, 1976, pp. 205-223.
8. Kennedy, R. P., (1976) "A Review of Procedures for the Analysis of Design of Concrete Structures to Resist Missile Impact Effects", Nuclear Engineering and Design, 37, 1976, p. 183-203.
9. Peterson, R. E., Editor, (1976), Proceedings of the Symposium on Tornadoes. Assessment of Knowledge and Implications for Man, Texas Technological University, Lubbock, Texas, June 22-24, 1976.
10. Wenzel, A. B. and Bessey, R. L., (1969) "Barricaded and Unbarricaded Blast Measurements", Final Report Contract No. DAHC04-69-C-0028, Subcontract 1-OU-431, Southwest Research Institute, San Antonio, Texas, October 1969.



## CHAPTER VI

### DISCUSSION AND RECOMMENDATIONS

We believe that this workbook should be a definite aid to designers and safety engineers in predicting damage and hazards from accidental explosions in ground handling systems. It should prove to be a useful adjunct to our earlier workbook for predicting explosion hazards in flight systems, NASA CR-134906. For the convenience of the reader, microfiche copies of the earlier work are attached to each copy of this report.

Parts of this work should have wider application than indicated by the title. The additional methods for rapid structural damage prediction can be used for any blast source, provided the peak overpressures and positive impulses can be predicted. The computer programs and methods for prediction of velocities and trajectories of lifting fragments and thrusting burst vessels can be effectively applied to transportation accidents with tank cars and tank trucks containing many types of pressurized fluids, in addition to rocket propellants. The methods for estimating explosive energy release for flash-evaporating fluids can be used to predict severity of boiler explosions, or severity of blast for any type of liquid and gas mixture stored under high pressure. The data and prediction methods for effects of impact of massive fragments or missiles are not limited to fragments generated by accidental explosions in ground handling systems, and indeed were taken from other related studies.

A number of prediction waves are given in this work for the characteristics of blast waves from bursting gas pressure vessels, and some for bursting vapor spheres. These waves exhibit some characteristics which are distinctly different from blasts from condensed explosives such as TNT, including pronounced negative phases and pronounced second shocks. Most structural response or damage analyses account only for pressures and impulses in the first positive phase, and we therefore recommend further study of responses to waves with characteristics such as in Figure 2-8. It would also be very desirable to conduct more scaled experiments with bursting, pressurized vessels, to generate additional blast prediction curves. These should probably include:

- 1) Tests with light gases such as helium.
- 2) Tests of bursting spheres filled with vapors of higher saturation pressure such as Freon-22, Freon-13, or sulfur hexafluoride ( $\text{SF}_6$ ) to better determine the effect of sphere pressure on the overpressures measured.





Looking into the future, we can perhaps anticipate an increasing shift to a hydrogen fuel economy. If this occurs, large volumes of hydrogen must be stored either as a compressed gas or as a cryogenic liquid near distribution points. As an aircraft fuel, the hydrogen would most probably be used as a cryogenic liquid, which would necessitate large volume storage near airports. Can this be done safely? A thorough safety study would have to precede any serious plans for such a change, with workbooks like this report providing part of the input to assess the hazards.



## APPENDIX A

### Calculations of Blast Wave Properties for Pressure Vessel Bursts

The method for predicting the overpressure and specific impulse from the burst of a thick-walled pressure vessel is the result of the following analysis.

TUTTI [Gentry, et al (1966)], a two dimensional finite difference computer program for compressible fluids, was used to calculate the axisymmetric flowfield surrounding a quadrant of a bursting pressure vessel. The geometry is shown in Figure A-1. During the calculation, the quadrant of the vessel moves along the axis of symmetry at a prescribed velocity. The velocity and position of the vessel are calculated by a computer program called FRAG [see Baker, et al (1975)]. These are supplied to TUTTI. (TUTTI was modified to allow a moving solid boundary.)

Six sets of initial conditions were used (Table A-1), with  $T_1/T_a = 1$  for all of them. The radius of the sphere is 0.19 m. Increments  $\Delta r = 0.0375$  m, and  $\Delta z = 0.0300$  m were chosen for the flowfield. The rather large  $\Delta r$  and  $\Delta z$  cause the shocks to be spread out, and some accuracy is lost, but this is necessary for economy.

$\bar{P}_s$  vs.  $\bar{R}$  is plotted for these computer runs in Figure A-2.  $\bar{I}$  vs.  $\bar{R}$  is plotted in Figure A-3.

Figure A-2 was used to derive the overpressure prediction method in the text. The point at the end of the dashed line is  $(\bar{P}_{s0}, \bar{R}_0)$ , where  $\bar{P}_{s0}^*$  is defined in the text and  $\bar{R}_0$  is  $\bar{R}$  corresponding to the edge of the sphere. The solid lines show the overpressure behavior after a shock has formed. On the dashed portion of the curves, a shock has not formed yet. Connecting the points of transition to a shock in Figure A-2 gives Curve A in Figure 2-5. It is observed that, for these bursts, the overpressure on curve A,  $\bar{P}_a$ , is related to  $\bar{P}_{s0}$  by  $\bar{P}_a \approx 0.21 \bar{P}_{s0}$ . This permits the location of a starting point for  $\bar{P}_s$  vs.  $\bar{R}$  behavior. A family of  $\bar{P}_s$  vs.  $\bar{R}$  curves has been drawn on Figure 2-5. Once the starting point has been found, the nearest curve(s) can be followed.

As was true for the one-dimensional study in Baker, et al (1975), the  $\bar{I}$  vs.  $\bar{R}$  behavior is not clear, and the pentolite curve

---

\* $\bar{P}_{s0}$  is calculated by assuming constant pressure across the contact surface between the stored gas and the atmosphere immediately after the vessel burst. See Baker, et al (1975).





TABLE A-1. INITIAL CONDITIONS FOR PRESSURE VESSEL BURSTS

Run Number	Gas	$\frac{P_1}{P_a}$	$\gamma_1$
1	air	987.2	1.4
2	H <sub>2</sub>	987.2	1.4
3	He	987.2	1.667
5	CO <sub>2</sub>	987.2	1.225
7	air	98.72	1.4
9	CO <sub>2</sub>	14.81	1.225

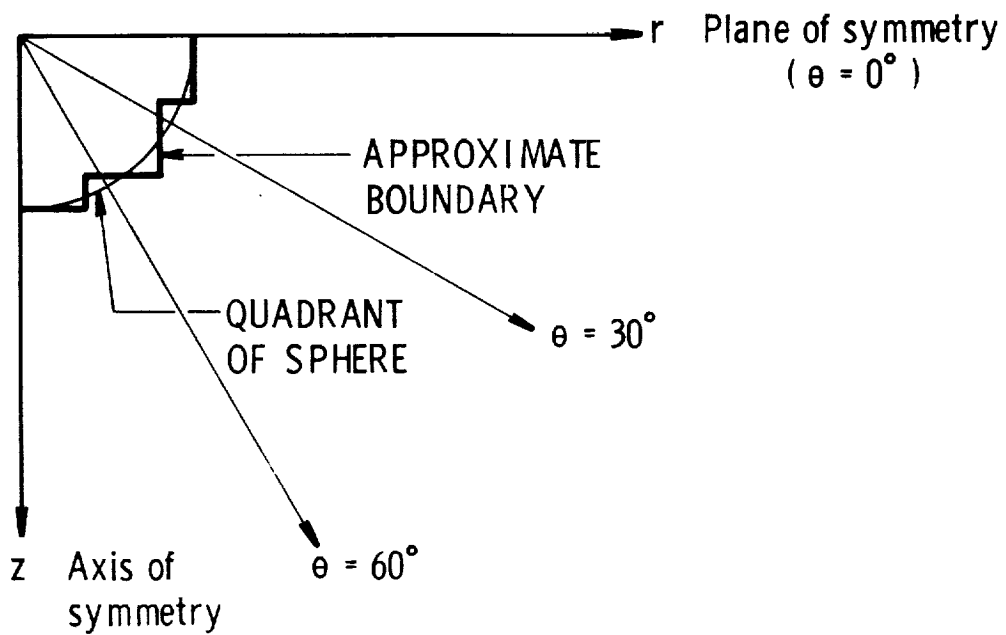


FIGURE A-1. QUADRANT OF FLOWFIELD FOR BURSTING PRESSURE VESSEL



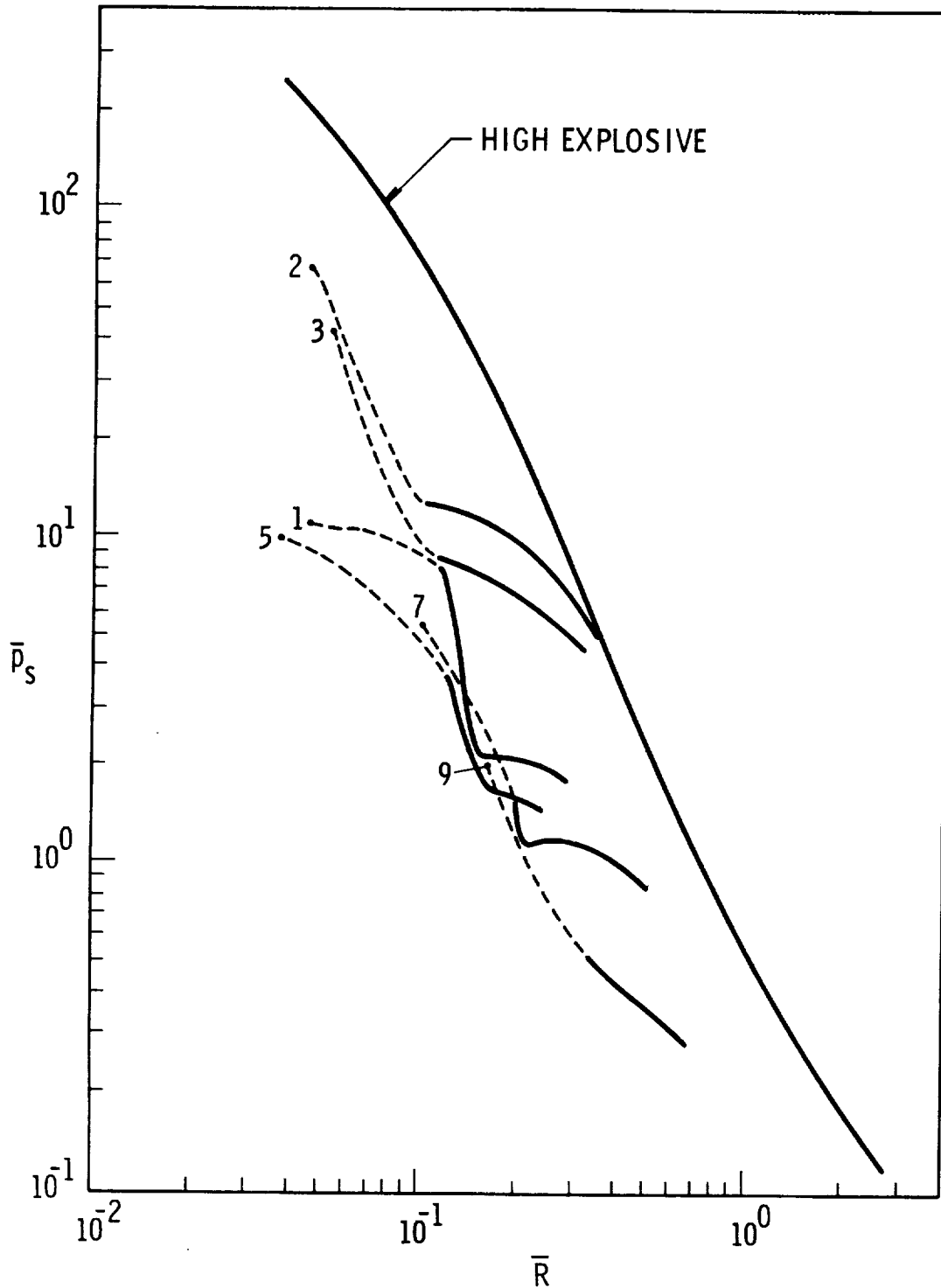


FIGURE A-2.  $\bar{p}_s$  VS  $\bar{R}$  FOR BURSTING PRESSURE VESSELS ALONG PLANE OF SYMMETRY



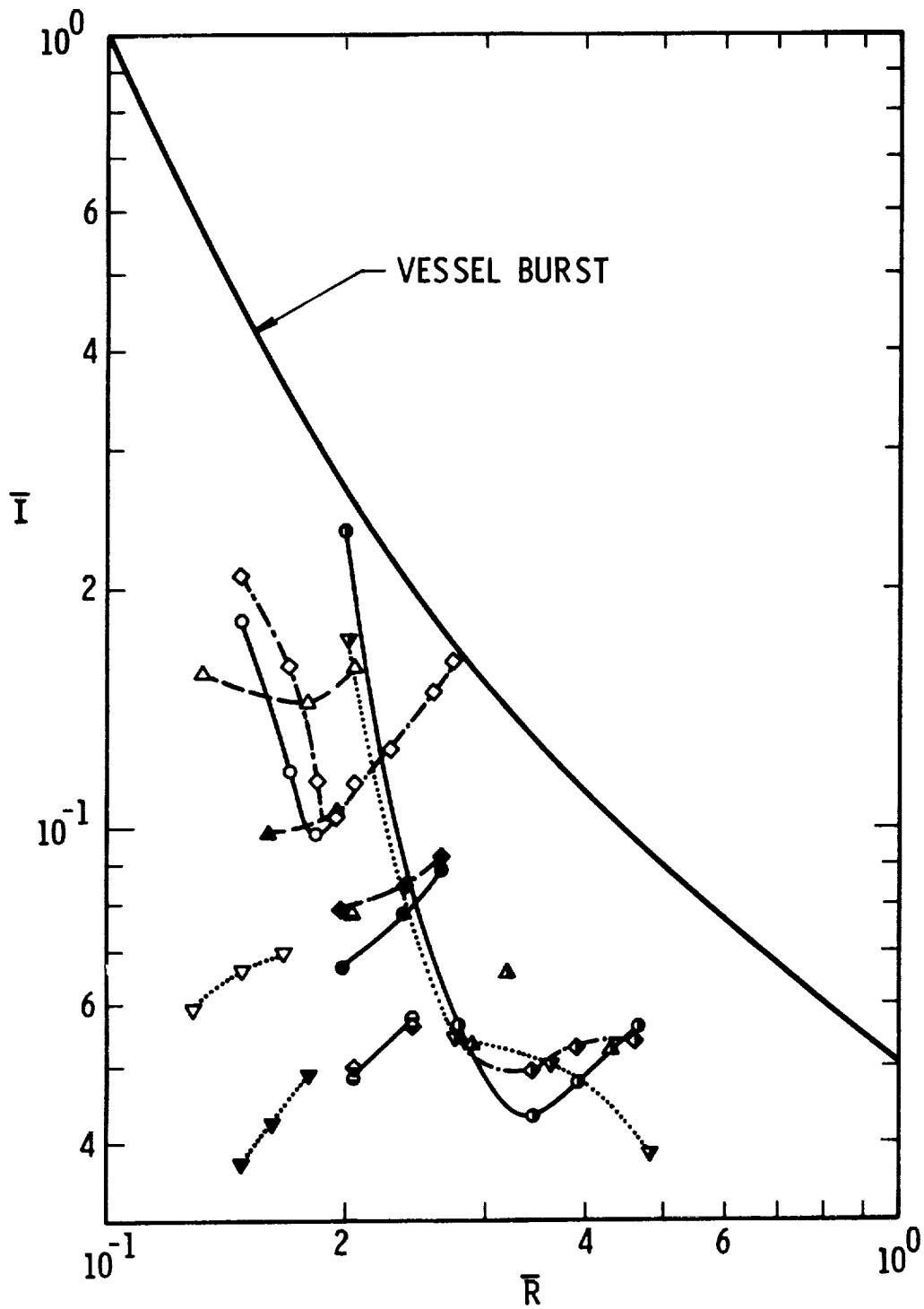


FIGURE A-3.  $\bar{I}$  VS  $\bar{R}$  FOR BURSTING PRESSURE VESSELS

ORIGINAL PAGE IS  
OF POOR QUALITY





LOCATION OF MTRL A AND INTERIOR WALLS.

PROBLEM NO. 2A BURSTING SPHERE 19CM RADIUS PRESSURE=10\*\*8PA  
 HYDROGEN

T= 1.084E-03 N= 126

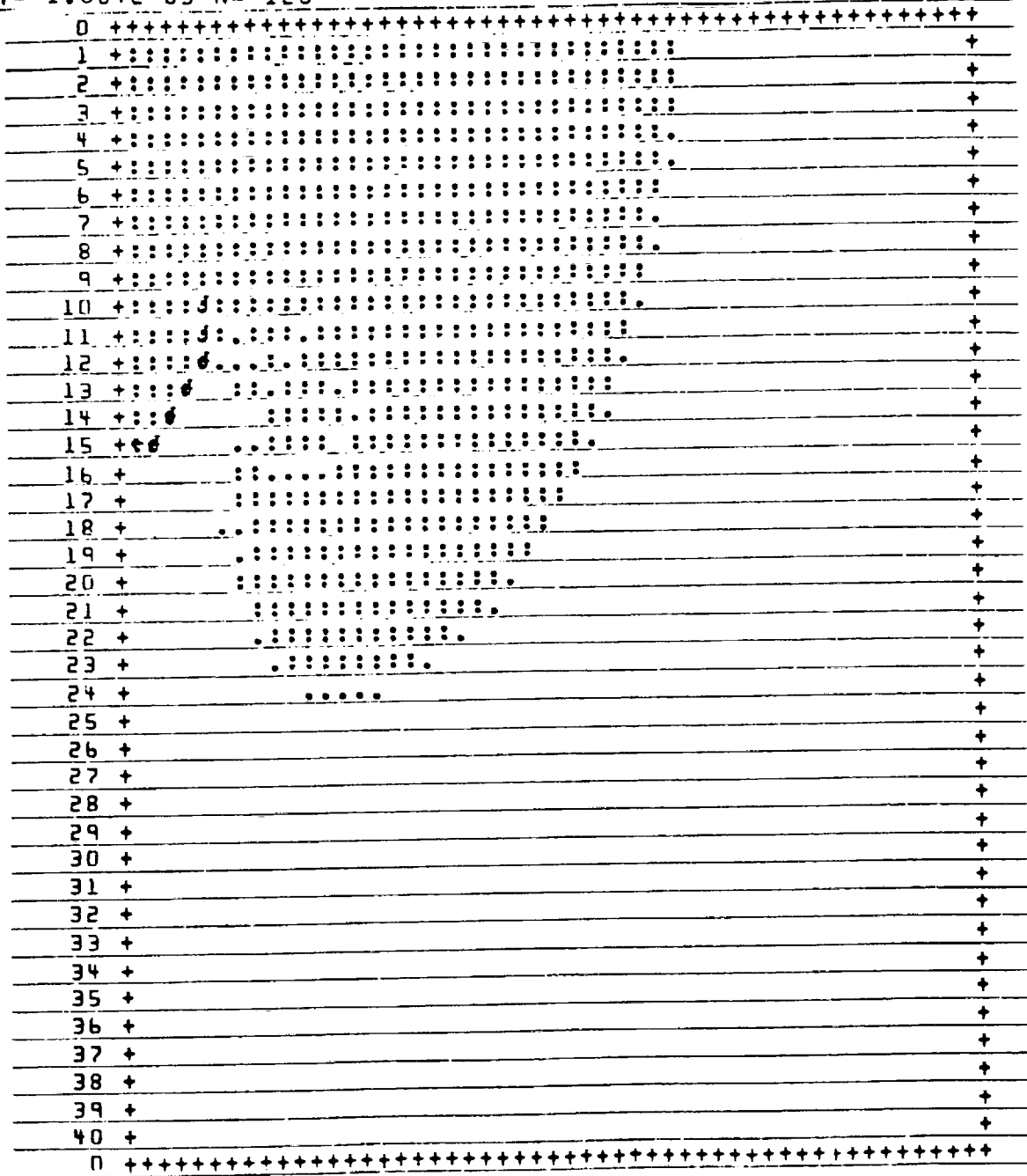
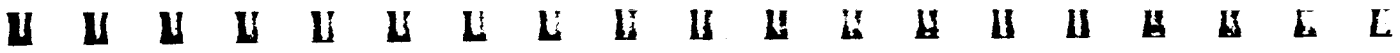


FIGURE A-5. SAMPLE PLOT FROM TUTTI FOR SPHERE BURSTING AS TWO HEMISPHERES



## APPENDIX B

### Development of Additional Prediction Methods for Structural Response to Blast Wave Loading

The elastic and elastic-plastic beam solutions which are presented in Figures 3-1 and 3-2 were derived using conservation of energy principles. To illustrate how these relationships can be derived, we will compute Figure 3-2 for an elastic, simply-supported beam. A deformed shape must be assumed in beam and plate like structures. Assuming a deformed shape which corresponds to the static deformed shape for a beam undergoing uniform loads gives:

$$Y = \frac{16}{5} w_o \left[ \frac{x}{\ell} - 2\left(\frac{x}{\ell}\right)^3 + \left(\frac{x}{\ell}\right)^4 \right] \quad (B-1)$$

This deformed shape is then differentiated twice with respect to  $x$  so that the elastic bending moment  $M$  can be obtained from  $M = -EI \frac{d^2 y}{dx^2}$ . This procedure gives for the bending moment

$$M = \frac{192}{5} \frac{EIw_o}{2} \left[ \left(\frac{w}{\ell}\right) - \left(\frac{w}{\ell}\right)^2 \right] \quad (B-2)$$

The strain energy S.E. stored in a deformed beam can then be determined by substitution into  $S. E. = \int_0^{\ell} \frac{M^2 dx}{2EI}$ . Substitution gives:

$$SE = \frac{(192)^2 EIw_o^2}{(50)\ell^4} \int_0^{\ell} \left[ \left(\frac{x}{\ell}\right)^2 - 2\left(\frac{x}{\ell}\right)^3 + \left(\frac{x}{\ell}\right)^4 \right] dx \quad (B-3)$$

Or after completing the integration

$$SE = 24.576 \frac{EIw_o^2}{\ell^3} \quad (B-4)$$

The asymptote which is impulse dependent is determined by equating the kinetic energy KE to the strain energy. The kinetic energy is given by:

$$KE = (1/2)m v_o^2 = \frac{I^2}{2m} \quad (B-5)$$



Substituting  $\rho A \ell$  for  $m$  and  $ib\ell$  for  $I$  gives:

$$KE = \frac{i^2 b^2 \ell}{2\rho A} \quad (B-6)$$

Equating  $U$  to  $KE$  gives the impulsive loading realm asymptote

$$\frac{i^2 b^2 \ell}{2\rho A} = 24.576 \frac{EI w_o^2}{\ell^3} \quad (B-7)$$

Equation (B-7) relates applied impulse to deformation. To relate impulse to bending stress we must use the moment-curvature relationships. The maximum moment as given by Equation (B-2) occurs at  $x/\ell = 1/2$ . The maximum moment is then given by:

$$M_{\max} = \frac{192}{20} \frac{EI w_o}{\ell^2} \quad (B-8)$$

Substituting  $\sigma_{\max} = \frac{M_{\max} H/2}{I}$  and solving for  $\frac{w_o}{\ell}$  gives:

$$\frac{w_o}{\ell} = \frac{5}{24} \frac{\sigma_{\max} \ell}{E H} \quad (B-9)$$

Finally, taking the square root of Equation (B-7) and substituting Equation (B-9) into Equation (B-7) to eliminate  $w_o$  gives the asymptote for the impulsive loading realm in terms of the maximum bending stress.

$$\frac{ibH}{\sqrt{\rho E I A}} = 1.461 \frac{\sigma_{\max}}{E} \quad (B-10)$$

Equation (B-10) is the impulsive loading realm asymptote plotted in Figure 3-2. The numerical coefficient 1.461 in Equation (B-10) is the  $\alpha_i$  coefficient for a simply-supported beam. In Equation (B-9), the number 5/24 is the  $C_w$  coefficient in Figure 3-2 to relate stress to deformations in a simply-supported beam.

The quasi-static asymptote in Figure 3-2 is computed by calculating the maximum possible work  $Wk$  and equating this quantity to the strain energy. This quantity equals:

$$Wk = \int_0^{\ell} pb(dx)Y \quad (B-11)$$





$$SE = Wk \tanh^2 \left[ \frac{KE}{Wk} \right]^{1/2} \quad (B-17)$$

of the argument, the tanh equals its argument and we obtain the impulsive loading realm asymptote from  $SE = KE$ . For large arguments the tanh equals 1.0, and we obtain the quasi-static loading realm asymptote from  $SE = Wk$ .

This approach, within the bounds of a Bernoulli-Euler, small deformation, beam solution, gives exact answers for both strain and deformation in the quasi-static loading realm. These "exact" answers occur because the deformed shape is correct in this domain. In the impulsive loading realm only approximate answers are given because the deformed shape is not quite right; however, the results are sufficiently accurate, especially when one realizes the uncertainties associated with the load. More accurate answers are obtained if a more accurate deformed shape is assumed. Actually the interrelationship of one variable with another remains the same irrespective of the assumed deformed shape. The only effect of using other deformed shapes is to slightly modify the numerical coefficients  $\alpha_i$ ,  $\alpha_p$ ,  $C_v$ , and  $C_w$ .

To compute the p-i diagram for cantilever, clamped-clamped, clamped-pinned, or beams with any other boundary condition, the same procedure can be followed. If the assumed deformed shape corresponds even approximately to a beam with the correct boundary conditions, then fairly accurate answers will result. The only difference in the solutions of beams with different boundary conditions is that different numerical values arise in the  $\alpha_i$ ,  $\alpha_p$ ,  $C_v$ , and  $C_w$  coefficients.

At this stage we will not compute the p-i diagram for the elastic-plastic beams as complex integrations are involved which must be performed on a computer. Response of a rigid-plastic beam can, however, be determined using hand calculations. The only differences are that after an assumed deformed shape is assumed and the curvature is obtained by differentiation, the strain energy is determined by integrating the plastic yield moment times the curvature over the entire span of the beam. The procedure of then equating strain energy to kinetic energy to obtain the impulsive-loading realm asymptote, and strain energy to work for the quasi-static asymptote remains the same. The deformations obtained from such a rigid-plastic analysis are residual permanent deformations and strains. In the elastic analysis, maximum deformations and strains are estimated.

Several observations should be noted from these numerical calculations. In the impulsive loading realm, maximum bending stress is independent of span  $l$ . This conclusion is mathematically correct. It is caused by span entering the strain energy



and kinetic energy expressions to the same power, so that it cancels. In the impulsive loading realm, the response depends only on the impulse or area under the applied pressure time history. In the quasi-static loading realm, response is independent of beam density and duration of the loading.

To derive the graphical solution presented in Figure 3-3, a deformed shape was assumed to be given by:

$$y = w_0 \sin \frac{\pi x}{l} \quad (B-18)$$

The extensional strain for small deformations is approximated by  $1/2 \left( \frac{dy}{dx} \right)^2$ . Differentiating Equation (B-18) and substituting gives:

$$\epsilon = \frac{\pi^2 w_0^2}{2l^2} \cos^2 \left( \frac{\pi x}{l} \right) \quad (B-19)$$

The maximum strain occurs when the cosine equals 1.0 or:

$$\epsilon_{\max} = \frac{\pi^2 w_0^2}{2l^2} \quad (B-20)$$

This equation is the relationship relating strains to deformation in Figure 3-3. If this solution is to be an elastic-plastic one, we need an elastic-plastic constitutive relationship. Equation (B-21) is assumed to be this relationship because it lets stress equal  $E\epsilon$  for values of  $E\epsilon/\sigma_y$  less than 0.5, and lets stress equal  $\sigma_y$  for values of  $E\epsilon/\sigma_y$  greater than 2.0.

$$\sigma = \sigma_y \tanh \left( \frac{E\epsilon}{\sigma_y} \right) \quad (B-21)$$

The strain energy per unit volume in an elastic-plastic system is the area under the stress strain curve. Equation (B-22) gives for the strain energy per unit volume

$$SE/Vol. = \int_0^\epsilon \sigma_y \tanh \left( \frac{E\epsilon}{\sigma_y} \right) d\epsilon \quad (B-22)$$

Or:

$$SE/Vol. = \frac{\sigma_y^2}{E} \log \cosh \left( \frac{E\epsilon}{\sigma_y} \right) \quad (B-23)$$



Substituting Equation (B-19) for  $\epsilon$  in Equation (B-23) and multiplying by the differential volume  $A, dx$  gives as an integral for the strain energy:

$$SE = \frac{\sigma_y^2 A}{E} \int_0^{\ell} \log \cosh \left[ \frac{\pi^2 E w_o^2}{2 \sigma_y \ell^2} \cos^2 \left( \frac{\pi x}{\ell} \right) \right] dx \quad (B-24)$$

Substituting in a dimensionless variable  $Z$  equal to  $\pi x/\ell$  and substituting in  $\epsilon_{\max}$  for  $\frac{\pi^2 w_o^2}{2 \ell^2}$  (Equation B-20) finally gives an integral for the strain energy:

$$SE = \frac{\sigma_y^2 A \ell}{\pi E} \int_0^{\pi} \log \cosh \left[ \frac{E \epsilon_{\max}}{\sigma_y} \cos^2 Z \right] dz \quad (B-25)$$

The asymptotes can now be calculated as before. The impulsive loading realm asymptote is obtained by equating kinetic energy KE to strain energy. The kinetic energy is given by:

$$KE = \frac{I^2}{2m} = \frac{i^2 b^2 \ell}{2 \rho A} \quad (B-26)$$

Equating Equations (B-26) and (B-24) plus rearranging terms gives:

$$\left[ \frac{i b E^{1/2}}{\rho^{1/2} \sigma_y A} \right]^2 = \frac{2}{\pi} \int_0^{\pi} \log \cosh \left[ \left( \frac{E \epsilon_{\max}}{\sigma_y} \right) \cos^2 Z \right] dz \quad (B-27)$$

A computer is needed to numerically integrate Equation (B-27) for various constant values of scaled strain  $\frac{E \epsilon_{\max}}{\sigma_y}$ . Equation (B-27) does show that the impulsive loading realm asymptote in functional format can be given by:

$$\frac{i b E^{1/2}}{\rho^{1/2} \sigma_y A} = \psi \left( \frac{E \epsilon_{\max}}{\sigma_y} \right) \quad (\text{Impulsive Realm}) \quad (B-28)$$

Equation (B-28) is plotted as the asymptotes to the impulsive loading realm in Figure 3-3.



To obtain the quasi-static loading realm asymptote, we calculate the work  $W_k$ .

$$W_k = pbw_o \int_0^{\ell} \sin \frac{\pi x}{\ell} dx \tag{B-29}$$

Or

$$W_k = \frac{2pb\ell w_o}{\pi} \tag{B-30}$$

Substituting Equation (B-20) for  $w_o$  in Equation (B-30), equating (B-30) to Equation (B-29), and rearranging terms gives an equation for the quasi-static asymptote.

$$\frac{pb\ell E^{1/2}}{\sigma_y^{3/2} A} = \frac{(\pi/2)^{3/2}}{\left(\frac{E\epsilon_{max}}{\sigma_y}\right)^{1/2}} \int_0^{\pi} \log \cosh \left[ \left(\frac{E\epsilon_{max}}{\sigma_y}\right) \cos^2 z \right] dz \tag{B-31}$$

A computer is also needed to numerically integrate Equation (B-31) for constant values of  $\frac{E\epsilon_{max}}{\sigma_y}$ . Equation (B-31) shows that the quasi-static loading realm asymptote is functionally given by:

$$\frac{pb\ell E^{1/2}}{\rho^{1/2} \sigma_y A} = \psi \left( \frac{E\epsilon_{max}}{\sigma_y} \right) \text{ (Quasi-Static Realm)} \tag{B-32}$$

Equation (B-32) with the proper functional format is plotted as the asymptotes to the quasi-static loading realm in Figure 3-3. An approximation still had to be made to establish a transition between the impulsive and quasi-static loading realms. The same hyperbolic tangent squared relationship, Equation (B-17), was used for this string solution as had been used in the beam solutions.

To derive the solution for buckling of a column, we must assume a deformed shape. If the column is simply-supported without side-sway, a sine wave as in Equation (B-33) is a good assumption

$$Y = w_o \sin \frac{\pi x}{\ell} \tag{B-33}$$

Differentiating Equation (B-33) twice and substituting into  $M = -EI \frac{d^2 y}{dx^2}$  gives the moment



$$M = \frac{\pi^2 EI w_0}{\ell^2} \sin \frac{\pi x}{\ell} \quad (B-34)$$

The strain energy is the integral  $\int_0^{\ell} \frac{M^2 dx}{2EI}$  or:

$$SE = 2 \int_0^{\ell/2} \frac{\pi^4 EI w_0^2}{2\ell^4} \sin^2 \left( \frac{\pi x}{\ell} \right) dx \quad (B-35)$$

Which, upon completion, gives:

$$SE = \frac{\pi^4 EI w_0^2}{4\ell^3} \quad (B-36)$$

The load on the column will act through a deflection  $\delta$  equal to  $S-\ell$ , where  $\ell$  is the original length of the column. The differential length  $ds$  is given by:

$$ds = dx \sqrt{1 + \left( \frac{dy}{dx} \right)^2} \quad (B-37)$$

Upon expanding with the binomial theorem and integrating this gives:

$$\delta = \int_0^{\ell} \left[ 1 + (1/2) \left( \frac{dy}{dx} \right)^2 + \dots \right] \quad (B-38)$$

Completing this integration and subtracting  $\ell$  from  $s$  to obtain  $\delta$  gives as a first approximation:

$$\delta = (1/2) \int_0^{\ell} \left( \frac{dy}{dx} \right)^2 dx \quad (B-39)$$

We can now proceed to solve for the work:

$$Wk = pA \delta = \frac{pA}{2} \int_0^{\ell} \left( \frac{dy}{dx} \right)^2 dx \quad (B-40)$$

Substituting in the first derivative of Equation (B-33) to integrate gives:



$$Wk = \frac{\pi^2 p A w_o^2}{2} \int_0^{\ell} \cos^2 \left( \frac{\pi x}{\ell} \right) dx \quad (B-41)$$

Or upon completion:

$$Wk = \frac{\pi^2 p A w_o^2}{4\ell} \quad (B-42)$$

The quasi-static asymptote is obtained when the strain energy is equated to the work:

$$\frac{\pi^4 E I w_o^2}{4\ell^3} = \frac{\pi^2 p A w_o^2}{4\ell} \quad (B-43)$$

Or:

$$\frac{p A \ell^2}{E I} = \pi^2 \quad (\text{quasi-static asymptote S.S. beam-no side sway}) \quad (B-44)$$

Equation (B-44) should look familiar. It is the Euler beam buckling solution. The dynamic load factor equals 1.0 instead of 2.0. Because the vertical load  $pA$  is independent of  $w_o$ , we have the classical small deformation Euler column instability. The factor  $\alpha_p$  in Figure 3-4 is equal to  $\pi^2$  for this pinned-pinned column without side-sway. The concept of effective column length with  $\ell$  being the distance between points of inflection can be applied in analysis. A review of  $\alpha_p$  for a pinned-pinned column with side-sway shows a column with only one quarter the strength because the effective length of the column is twice as long. Similarly  $\alpha_p$  for a clamped-clamped column without side-sway is four times stronger than the simply-supported column because the effective length of the column is halved.

To compute buckling in the impulsive loading realm, we need the kinetic energy imparted to the overlying mass. This kinetic energy equals:

$$KE = (1/2) m v_o^2 = (1/2) m \left( \frac{iA}{m} \right)^2 \quad (B-45)$$

Or

$$KE = \frac{i^2 A^2}{2m} \quad (B-46)$$

Equating KE to SE gives the impulsive loading realm asymptote.

$$\frac{(iA)^2}{2m} = \frac{\pi^4 EI w_0^2}{4\ell^3} \quad (B-47)$$

Notice that, unlike the quasi-static loading realm result, the deformation  $w_0$  does not cancel out of Equation (B-47). This result means that "stable buckling" occurs in the impulsive loading realm. A certain quantity of kinetic energy is being put into the column, which strain energy can dissipate until the deformations are large enough to cause yielding. This observation means that we must use Equation (B-34) to obtain the maximum moment,  $\sin \pi x/\ell$  equal 1.0, and substitute into a  $\sigma = MH/2\ell$  to relate the maximum bending stress (to be limited by  $\sigma_y$ ) to the deformation  $w_0$ . This substitution gives:

$$\sigma_y = \frac{\pi^2 E H w_0}{2\ell^2} \quad (B-48)$$

Substituting Equation (B-48) into Equation (B-47), rearranging terms algebraically, and taking the square root of the result finally gives:

$$\frac{(iA)H\sqrt{E}}{\sigma_y \sqrt{m \ell I}} = \sqrt{2.0} \quad \begin{array}{l} \text{(impulse asymptote} \\ \text{s.s. beam, no side-sway)} \end{array} \quad (B-49)$$

The numerical coefficient  $\sqrt{2.0}$  is the  $\alpha_i$  coefficient in Figure 3-4. Other  $\alpha_i$  coefficients must be computed independently. The static concept of effective length no longer applies in the impulsive loading realm; hence, it should not be used. We have already mentioned that in the impulsive loading realm, it is a "stable buckling" or actually bending phenomenon that occurs. Permanent deformation does not occur until the column yields. The same Equation (B-17) was used to estimate a transition between the quasi-static and impulsive loading realms as has been used to approximate this transition in all earlier analysis.





TABLE C-1. PERTINENT PARAMETERS FOR BURSTING SPHERICAL AND CYLINDRICAL CONTAINMENT VESSELS

<u>Symbol</u>	<u>Description</u>	<u>Dimensions*</u>
d	diameter	L
h	thickness	L
l	length	L
V	volume	L <sup>3</sup>
M <sub>C</sub>	mass of container	FT <sup>2</sup> /L
σ <sub>y</sub>	yield strength of material	F/L <sup>2</sup>
n	number of fragments	--
γ	ratio of specific heats	--
R <sub>M</sub>	ideal gas constant (adjusted for molecular weight)	L <sup>2</sup> /T <sup>2</sup> θ
a <sub>0</sub>	speed of sound in gas	L/T
P <sub>0</sub>	burst pressure	F/L <sup>2</sup>
T <sub>0</sub>	initial temperature of gas	θ
E	energy of gas	FL
P <sub>a</sub>	atmospheric pressure	F/L <sup>2</sup>
u	velocity of fragment	L/T

---

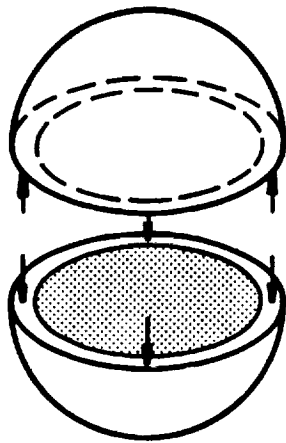
\* L = length  
 F = force  
 T = time  
 θ = temperature



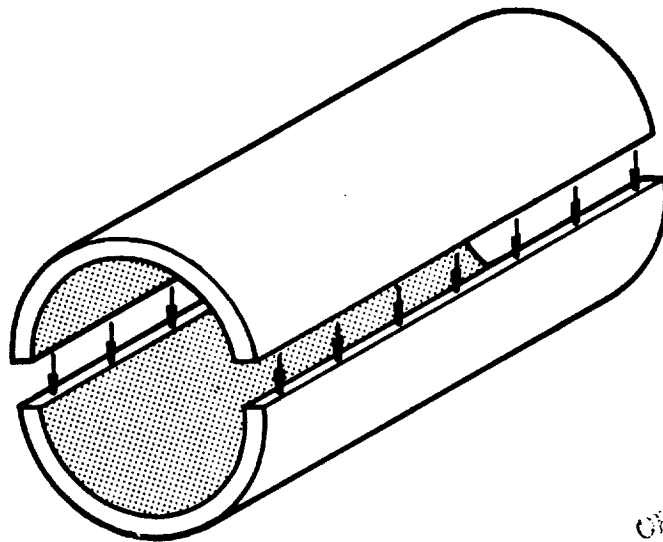
TABLE C-2. LIST OF Pi TERMS FOR BURSTING CONTAINMENT VESSELS

$\pi_1$	$\frac{h}{d}$	proportional to $(P_o - p_a)\sigma_y$
$\pi_2$	$\frac{l}{d}$	constant (equals 1.0 or 10.0)
$\pi_3$	$\frac{V_o}{d^3}$	
$\pi_4$	$\frac{M_c a_o^2}{p a d^3}$	
$\pi_5$	$\frac{\sigma_y}{P_a}$	constant
$\pi_6$	$n$	
$\pi_7$	$\gamma$	$a_o = \sqrt{\gamma R_M T_o}$ (see $\pi_4$ and $\pi_{11}$ )
$\pi_8$	$\frac{R_M T_o}{a_o^2}$	
$\pi_9$	$\frac{P_o}{P_a}$	
$\pi_{10}$	$\frac{E}{p_a h d^2}$	$E = \frac{(P_o - p_a)V_o}{(\gamma - 1)}$ (see $\pi_3$ , $\pi_7$ and $\pi_9$ )
$\pi_{11}$	$\frac{u}{a_o}$	





(a) Sphere



(b) Cylinder

ORIGINAL PAGE IS  
OF POOR QUALITY

FIGURE C-1. DETERMINATION OF VESSEL THICKNESS



the vessel will burst when the force exerted on the vessel walls by the internal pressure equals the force required to break the vessel. If one considers that the vessel (sphere) bursts in half, one has

$$(P_o - p_a) \frac{\pi d^2}{4} = \sigma_y \pi d h \quad (C-2)$$

or

$$\frac{h}{d} = \frac{P_o - p_a}{4\sigma_y} \quad (C-3)$$

Cylinders must have thicker walls than spheres to contain equal amounts of internal pressures. A simplified design for a cylinder can be based on Figure C-1b which shows a cylinder without hemispherical endcaps.

The most likely plane of fracture of a cylinder made of a homogeneous material is along the longitudinal axis as shown in Figure C-1b. For vessels whose thickness is much smaller than its diameter, the vessel will burst when the force exerted on the vessel walls by the internal pressure equals the force required to break the vessel. If one considers that the vessel (cylinder) bursts into two pieces as shown in Figure C-1b, one has

$$(P_o - p_a) d l = \sigma_y 2 l h \quad (C-4)$$

or

$$\frac{h}{d} = \frac{(P_o - p_a)}{2\sigma_y} \quad (C-5)$$

Equations C-3 and C-5 indicate that  $(h/d)$  is proportional to  $(P_o - p_a)/\sigma_y$  and thus pi term  $\pi_1$  can be eliminated. If one assumes that only one material with one yield strength will be used in constructing the vessel, then pi term  $\pi_5$  can also be eliminated.

Energy  $E$  in the gas is defined as

$$E = \frac{(P_o - p_a) V_o}{(\gamma - 1)} \quad (C-6)$$



Pi term  $\pi_9$  contains  $p_o$  and  $p_a$ ,  $\pi_3$  contains  $V_o$ , and  $\pi_7$  contains  $\gamma$ . Therefore, the energy of the gas is completely defined by these other pi terms and pi term  $\pi_{10}$  can be eliminated.

Variables in  $\pi_7$  and  $\pi_8$  appear in  $\pi_4$  and  $\pi_{11}$ . It seems logical that the problem has been overdefined and that  $\pi_7$  and  $\pi_8$  can be eliminated from the analysis.

Since  $\pi_3$ ,  $\pi_4$  and  $\pi_9$  have some terms in common, it appeared beneficial to combine them. Thus, one has

$$\frac{\pi_9 \times \pi_3}{\pi_4} = \frac{\frac{p_o}{p_a} \times \frac{V_o}{d^3}}{\frac{M_c a_o^2}{p_a d^3}} \quad (C-7)$$

Rearranging Equation C-7 and substituting Equation C-1 for  $a_o$ , one has

$$\pi'_9 = \frac{P_o V_o}{M_c \gamma R_m T_o} \quad (C-8)$$

Substituting  $(P_o - p_a)$  for  $P_o$  in order to emphasize the importance of the differential in pressure between the inside and outside of the vessel walls, one obtains the abscissa of Figure 4-2. Plotting  $\pi_{11}$  with equation C-1 substituted for  $a_o$ , versus the modified version of Equation C-8 yields the desired result. Figure 4-2 in the text consolidates the presentation of the analysis by allowing one to plot several curves for different L/D ratios and numbers of fragments n on one curve and still maintain accurate estimation of fragment velocity u. Several computer checks have shown that the curves presented in Figure 4-2 can be used for materials of different densities and yield strengths, provided that the thickness of the vessel is less than 1/3 of the diameter of the vessel. For cylinders bursting into three or more "strip" fragments as explained in Baker, Kulesz, et al (1975), the hemispherical endcaps were ignored.

Some cases were run for cylinders with hemispherical endcaps and an L/D ratio of 10.0 which burst into two unequal segments perpendicular to the cylindrical axis of symmetry. It seemed reasonable that the velocity of each fragment would be related to the velocity of the fragments from cylinders bursting in half by some constant k which depends on the unequal fragment's fraction of the total mass of the container. Figure 4-4 in the text was





## APPENDIX D

### Estimate of Initial Velocities of Fragments from Spheres and Cylinders Bursting Into Two Unequal Fragments

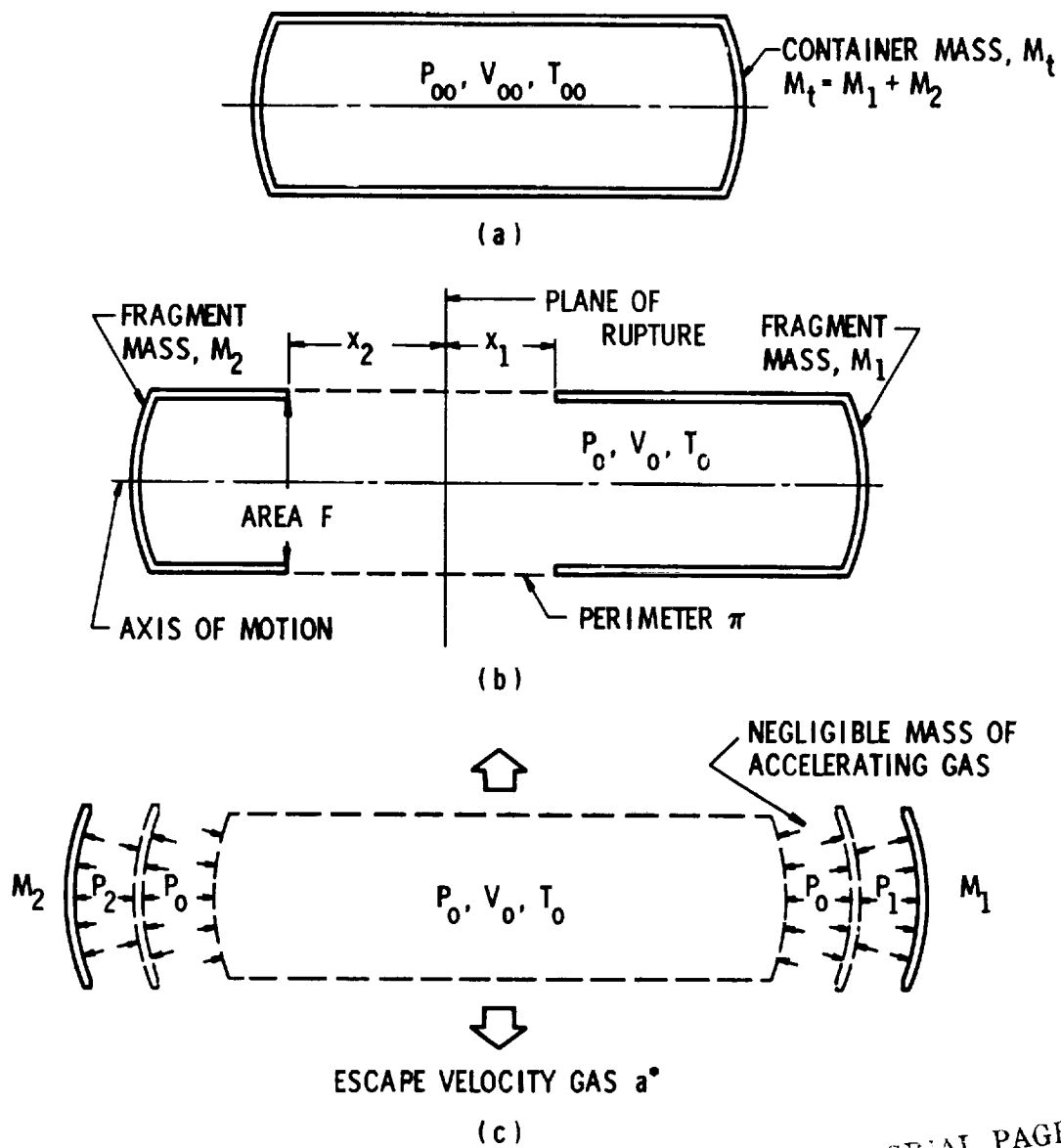
The method developed by Taylor and Price (1971) and modified by Baker, et al (1975) for calculating velocities of fragments from bursting spherical and cylindrical gas reservoirs was further adapted to provide velocity calculations for unequal fragments from cylindrical gas vessels. To compute the velocity of fragments from bursting cylinders which contain gas under pressure, the following assumptions were made:

- (1) The vessel with gas under pressure breaks into two unequal fragments along a plane perpendicular to the cylindrical axis, and the two container fragments are driven in opposite directions.
- (2) Gas within the vessel obeys the ideal gas law.
- (3) Originally contained gas escapes from the vessel through the opening between the fragments into a surrounding vacuum. The escaping gas travels perpendicular to the direction of motion of the fragments with local sonic velocity.
- (4) Energy necessary to break the vessel walls is negligible compared to the total energy of the system.
- (5) Drag and lift forces are ignored since the distance the fragment travels before it attains its maximum velocity are too short for drag and lift forces to have a significant effect.

A schematic depicting the essential characteristics of the modified solution for bursting cylinders is shown in Figure (D-1). Before accelerating into an exterior vacuum, the cylinder has internal volume  $V_{00}$  and contains a perfect gas of adiabatic exponent (ratio of specific heats)  $\gamma$  and gas constant  $R_M$  with initial pressure  $P_{00}$  and temperature  $T_{00}$  (Figure D-1a). At a time  $T = 0$ , rupture occurs along a perimeter  $\Pi$ , and the two fragments are propelled in opposite directions due to forces applied against the area  $F$  which is perpendicular to the axis of motion of the fragments (Figure D-1b). The masses of the fragments,  $M_1$  and  $M_2$ , are considered large relative to the mass of the remaining gas at elevated pressure (Figure D-1c).

Figure D-2 contains the geometric parameters associated with cylindrical vessels. The generalized fragment velocity solution and subsequent computer program allow for computation of the velocities of both segments of the cylinder. The vessel is assumed





ORIGINAL PAGE IS  
OF POOR QUALITY

FIGURE D-1. PARAMETERS FOR CYLINDER BURSTING INTO TWO UNEQUAL SEGMENTS



to break into two unequal segments along a plane perpendicular to its cylindrical axis. The cylinder can have spherical segment end caps or can have flat faces. The vessel has cylindrical radius  $r$ , cylindrical thickness  $C_t$ , end cap thickness  $E_t$ , cylindrical length  $C_\ell$ , and end cap length  $E_\ell$  beyond the cylindrical portion.

The Taylor and Price (1971) solution, generalized to allow for cylindrical vessels bursting into unequal fragments, follows. The equations of motion and initial conditions of the two fragments are

$$M_1 \frac{d^2 X_1(\tau)}{d\tau^2} = FP_1(\tau), \text{ with } X_1(0) = 0, \frac{dX_1(0)}{d\tau} = 0 \quad (D-1)$$

$$M_2 \frac{d^2 X_2(\tau)}{d\tau^2} = FP_2(\tau) \text{ with } X_2(0) = 0, \frac{dX_2(0)}{d\tau} = 0 \quad (D-2)$$

where subscripts refer to each fragment and  $X_1$  is a displacement distance taken along the axis of motion. To allow for cylindrical containment vessels, the cross sectional area  $F$  over which the force is applied becomes

$$F = \pi (r - C_t)^2 \quad (D-3)$$

The equation of state for the unaccelerated gas remaining within the confinement of the container fragments is

$$P_o(\tau) V_o(\tau) = C(\tau) RT_o(\tau) \quad (D-4)$$

where subscript "o" denotes reservoir conditions immediately after failure,  $R$  is the gas constant,  $P$  is pressure,  $V$  is volume,  $T$  is temperature and  $C(\tau)$  is the mass of gas confined at high pressure as a function of time. The rate of change of the confined mass is

$$\frac{dC(\tau)}{d(\tau)} = k \Pi X \rho_* a_* \quad (D-5)$$

where

$$X = X_1 + X_2, \quad (D-6)$$

$K$  is the coefficient of discharge of the area between the fragments and  $\rho_*$  is the gas density at critical gas velocity  $a_*$ . The expression for perimeter  $\Pi$  is





$$\Pi = 2\pi r \quad (D-7)$$

Gas density  $\rho_*$  and  $a_*$  are standard expressions

$$\rho_* = \rho_o(\tau) \left( \frac{2}{\gamma + 1} \right)^{1/(\gamma-1)}$$

$$a_* = a_o(\tau) \left( \frac{2}{\gamma + 1} \right)^{1/2} \quad (D-8)$$

where  $\gamma$  is the adiabatic exponent (ratio of specific heats) for an ideal gas. The volume is assumed to be variable and can be described by

$$V_o(\tau) = V_{oo} + Fx \quad (D-9)$$

where  $x = x_1 + x_2$ .

Nearly all of the gas is assumed to be accelerated with the fragments, with gas immediately adjacent to the fragments being accelerated to the velocity of the fragments. From simple one-dimensional flow relationships,

$$P_1(\tau) = P_o(\tau) \left( 1 - \left\{ \frac{\gamma - 1}{2[a_o(\tau)]^2} \right\} \left[ \frac{dx_1(\tau)}{d\tau} \right]^2 \right)^{\gamma/(\gamma-1)}$$

$$P_2(\tau) = P_o(\tau) \left( 1 - \left\{ \frac{\gamma - 1}{2[a_o(\tau)]^2} \right\} \left[ \frac{dx_2(\tau)}{d\tau} \right]^2 \right)^{\gamma/(\gamma-1)} \quad (D-10)$$

To generalize the solution, one can use the following nondimensional forms of the variables:

$$\text{Dimension: } x(\tau) = Xg(\zeta), \quad x_1(\tau) = Xg_1(\zeta), \quad x_2(\tau) = Xg_2(\zeta)$$

$$\text{Time: } \tau = \theta\zeta \quad (D-11)$$

$$\text{Pressure: } P_o(\tau) = P_{oo}P_*(\zeta)$$

From appropriate solutions and initial conditions:

$$\frac{dx_1(\tau)}{d\tau} = \frac{X}{\theta} g'_1(\zeta), \quad \frac{dx_2(\tau)}{d\tau} = \frac{X}{\theta} g'_2(\zeta)$$





$$V_{oo} = \pi \left\{ (r - c_t)^2 c_\ell + (E_\ell - E_t) \left[ (r - E_t)^2 + \frac{(E_\ell - E_t)^2}{3} \right] \right\} \quad (D-15)$$

for the adiabatic case,

$$\frac{P_o(\tau)}{P_{oo}} = \left[ \frac{\rho_o(\tau)}{\rho_{oo}} \right]^\gamma = \left[ \frac{T_o(\tau)}{T_{oo}} \right]^{\frac{\gamma}{\gamma-1}} = \left[ \frac{a_o(\tau)}{a_{oo}} \right]^{\frac{2\gamma}{\gamma-1}} \quad (D-16)$$

Substitution of Equations (D-10), (D-12) through (D-14), and (D-16) into Equations (D-1) and (D-2) gives

$$\frac{M_1}{M_t} g_1'' = P_* \left[ 1 - \left( \frac{g_1'^2}{P_*^{(\gamma-1)/\gamma}} \right) \right]^{\gamma/(\gamma-1)} \quad (D-17a)$$

by analogy,

$$\frac{M_2}{M_t} g_2'' = P_* \left[ 1 - \left( \frac{g_2'^2}{P_*^{(\gamma-1)/\gamma}} \right) \right]^{\gamma/(\gamma-1)} \quad (D-17b)$$

Differentiation of Equation (D-4) and substitution of Equations (D-5) through (D-9), (D-11) and (D-12) yields

$$\left[ \left( \frac{\gamma-1}{2} \right) \alpha + g \right] \frac{P_*'}{P_*} = - \frac{\beta\gamma}{\alpha} g P_*^{(\gamma-1)/2\gamma} - \gamma g' \quad (D-18)$$

In the solution for equal fragments, the fragment masses are equal, and the equations for the motion of the two fragments become identical. However, since the fragment masses in the new solution are unequal, the equations of motion become

$$g_1'' = \frac{M_t}{M_1} P_* \left[ 1 - \left( \frac{g_1'^2}{P_*^{(\gamma-1)/\gamma}} \right) \right]^{\gamma/(\gamma-1)} \quad (D-19)$$

$$g_2'' = \frac{M_t}{M_2} P_* \left[ 1 - \left( \frac{g_2'^2}{P_*^{(\gamma-1)/\gamma}} \right) \right]^{\gamma/(\gamma-1)}$$

Rearranging terms in Equation (D-18) produces







Table D-1. Computer Program Entitled /UNQL/ in Basic

Function: This program computes the velocity of a fragment from a bursting sphere or cylinder, with or without spherical segment end caps with one base, which contains gas under pressure. It is assumed that the vessel breaks into two unequal fragments along a plane perpendicular to the cylindrical axis. Distance, acceleration and residual pressure as a function of time are also computed.

Input-Output Considerations: The program accepts input in English units only and prints output in SI and English units making any conversions needed internally. The program considers SI units of mass in kilograms, length in meters and time in seconds. The program considers English units of mass in pounds of force (weight measure used for convenience), length in inches and time in seconds. Input data are:

(A) Gas characteristics:

(CØ) Adiabatic exponent (ratio of specific heats) for gas in the containment vessel

(AØ) Speed of sound in gas of vessel

(PØ) Initial pressure of gas in vessel

(B) Vessel characteristics:

(RØ) Cylinder radius

choice of

(Z1) = 1: (A) Cylinder length  
(B) Length of end cap  
(C) Cylinder thickness  
(D) Thickness of end cap  
(E) Wall density

(Z1) = 2: (A) Volume of containment vessel  
(B) Mass of reservoir  
(C) Cylinder thickness

(C) Dynamic variables:

(KØ) Discharge coefficient

(X8) Nondimensional time increment for calculations

(X9) Maximum nondimensional time calculation



(D) Input/Output format:

(F9) Fraction of total cylinder length (or mass) for first fragment

(F1) Display nondimensional dynamic variance  
1. = Yes  
2. = No

(F2) Display dimensional dynamic variance  
1. = Yes  
2. = No

Variables: The definition and units of variables in this program follow.

<u>Program Variable</u>	<u>Variable</u>	<u>Definition</u>	<u>SI</u>	<u>Units English</u>
F2	--	if-1., program displays normal time, distance, velocity, accelerations and pressure	--	--
C1	$C_\ell$	cylinder length	m	in
E1	$E_\ell$	end length	m	in
C2	$C_t$	cylinder thickness	m	in
E2	$E_t$	end thickness	m	in
DØ	--	wall density	kg/m <sup>3</sup>	lb-f/in <sup>3*</sup>
VØ	--	outside volume of vessel	m <sup>3</sup>	in <sup>3</sup>
V1	$V_{\text{oo}}$	internal volume of vessel	m <sup>3</sup>	in <sup>3</sup>
V2	--	wall volume of vessel	m <sup>3</sup>	in <sup>3</sup>
MØ	$M_t$	total mass of reservoir	kg	lb-f*
V5	--	outside volume of frag #1	m <sup>3</sup>	in <sup>3</sup>

\*lb-f indicates English weight measurement of pounds of force. Sea level gravitation is assumed.



<u>Program Variable</u>	<u>Variable</u>	<u>Definition</u>	<u>Units</u>	
			<u>SI</u>	<u>English</u>
V6	--	internal volume of frag #1	m <sup>3</sup>	in <sup>3</sup>
V7	--	wall volume of frag #1	m <sup>3</sup>	in <sup>3</sup>
M7	M <sub>1</sub>	mass of frag #1	kg	lb-f*
M8	M <sub>2</sub>	mass of frag #2	kg	lb-f*
CØ	γ	adiabatic exponent	--	--
AØ	a <sub>oo</sub>	sound speed	m/s	in/sec
PØ	P <sub>oo</sub>	initial pressure	Pa	psi
RØ	r	cylinder radius	m	in
Z1	--	if = 1., input is if = 2., input is	--	--
KØ	--	gas discharge coefficient	--	--
X8	--	dimensionless time interval of iteration	--	--
X9	--	maximum dimensionless time of iteration	--	--
F9	--	fraction of total cylinder length (or mass) for frag #1	--	--
F1	--	if = 1., program displays	--	--
F2	--	if = 1., program displays	--	--
P5	Π	perimeter(calculated)	m	in
F5	F	area of cross-section to which force is applied(calculated)	m <sup>2</sup>	in <sup>2</sup>
X2	X	characteristic dimension(calculated)	m <sup>2</sup>	in <sup>2</sup>

Program Variable	Variable	Definition	Units	
			SI	English
O	$\theta$	characteristic time (calculated)	s	sec
C7	--	quantity $(\gamma/(\gamma-1))$	--	--
C8	--	quantity $(3\gamma-1)/2\gamma$	--	--
C9	--	quantity $(\gamma+1)/2(\gamma-1)$	--	--
Q1	$\alpha$	dimensionless parameter	--	--
B1	$\beta$	dimensionless geometry parameter	--	--
X	--	normalized time	--	--
Y(1)	--	normalized initial displacement of frag #1	--	--
Y(2), F(1)*	--	normalized velocity of frag #1	--	--
Y(3)	--	normalized pressure	--	--
Y(4)	--	normalized initial displacement of frag #2	--	--
Y(5), F(4)*	--	normalized velocity of frag #2	--	--
F(2)*	--	normalized accelera- tion of frag #1	--	--
F(3)*	--	normalized rate of change of pressure	--	--
F(5)*	--	normalized acceleration of frag #2	--	--
Q2	--	quantity $[(\gamma-1)/2]\alpha +$ $(g_1 + g_2)$	--	--
U	$g'$	$(g'_1 + g'_2)$ quantity	--	--
T9	--	normalized time(output)	--	--

\*indicates differential equations solved.







PRECEDING PAGE BLANK NOT ~~REPRODUCED~~

SAMPLE INPUT AND OUTPUT

1

Preceding page blank

155

U U U E E U U E E E E E E E E E E E E E E E

```

100 INIT
110 PAGE
120 REN
130 REN /UNOL/--VELOCITY OF FRAGMENTS FROM CYLINDRICAL
140 REN PRESSURE VESSELS BURSTING INTO TWO UNEQUAL SEGMENTS
150 REM PERPENDICULAR TO AXIS OF SYMMETRY
160 REM ENGLISH INPUT UNITS ONLY (IN,LBF,PSI)
170 REN
180 REN
190 REM
200 DIM F(5),Y(5),W1(5),W2(5),P9(50),T9(50),G(50),G1(50),G2(50)
210 DIM G3(50),G4(50),G5(50)
220 PRINT "GAMMA, SOUND SPEED, INITIAL PRESSURE? ";
230 INPUT C5,A5,P0
240 PRINT "CYLINDER RADIUS? ";
250 PRINT R0
260 INPUT R0
270 PRINT "IF PARAMETERS ARE:"
280 PRINT "CYL LEN, END LEN, CYL THICK, END THICK, WALL DENS--ENTER 1"
290 PRINT "VOLUME, MASS OF RESERVOIR, CYL THICK--ENTER 2-----";
300 INPUT Z1
310 PRINT "READ IN VALUES ";
320 PRINT A,B,C,D,E
330 PRINT "FRACTION OF TOTAL CYLINDER LENGTH(COR MASS) FOR FRAG#1? ";
340 INPUT F9
350 PRINT "DISCHARGE COEF.? ";
360 INPUT K0
370 PRINT "TIME INTERVAL, MAXIMUM TIME? ";
380 INPUT X0,X9

```

```
440 PRINT "DISPLAY NONDIMENSIONAL DYNAMIC VAR.? YES=1 NO=2--";
450 INPUT F1
460 PRINT "DISPLAY DIMENSIONAL DYNAMIC VAR.? YES=1 NO=2--";
470 INPUT F2
480 A$="ITEM"
490 B$="ENGLISH UNITS"
500 D$="GAMMA"
510 E$="SOUND SPEED"
520 F$="PRESSURE"
530 G$="RADIUS"
540 H$="CYL. LENGTH"
550 I$="END. LENGTH"
560 J$="CYL. THICK."
570 K$="END. THICK."
580 L$="WALL DENSITY"
590 M$="RESERVOIR MASS"
600 O$="IN"
610 P$="VOLUME"
620 PAGE
630 PRINT "DATE ";
640 INPUT Z$
650 PRINT "PAGE NO. ";
660 INPUT J9
670 PRINT
680 IF Z1=2 THEN 1100
690 C1=A
700 E1=B
710 C2=C
720 E2=D
730 D0=E
740 V0=PI*(R0*R0*C1+E1*R0*R0+E1*E1*E1/3)
750 V1=PI*((R0-C2)^2*C1+(E1-E2)*((R0-E2)^2+(E1-E2)^2/3))
760 V2=V0-V1
```

```

790 M0=D0*V2
900 REM CALCULATE MASS OF FRAG #1(M7) AND FRAG #2(M8)
910 V5=PI*(R0*R0*F9*C1+E1*R0*R0/2+E1*E1*E1/6)
920 V6=PI*(R0-C2)^2*F9*C1+(E1-E2)*(R0-E2)^2/2+(E1-E2)^2/6)
930 V7=V5-V6
940 M7=D0*V7
950 M8=M0-M7
960 PRINT "FRACTION OF TOTAL CYL. LENGTH<LESS END CAPS> FOR FRAG#1 IS ";
970 PRINT USING 10.40
980 IMAGE 100: "ENGLISH INPUT/ENGLISH OUTPUT", A$, B$, D$, C0
990 IMAGE 110: 2/, 4A, 13X, 13A, /, 50, 11X, 3E
1000 IMAGE 120: E$, A0, "IN/SEC", F$, P$, "PSI", G$, R0, 0$
1010 IMAGE 130: 1X, 6A, /, 8A, 8X, 3E, 1X, 3A, /, 6A, 10X, 3E, 1X, 2A
1020 IMAGE 140: H$, C0, 0$, I$, E1, 0$, J$, C2, 0$
1030 IMAGE 150: 5X, 3E, 1X, 2A, /, 10A, 6X, 3E, 1X, 2A, /, 11A, 5X, 3E, 1X, 2A
1040 IMAGE 160: K$, E2, 0$, L$, D0, "LBF/QU IN", P$, V1, "CU IN"
1050 IMAGE 170: 1A, 5X, 3E, 1X, 2A, /, 12A, 4X, 3E, 1X, 5A, /, 6A, 10X, 3E, 1X, 5A
1060 IMAGE 180: M$, M0, "LBF"
1070 IMAGE 190: 2X, 3E, 1X, 3A
1080 IMAGE 200: "FRAG#1 CYL L", F9*C1, 0$
1090 IMAGE 210: 4X, 3E, 1X, 2A
1100 PRINT USING 1020: "FRAG#1 MASS", M7, "LBF"
1110 IMAGE 220: 5X, 3E, 1X, 3A
1120 PRINT USING 1090: "FRAG#2 CYL L", (1-F9)*C1, 0$
1130 PRINT USING 1020: "FRAG#2 MASS", M8, "LBF"
1140 D0=D0/386.0886
1150 M0=M0/386.0886
1160 M7=M7/386.0886
1170 M8=M8/386.0886
1180 GO TO 1350
1190 V1=A
1200 M0=B
1210 M7=F9*M0
1220 M8=M0-M7

```



```
1149 C2=C
1150 PRINT "FRACTION OF TOTAL VESSEL MASS FOR FRAG#1 IS "J
1160 PRINT USING 1170:F9
1170 IMAGE 10.4D
1180 PRINT USING 1190:"ENGLISH INPUT/ENGLISH OUTPUT",A$,B$,D$,C0
1190 IMAGE /,20A,2/,4A,13X,13A,/,5A,11X,3E
1200 PRINT USING 1210:E$,A0,"IN/SEC",F$,P0,"PSI",G$,R0,0$
1210 IMAGE 11A,5X,3E,1X,6A,/,8A,8X,3E,1X,3A,/,GA,10X,3E,1X,2A
1220 PRINT USING 1230:P$,V1,"CU IN",M$,M0,"LBF",J$,C2,0$
1230 IMAGE 6A,15X,3E,1X,5A,/,14A,2X,3E,1X,3A,/,11A,5X,3E,1X,2A
1240 PRINT USING 1250:"FRAG#1 MASS",M7,"LBF"
1250 IMAGE 11A,5X,3E,1X,3A
1260 PRINT USING 1250:"FRAG#2 MASS",M8,"LBF"
1270 M9=M0/386.1896
1280 M7=M7/306.1986
1290 M8=M8/306.1886
1300 REM
1310 REM
1320 REM BEGIN VELOCITY CALCULATIONS
1330 REM
1340 REM
1350 J1=0
1360 P5=2*PI*70
1370 F5=PI*(70-C2)^2
1380 X2=M0*V0*(2/(C0-1))/(F5*P0)
1390 O=M0*V0*(2/(C0-1))^0.5/(F5*P0)
1400 C7=C0/(C0-1)
1418 C8=(3*C0-1)/(2*C0)
1420 C9=(C0+1)/(2*(C0-1))
1430 Q1=P0*V1/(M0*V0*A0)
1448 B1=K0*(2/(C0+1))^C9*(2/(C0-1))^0.5*P5*V1/(F5*F5)
1450 REM
1460 REM
1479 REM
1480 REM
X=T-NORM
Y(I)=G#1
```

```

1490 REM Y(2)=F(1)=G'#1
1500 REM Y(3)=P-NORM
1510 REM F(2)=G'#1
1520 REM F(3)=P-NORM PRIME
1530 REM
1540 REM Y(4)=G#2
1550 REM Y(5)=F(4)=G'#2
1560 REM F(5)=G'#2
1570 REM -----
1580 REM
1590 X=0
1600 Y(1)=0
1610 Y(2)=0
1620 Y(3)=1
1630 Y(4)=0
1640 Y(5)=0
1650 PRINT
1660 PRINT "INITIAL CONDITIONS"
1670 PRINT USING 1680: "X(0)=", X, "G1(0)=", Y(1), "G1'(0)=", Y(2)
1680 PRINT USING 1680: "Y(0)=", Y(3), "G2(0)=", Y(4), "G2'(0)=", Y(5)
1690 PRINT USING 1680: "Y(0)=", Y(4), "G2'(0)=", Y(5)
1700 PRINT USING 1680: "Y(0)=", Y(4), "G2'(0)=", Y(5)
1710 H=5
1720 F(1)=Y(2)
1730 F(2)=M0/M7*Y(3)*(1-Y(2))*Y(2)/Y(3)↑(1/C7)↑C7
1740 Q2=(C0-1)/2*Q1+Y(1)+Y(4)
1750 F(3)=(-B1*C0/Q1*(Y(1)+Y(4))*Y(3)↑C8-C0*(Y(2)+Y(5))*Y(3))/Q2
1760 F(4)=Y(5)
1770 F(5)=M0/M8*Y(3)*(1-Y(5))*Y(5)/Y(3)↑(1/C7)↑C7
1780 STOP
1790 PAGE
1800 PRINT "CHARACTERISTICS OF MOTION OF FRAGMENTS <NORMALIZED>"
1810 PRINT "T-NORM G' G' P-NORM"
1820 U=1000
1830 N2=0

```

```
1840 GOSUB 2990
1850 F(1)=Y(2)
1860 F(2)=M0/M7*Y(3)*(1-Y(2))*Y(2)/Y(3)↑(1/C7)↑C7
1870 Q2=(C0-1)/2*Q1+Y(1)+Y(4)
1880 F(3)=(-B1*C0/Q1*(Y(1)+Y(4))*Y(3)↑C8-C0*(Y(2)+Y(5))*Y(3))/Q2
1890 F(4)=Y(5)
1900 F(5)=M0/M8*Y(3)*(1-Y(5))*Y(5)/Y(3)↑(1/C7)↑C7
1910 IF S=1 THEN 1840
1920 PRINT
1930 PRINT USING 1940:"1",X,Y(1),Y(2),F(2),Y(3)
1940 IMAGE 10,1X,3E,4(1X,3E)
1950 PRINT USING 1960:"2",X,Y(4),Y(5),F(5)
1960 IMAGE 10,1X,3E,3(1X,3E)
1970 J1=J1+1
1980 T9(J1)=X
1990 G(J1)=Y(1)
2000 G1(J1)=Y(2)
2010 G2(J1)=F(2)
2020 P9(J1)=Y(3)
2030 G3(J1)=Y(4)
2040 G4(J1)=Y(5)
2050 G5(J1)=F(5)
2060 IF X>X9 THEN 2100
2070 IF ABS(LOG(U))-LOG(Y(2)+Y(5))<=3.0E-5 THEN 2100
2080 U=Y(2)+Y(5)
2090 GO TO 1830
2100 STOP
2110 PAGE
2120 IF F1=2 THEN 2400
2130 I=0
2140 K=I+1
2150 IF K>J1 THEN 2350
2160 PRINT USING 2170:"DATE ",Z$
2170 IMAGE 50,10A
2180 PRINT USING 2190:"PAGE NO. ",J9+1
```

```

2190 IMAGE 90,30
2200 J9=J9+1
2210 PRINT
2220 PRINT "CHARACTERISTICS OF MOTION OF FRAGMENTS (NORMALIZED)"
2230 PRINT "      G'      G'      P-NORM"
2240 FOR I=K TO J1
2250 PRINT
2260 PRINT USING 2270:"1",T9(I),G(I),G1(I),G2(I),P9(I)
2270 IMAGE 10,1X,3E,4(1X,3E)
2280 PRINT USING 2290:"2",T9(I),G3(I),G4(I),G5(I)
2290 IMAGE 10,1X,3E,3(1X,3E)
2300 IF I=10 THEN 2140
2310 IF I/2=10 THEN 2140
2320 IF I/3=10 THEN 2140
2330 IF I/4=10 THEN 2140
2340 NEXT I
2350 STOP
2360 PAGE
2370 I=0
2380 K=I+1
2390 IF K>J1 THEN 2600
2400 PRINT USING 2410:"DATE ",Z$
2410 IMAGE 50,10
2420 PRINT USING 2430:"PAGE NO. ",J9+1
2430 IMAGE 90,30
2440 J9=J9+1
2450 IF F2=2 THEN 2600
2460 PRINT
2470 PRINT "CHARACTERISTICS OF MOTION OF FRAGMENTS (ENGLISH UNITS)"
2480 PRINT "      TIME      VELOCITY      ACCEL.      PRESSURE"
2490 FOR I=K TO J1
2500 T1=0*TS(I)
2510 H1=X2*G(I)
2520 H2=X2*G(I)
2530 H3=X2*(G(I)*G2(I)

```

ORIGINAL PAGE IS  
OF POOR QUALITY

```
2540 H4=P0*P9(I)
2550 H5=X2*G3(I)
2560 H6=X2/0*G4(I)
2570 H7=X2/(0*0)*G5(I)
2580 PRINT
2590 PRINT USING 2600:"1",Y1,H1,H2,H3,H4
2600 IMAGE 1A,1X,5(3E)
2610 PRINT USING 2620:"2",Y1,H5,H6,H7
2620 IMAGE 1A,1X,4(3E)
2630 IF I=10 THEN 2300
2640 IF I/2=10 THEN 2380
2650 IF I/3=10 THEN 2380
2660 IF I/4=10 THEN 2380
2670 NEXT I
2680 E5=0*X
2690 E6=X2*Y(1)
2700 E7=X2/0*Y(2)
2710 E8=X2/(0*0)*F(2)
2720 E9=P0*Y(3)
2730 S6=X2*Y(4)
2740 S7=X2/0*Y(5)
2750 S8=X2/(0*0)*F(5)
2755 IF F2=2 THEN 2820
2760 STOP
2770 PAGE
2780 PRINT USING 2790:"DATE ",Z$
2790 IMAGE 5A,10A
2800 PRINT USING 2810:"PAGE NO. ",J9+1
2810 IMAGE 5A,30
2820 PRINT
2830 PRINT USING 2840:"FINAL VALUES",TIME="E5," SEC"
2840 IMAGE 12A,/,6A,3E,4A
2850 PRINT USING 2860:"DISTANCE #1=",E6," IN ("E6*0.0254," METERS)"
2860 IMAGE 13A,3E,5A,3E,8A
2870 PRINT USING 2880:"VELOCITY #1=",E7," IN/SEC ("E7*0.0254," M/SEC)"
```

```

2880 IMAGE 130,3E,9A,7E,7A
2890 PRI USI 2900:"ACCEL. #1=" ,E8," IN/SQ-SEC (",E8*0.0254," M/SQ-SEC)"
2900 IMAGE 110,3E,120,3E,100
2910 PRINT USING 2920:"PRESSURE=" ,E9," PSI (",E9*6894.757," PASCALS)"
2920 IMAGE 160,3E,60,3E,90
2930 PRINT
2940 PRINT USING 2860:"DISTANCE #2=" ,S6," IN (",S6*0.0254," METERS)"
2950 PRINT USING 2900:"VELOCITY #2=" ,S7," IN/SEC (",S7*0.0254," M/SEC)"
2960 PRI USI 2900:"ACCEL. #2=" ,S8," IN/SQ-SEC (",S8*0.0254," M/SQ-SEC)"
2970 REM
2980 REM-----
2990 REM SUBROUTINE RUNGE-KUTTA
3000 REM-----
3010 REM
3020 DIM Q(5)
3030 N2=N2+1
3040 IF N2=1 THEN 3080
3050 IF N2=2 THEN 3140
3060 IF N2=3 THEN 3160
3070 IF N2=4 THEN 3190
3080 FOR J=1 TO 4
3090 Q(J)=0
3100 NEXT J
3110 A=0.5
3120 X=X+X8/2
3130 GO TO 3250
3140 A=0.2929321801
3150 GO TO 3250
3160 A=1.7071067812
3170 X=X+X8/2
3180 GO TO 3250
3190 FOR I=1 TO 4
3200 Y(I)=Y(I)+X8*F(I)/6-Q(I)/3
3210 NEXT I
3220 N2=N2+1

```



APPENDIX E

MODEL ANALYSIS FOR FRAGMENT TRAJECTORIES

In order to generalize the analysis for determining the range of a flying fragment from a bursting spherical or cylindrical container, a model analysis was performed. The analysis for calculating the fragment range and the subsequent computer program (FRISB) are presented in detail in Baker, et al (1975). However, for the sake of clarity, a brief discussion of this analysis is presented below.

The equations for calculating the horizontal and vertical (X and Y) accelerations of a fragment are as follows:

$$\ddot{Y} = -g - \frac{A_D C_D \rho_o (\dot{X}^2 + \dot{Y}^2) \sin \alpha}{2M} + \frac{A_L C_L \rho_o (\dot{X}^2 + \dot{Y}^2) \cos \alpha}{M} \quad (E-1)$$

$$\ddot{X} = \frac{-A_D C_D \rho_o (\dot{X}^2 + \dot{Y}^2) \cos \alpha}{2M} - \frac{A_L C_L \rho_o (\dot{X}^2 + \dot{Y}^2) \sin \alpha}{M} \quad (E-2)$$

where

- X = range, m
- Y = altitude, m
- $\dot{X}$  = horizontal velocity
- $\dot{Y}$  = vertical velocity
- $\ddot{X}$  = horizontal acceleration
- $\ddot{Y}$  = vertical acceleration
- $C_D$  = drag coefficient
- $A_D$  = drag area
- $C_L$  = lift coefficient
- $A_L$  = lift area
- $\rho_o$  = density of air, kg/m<sup>3</sup>
- M = mass, kg
- $\alpha$  = trajectory angle, rad
- $\alpha_i$  = initial trajectory angle, rad
- g = acceleration of gravity

ORIGINAL PAGE IS  
OF POOR QUALITY





TABLE E-1  
LIST OF DIMENSIONAL PARAMETERS

<u>Parameter</u>	<u>Dimension</u>
$C_D A_D \rho_o$	M/L
$C_L A_L \rho_o$	M/L
V	L/T
M	M
g	L/T <sup>2</sup>
R	L
$\alpha$	-

TABLE E-2  
DIMENSIONLESS PARAMETERS (PI TERMS)

$\pi_1$	$\alpha$
$\pi_2$	$\frac{\rho_o C_D A_D V^2}{Mg}$
$\pi_3$	$\frac{\rho_o C_D A_D R}{M}$
$\pi_4$	$\frac{C_L A_L}{C_D A_D}$



## APPENDIX F

### ROCKETING OF STORAGE AND TRANSPORTATION VESSELS

In an accident involving propellant (propane, butane, etc.) storage systems, fragments are often generated and propelled by the force of an explosion. The fragments generated in an explosion which travel large distances typically are of much smaller mass than that of the storage vessel. However, in some instances, a large portion or portions of the vessel (greater than one-fourth) will break free intact and will travel larger distances than would be possible solely from the force of the explosion. These large fragments exhibit a rocketing behavior (see Appendix H) which results from the changing of the liquid propellant into a gas when the external pressure is released during the fracturing of the vessel. The gas escapes from the opening in the vessel in a manner similar to gas exiting a rocket motor and propels the, somewhat stabilized, fragment to great distances.

Figure F-1 schematically demonstrates the fragment rocketing process. After a portion of the vessel breaks off, the remaining portion of the tank emits gas out of its open end as the fluid in the tank vaporizes. This mass flows out of the aft end of the tank and produces a force  $F(t)$  in the direction opposite to the mass flow which varies as a function of time  $t$ , and the tank accelerates along a trajectory angle  $\theta$  with respect to the horizontal axis (ground). The force of gravity  $Mg$  also acts on the vessel inhibiting its vertical ascent. Since every action has an equal and opposite reaction, the vertical and horizontal inertial forces  $M\ddot{y}$  and  $M\ddot{x}$ , respectively, complete the simplified free-body diagram in Figure F-1. Note that for the purposes of this analysis, drag and lift forces are assumed to be much smaller than the thrust and gravitational forces and are ignored. It is also assumed that the "rocket" never changes its angle of attack  $\theta$  during its flight.

The equations of motion for this simplified rocketing problem are then

$$M(t)g + M(t)\ddot{y} - F(t)\sin \theta = 0 \quad (F-1)$$

and

$$M(t)\ddot{x} - F(t)\cos \theta = 0 \quad (F-2)$$

Note that the mass (mass of the fragment and its contents) as well as the force, changes with time. From basic rocketry, the thrust  $F$  is





$$F = A_e \left( \frac{U_e^2}{v_e g} + p_e - p_o \right) \quad (F-3)$$

where

- $A_e$  = exit area
- $U_e$  = exit velocity
- $v_e$  = specific volume of the gas
- $g$  = gravity constant
- $p_e$  = exit pressure
- $p_o$  = atmospheric pressure

Balancing the energy in the system, one has

$$h_i + q = h_e + \frac{U_e^2}{2g} \quad (F-4)$$

where

- $h_i$  = enthalpy of the gas at time  $t_i$
- $q$  = energy expended in heating the gas
- $h_e$  = enthalpy of the gas at the nozzle (exit)

If the gas expansion is isentropic,  $q = 0$ , and Equation (F-4) reduces to

$$\frac{v_e^2}{2g} = h_i - h_e \quad (F-5)$$

Flow continuity gives

$$\dot{w}v = AU \quad (F-6)$$

where  $\dot{w}$  is the mass flow rate.

To determine the fragment's trajectory, one starts with a wet vapor in a tank having known initial state conditions of pressure  $p_i$ , specific volume  $v_i$ , entropy  $s_i$ , and enthalpy  $h_i$  which can be determined from tables of thermodynamic properties. One next assumes isentropic expansion through the nozzle, That is,

$$s_{i+1} = s_e = s_i \quad (F-7)$$



where  $s_e$  is the entropy of the gas at the nozzle (exit) and  $s_{i+1}$  is the entropy at time  $t_{i+1}$ .

When the backpressure  $p_o$  is less than the critical pressure  $p_c$  given by

$$p_c = 0.58 p_i \quad (F-8)$$

the flow will be sonic and  $p_e$  in Equation (F-3) equals  $p_c$ . When the backpressure  $p_o$  is greater than the critical pressure  $p_c$ , then  $p_e$  equals  $p_o$  in Equation (F-3). Also, the pressure in the vessel at time  $t_{i+1}$  is given by

$$p_{i+1} = p_e \quad (F-9)$$

Equations (F-7) and (F-9) allow one to obtain the value for  $h_2$ , the enthalpy at time  $t_{i+1}$ , from the table of thermodynamic properties once one knows the values of  $s_e$  and  $p_e$ . Equation (F-5) gives  $U_e$ , and the thrust obtained by substitution into Equation (F-3). At the exit, Equation (F-6) gives

$$\dot{w}v_e = A_e U_e \quad (F-10)$$

where  $v_e$  is also obtained from the thermodynamic tables. In reality, the state variables of the gas within the tank change continuously, but, for computational purposes, we will assume quasi-steady flow. From Equation (F-10), one can obtain the mass flow rate  $\dot{w}$  and calculate a new total mass of the fluid after a small time  $\Delta t$  from

$$M_{i+1} = M_i - \frac{\dot{w}}{g} \Delta t \quad (F-11)$$

After this time, a new specific volume can be determined from

$$v_{i+1} = \frac{V}{gM_{i+1}} \quad (F-12)$$

where  $V$  is the total volume of the fragment. Knowing  $v_{i+1}$  one can then obtain  $p_{i+1}$  from the table of thermodynamic properties of the gas and start a second iteration.

The above iteration process continues until backpressure  $p_o$  is greater than the critical pressure in Equation (F-8). Then the flow becomes subsonic and Equation (F-3) reduces to





$$y_{i+1} = \frac{\Delta t^2}{2} \left( \frac{F_i \sin \theta}{M_i} - g \right) + \dot{y}_i \Delta t + y_i \quad (\text{F-18})$$

and

$$x_{i+1} = \frac{\Delta t^2}{2} \left( \frac{F_i \cos \theta}{M_i} \right) + \dot{x}_i \Delta t + x_i \quad (\text{F-19})$$

where  $y(0) = x(0) = 0$ .

The thermodynamic processes followed by the expanding fluids are shown on the pressure-volume ( $p - v$ ) plane and temperature-entropy ( $T - s$ ) plane in Figures 1-1 and 1-2, respectively.

A computer program entitled "THRUST" was written to perform computations for determining acceleration, velocity, and position of a thrusting fragment as a function of time, as explained. The program was written in BASIC and was run on a Tektronix 4051 microprocessor. The program was exercised using the state properties of propane gas to compare with measurements made after propane/butane accidents (Appendix H). The program was written with enough flexibility to allow for rocketing calculations of large portions of vessels containing other types of gases. To change the contained gas, one merely inputs the state variables of the appropriate gas at the beginning of the program. Linear interpolation was used to estimate values of the state variables between those acquired from the thermodynamic properties tables [Din (1962)]. Table F-1 contains a list of the program variables, a listing of the program, and sample input and output.







### VARIABLES

The program variable, identifying variable in the derivation above, definition, and units of variables in this program follow.

U U

<u>PROGRAM VARIABLE</u>	<u>VARIABLE</u>	<u>DEFINITION</u>	<u>UNITS</u>
S	s	Array of entropy liquid/vapor values for propane	cal/mole, °K
H	h	Array of enthalpy liquid/vapor values for propane	cal/mole
V	v	Array of specific volume liquid/vapor values for propane	cm <sup>3</sup> /mole
A1	--	Array for storing launch angles to be tested	degrees
P1	p1	Initial pressure	Pa
VØ		Volume of the container	m <sup>3</sup>
V1		Volume of fragment enclosure	m <sup>3</sup>
V8		Volume of liquid in the container	m <sup>3</sup>
V9		Volume of vapor in the container	m <sup>3</sup>
A		Exit area	m <sup>2</sup>
M		Mass of fragment	kg
T		Time step	s
BØ	Ø	Current launch angle	degrees
J	--	Counter used once to determine mass of gas and specific volume of frag portion immediately after breakup	--
PØ	Po	Atmospheric pressure	Pa
E1		Horizontal velocity at current time	m/s
E1		Vertical velocity at current time	m/s
T1		Current time	s
N	--	Unit conversion constant for interpolations in specific volume	J · mole/cal · kg
NI	--	Unit conversion constant for interpolations in entropy or enthalpy	m <sup>3</sup> · mole/cm <sup>3</sup> · kg
P8		Nondimensional internal pressure	--
V3		Interpolated liquid specific volume	m <sup>3</sup> /kg
V4		Interpolated vapor specific volume	m <sup>3</sup> /kg
M1		Initial mass of gas/liquid	kg
V2		Initial specific volume	m <sup>3</sup> /kg
Q1		Initial quality (based on specific volume)	--

ORIGINAL PAGE IS  
OF POOR QUALITY

<u>PROGRAM VARIABLE</u>	<u>VARIABLE</u>	<u>DEFINITION</u>	<u>UNITS</u>
P3		Pressure at nozzle	Pa
Q8		Quality after pressure release (based on specific volume)	--
Q9		Quality after pressure release (based on entropy)	--
D1		Stabilization time (no more thrust)	s
D2		Stabilization distance (no more thrust)	m
D3		Stabilization height (no more thrust)	m
T2		Time from stabilization until maximum height is reached	l
H1		Maximum height reached by fragment	m
Y3		Final vertical velocity	m/s
T3		Time from point of maximum height to the end of flight	s
T4		Total time fragment is in air	s
D		Total range of the thrusting fragment	m
X9		Horizontal (X) position of fragment at maximum height	m

ORIGINAL PAGE IS  
OF POOR QUALITY

H H H H H H H H H H H H H H H H H H H

<u>PROGRAM VARIABLE</u>	<u>VARIABLE</u>	<u>DEFINITION</u>	<u>UNITS</u>
M2		Mass of gas/liquid in thrusting portion of tank	kg
S3		Interpolated liquid entropy	J/kg
S4		Interpolated vapor entropy	J/kg
S5		Calculated entropy	J/kg
H3		Interpolated liquid enthalpy	J/kg
H4		Interpolated vapor enthalpy	J/kg
H5		Calculated enthalpy	J/kg
C		Constant (1/0.58)	--
P9		Nondimensional exit pressure	--
S6		Interpolated liquid entropy at nozzle (exit)	J/kg
S7		Interpolated vapor entropy at nozzle (exit)	J/kg
Q2		Quality at nozzle (exit)	--
H6		Interpolated liquid enthalpy at nozzle (exit)	J/kg
H7		Interpolated vapor enthalpy at nozzle (exit)	J/kg
H9		Calculated enthalpy at nozzle (exit)	J/kg
V6		Interpolated liquid specific volume at nozzle	m <sup>3</sup> /kg
V7		Interpolated vapor specific volume at nozzle	m <sup>3</sup> /kg
V5		Calculated specific volume at nozzle	m <sup>3</sup> /kg
U		Exit velocity	m/s
F		Thrust	N
W		Mass flow rate	kg/s
X2		Horizontal acceleration	m/s <sup>2</sup>
Y2		Vertical acceleration	m/s <sup>2</sup>
X1		New horizontal velocity	m/s
Y1		New vertical velocity	m/s
X		Horizontal distance (range)	m
Y		Vertical distance (height)	m
P2		Pressure in container	Pa

COMPUTER PROGRAM LISTING AND SAMPLE OUTPUT

U U



100 REM THRUST--THIS PROGRAM CALCULATES THE ACCELERATION, VELOCITY, AND  
110 REM DISTANCE TRAVELED BY A THRUSTING LIQUID  
120 REM HYDROCARBON STORAGE TANK

130 REM  
140 PAGE  
150 INIT

160 SET DEGREES

170 REM INPUT ENTROPY(S), ENTHALPY(H), AND SPECIFIC VOLUME(V) LIQUID/  
180 REM VAPOR VALUES

190 DIM S(18,4), H(18,4), V(18,4), A1(5)

200 FIND 5

210 INPUT @33:S

220 FIND 6

230 INPUT @33:H

240 FIND 7

250 INPUT @33:V

260 REM INPUT INITIAL CONDITIONS

261 DATA 5, 10, 15, 30, 45

262 READ A1(1), A1(2), A1(3), A1(4), A1(5)

270 PRINT "INITIAL PRESSURE (PA) = ";

280 INPUT P1

290 PRINT "VOLUME OF CONTAINER (CU M) = ";

300 INPUT V0

310 PRINT "VOLUME OF FRAG ENCLOSURE (CU M) = ";

320 INPUT V1

330 PRINT "VOLUME OF LIQUID (CU M) = ";

340 INPUT V8

350 PRINT "VOLUME OF VAPOR (CU M) = ";

360 INPUT V9

370 PRINT "EXIT AREA (SQ M) = ";

380 INPUT A

390 PRINT "MASS OF FRAG (KG) = ";

400 INPUT M

401 A\$="DATE "

```

402 B$="PAGE NO. "
403 PRINT "INPUT DATE";
404 INPUT Z$
430 PRINT "TIME STEP (SEC) = ";
440 INPUT T
450 FOR J1=1 TO 5
460 B0=A1(J1)
470 Z=J1
705 J=0
710 X=0
720 Y=0
730 P0=101353
740 E1=0
750 E2=0
760 T1=0
860 N=94.96
870 N1=44094
880 P8=P1/P0
890 FOR I=1 TO 18
900 IF V(I,1)>P8 THEN 920
910 NEXT I
920 V3=(V(I-1,3)+(P8-V(I-1,1))/V(I,1))-V(I-1,3))/N1
930 V4=(V(I-1,4)+(P8-V(I-1,1))/V(I,1))-V(I-1,4))/N1
940 REM
950 REM DETERMINE INITIAL MASS-F, GAS, SPECIFIC VOLUME, QUALITY, AND
960 REM MASS OF GAS WITH FRAG
970 REM
980 M1=V8/V3+V9/V4
990 V2=V0/M1
1000 Q1=(V2-V3)/(V4-V3)
1010 M2=V1/V2
1020 REM
1030 REM DETERMINE ENTROPY
1040 REM
1070 S3=(S(I-1,3)+(P8-S(I-1,1))/(S(I,1)-S(I-1,1)))*(S(I,3)-S(I-1,3)))*N

```

```

1080 S4=(S(I-1,4)+(P8-S(I-1,1))/(S(I,1)-S(I-1,1)))*(S(I,4)-S(I-1,4)))*M
1090 S5=S3+Q1*(S4-S3)
1100 IF P8<1 THEN 1582
1110 IF E1=0 THEN 1210
1120 FOR I=1 TO 18
1130 IF V(I,1)=>P8 THEN 1150
1140 NEXT I
1150 V3=(V(I-1,3)+(P8-V(I-1,1))/(V(I,1)-V(I-1,1)))*(V(I,3)-V(I-1,3)))/N1
1160 V4=(V(I-1,4)+(P8-V(I-1,1))/(V(I,1)-V(I-1,1)))*(V(I,4)-V(I-1,4)))/N1
1170 Q1=(V2-V3)/(V4-V3)
1180 REM
1190 REM DETERMINE INITIAL ENTHALPY
1200 REM
1210 H3=(H(I-1,3)+(P8-H(I-1,1))/(H(I,1)-H(I-1,1)))*(H(I,3)-H(I-1,3)))*M
1220 H4=(H(I-1,4)+(P8-H(I-1,1))/(H(I,1)-H(I-1,1)))*(H(I,4)-H(I-1,4)))*M
1230 H5=H3+Q1*(H4-H3)
1240 C=1/0.58
1250 IF P8<=C THEN 1280
1260 P9=0.58*P8
1270 GO TO 1290
1280 P9=1
1290 FOR I=1 TO 18
1300 IF S(I,1)=>P9 THEN 1350
1310 NEXT I
1320 REM
1330 REM DETERMINE QUALITY AT NOZZLE (EXIT)
1340 REM
1350 S6=(S(I-1,3)+(P9-S(I-1,1))/(S(I,1)-S(I-1,1)))*(S(I,3)-S(I-1,3)))*M
1360 S7=(S(I-1,4)+(P9-S(I-1,1))/(S(I,1)-S(I-1,1)))*(S(I,4)-S(I-1,4)))*M
1370 Q2=(S5-S6)/(S7-S6)
1380 REM
1390 REM DETERMINE ENTHALPY AT NOZZLE (EXIT)
1400 REM
1410 H6=(H(I-1,3)+(P9-H(I-1,1))/(H(I,1)-H(I-1,1)))*(H(I,3)-H(I-1,3)))*M
1420 H7=(H(I-1,4)+(P9-H(I-1,1))/(H(I,1)-H(I-1,1)))*(H(I,4)-H(I-1,4)))*M

```

```

1430 H9=H6+Q2*(H7-H6)
1440 REM
1450 REM DETERMINE SPECIFIC VOLUME AT NOZZLE (EXIT)
1460 REM
1470 V6=(U(I-1,3)+(P9-U(I-1,1)))/(U(I,1)-U(I-1,1))*((U(I,3)-U(I-1,3)))/M1
1480 V7=(U(I-1,4)+(P9-U(I-1,1)))/(U(I,1)-U(I-1,4))*((U(I,4)-U(I-1,4)))/M1
1490 V5=V6+Q2*(V7-V6)
1500 REM DETERMINE EXIT VELOCITY, THRUST, AND MASS FLOW RATE
1510 REM
1520 U=SQR(2*(H5-H9))
1530 F=A*(U*U/V5+(P9*P0-P0))
1540 W=A*U/V5
1550 M2=M2-W*T
1560 REM
1570 REM DETERMINE ACCELERATION
1580 REM
1581 IF P8>1 THEN 1590
1582 P8=1
1583 F=0
1590 X2=F*COS(B0)/(M+M2)
1600 Y2=F*SIN(B0)/(M+M2)-9.80665
1610 REM
1620 REM DETERMINE VELOCITY
1630 REM
1640 X1=F*COS(B0)/(M+M2)*T+E1
1650 Y1=(F*SIN(B0)/(M+M2)-9.80665)*T+E2
1660 REM
1670 REM DETERMINE POSITION
1680 REM
1690 X=F*COS(B0)/(M+M2)*T*T/2+E1*T+X
1700 Y=(F*SIN(B0)/(M+M2)-9.80665)*T*T/2+E2*T+Y
1710 P2=P8*P0
1720 P3=P9*P0
1730 T1=T1+T
1771 E1=X1

```

ORIGINAL PAGE IS  
OF POOR QUALITY

```
1772 E2=Y1
1775 IF F=0 THEN 2091
1780 REM
1790 REM DETERMINE NEW MASS OF GAS AND SPECIFIC VOLUME OF FRAG PORTION
1800 REM
1810 IF Y<=0 THEN 2091
1811 IF P8=1 THEN 1590
1820 V2=V1/M2
1825 IF J>0 THEN 1910
1830 FOR J=1 TO 18
1840 IF V(J,1)>P8 THEN 1910
1850 NEXT J
1860 REM
1870 REM DETERMINE PRESSURE AT WHICH QUALITIES Q8(SPECIFIC VOLUME) AND
1880 REM Q9(ENTROPY) ARE EQUAL--THIS IS THE NEW INTERNAL
1890 REM PRESSURE.
1900 REM
1910 Q8=(U2-V(J,3))/V(J,4)-V(J,3)
1920 Q9=(S5-S(J,3))/S(J,4)-S(J,3)
1930 IF V(J,1)<=0.5 THEN 1950
1940 GO TO 1960
1950 P8=1
1951 GO TO 1100
1960 IF X>0 THEN 1970
1961 P8=V(J,1)
1970 IF ABS(Q9-Q8)<=1.0E-3 THEN 1100
1971 IF P8>2 THEN 1980
1972 P8=P8-T#0.1
1973 GO TO 1990
1980 P8=P8-T
1990 IF P8>V(J-1,1) THEN 2020
2000 J=J-1
2010 GO TO 1910
2020 U6=(V(J,3)-(V(J,1)-P8)/(V(J,1)-V(J-1,1)))*(V(J,3)-V(J-1,3))
2030 U7=(V(J,4)-(V(J,1)-P8)/(V(J,1)-V(J-1,1)))*(V(J,4)-V(J-1,4))
```

```

2040 Q8=(U2-U6)/(U7-U6)
2050 S6=(S(J,3)-(S(J,1)-P8)/(S(J,1)-S(J-1,1)))*(S(J,3)-S(J-1,3)))*94.96
2060 S7=(S(J,4)-(S(J,1)-P8)/(S(J,1)-S(J-1,1)))*(S(J,4)-S(J-1,4)))*94.96
2070 Q9=(S5-S6)/(S7-S6)
2080 IF ABS(Q9-Q8)<=1.0E-3 THEN 1100
2090 GO TO 1971
2091 D1=TI
2092 D2=X
2093 D3=Y
2100 PAGE
2140 PRINT A$;Z$;
2150 PRINT B$;Z;
2160 PRINT
2180 PRINT "INITIAL CONDITIONS"
2200 PRINT
2210 PRINT USING 2220:"INITIAL PRESSURE",P1,"PASCALS"
2220 IMAGE 16A,8X,4E,1X,7A
2230 PRINT USING 2240:"VOLUME OF CONTAINER",V0,"CU M"
2240 IMAGE 19A,5X,4E,1X,4A
2250 PRINT USING 2260:"VOLUME OF FRAG ENCLOSURE",V1,"CU M"
2260 IMAGE 24A,4E,1X,4A
2270 PRINT USING 2280:"VOLUME OF LIQUID",V8,"CU M"
2280 IMAGE 16A,8X,4E,1X,4A
2290 PRINT USING 2300:"VOLUME OF VAPOR",V9,"CU M"
2300 IMAGE 15A,9X,4E,1X,4A
2310 PRINT USING 2320:"EXIT AREA",A,"SQ M"
2320 IMAGE 9A,15X,4E,1X,4A
2330 PRINT USING 2340:"MASS OF FRAG",M,"KG"
2340 IMAGE 12A,12X,4E,1X,4A
2350 PRINT USING 2360:"LAUNCH ANGLE",B0,"DEGREES"
2360 IMAGE 12A,12X,4E,1X,7A
2361 PRINT USING 2362:"TIME STEP",T,"SEC"
2362 IMAGE 9A,15X,4E,1X,3A
2370 T2=E2/9.80665

```

2380 H1=Y+0.5\*E2\*T2  
2390 Y3=SOR(2\*9.80665\*H1)  
2400 T3=Y3/9.80665  
2410 T4=T1+T2+T3  
2420 D=X+E1\*(T2+T3)  
2425 X9=D-E1\*T3  
2430 PRINT  
2440 PRINT "FINAL VALUES";  
2450 PRINT  
2451 PRINT USING 2452:"STABILIZATION X-VEL.",E1,"M/SEC"  
2452 IMAGE 20A,4X,4E,1X,5A  
2453 PRINT USING 2452:"STABILIZATION Y-VEL.",E2,"M/SEC"  
2454 PRINT USING 2455:"STABILIZATION TIME",D1,"SEC"  
2455 IMAGE 18A,6X,4E,1X,3A  
2456 PRINT USING 2457:"STABILIZATION DISTANCE",D2,"M"  
2457 IMAGE 22A,2X,4E,1X,1A  
2458 PRINT USING 2459:"STABILIZATION HEIGHT",D3,"M"  
2459 IMAGE 20A,4X,4E,1X,1A  
2460 PRINT USING 2470:"TOTAL RANGE",D,"M"  
2470 IMAGE 11A,13X,4E,1X,1A  
2480 PRINT USING 2490:"FINAL VERT. VELOCITY",Y3,"M/SEC"  
2490 IMAGE 20A,4X,4E,1X,5A  
2500 PRINT USING 2490:"FINAL HORZ. VELOCITY",E1,"M/SEC"  
2510 PRINT USING 2520:"TOTAL TIME",T4,"SEC"  
2520 IMAGE 10A,14X,4E,1X,3A  
2530 PRINT USING 2540:"MAXIMUM HEIGHT",H1,"M"  
2540 IMAGE 14A,10X,4E,1X,1A  
2541 PRINT USING 2542:"X POSITION AT MAX.HT.",X9,"M"  
2542 IMAGE 21A,3X,4E,1X,1A  
2543 PRINT USING 2544:"TIME AT MAX.HT.",T1+T2,"SEC"  
2544 IMAGE 15A,9X,4E,1X,3A  
2545 PRINT USING 2546:"INTERNAL PRESSURE",P2,"PASCALS"  
2546 IMAGE 17A,7X,4E,1X,7A  
2550 COPY  
2560 NEXT J1  
2570 END

DATE 9/30/77

PAGE NO. 1

INITIAL CONDITIONS

INITIAL PRESSURE	7.0120E+005	PASCALS
VOLUME OF CONTAINER	3.8020E+001	CU M
VOLUME OF FRAG ENCLOSURE	2.8230E+001	CU M
VOLUME OF LIQUID	3.3100E+001	CU M
VOLUME OF VAPOR	4.9160E+000	CU M
EXIT AREA	3.7500E+000	SQ M
MASS OF FRAG	3.8850E+003	KG
LAUNCH ANGLE	5.0000E+000	DEGREES
TIME STEP	5.0000E-003	SEC

FINAL VALUES

STABILIZATION X-VEL.	1.9383E+002	M/SEC
STABILIZATION Y-VEL.	6.0238E+000	M/SEC
STABILIZATION TIME	1.1150E+000	SEC
STABILIZATION DISTANCE	1.0779E+002	M
STABILIZATION HEIGHT	3.3347E+000	M
TOTAL RANGE	4.2617E+002	M = 1398 ft
FINAL VERT. VELOCITY	1.0084E+001	M/SEC
FINAL HORIZ. VELOCITY	1.9383E+002	M/SEC
TOTAL TIME	2.7576E+000	SEC
MAXIMUM HEIGHT	5.1848E+000	M = 17.01 ft
X POSITION AT MAX.HT.	2.2686E+002	M
TIME AT MAX.HT.	1.7293E+000	SEC
INTERNAL PRESSURE	1.0135E+005	PASCALS

actual range = 1029 ft = before first hitting ground

ORIGINAL PAGE IS  
OF POOR QUALITY



TABLE F-2

PROGRAM FOR STORING DATA ARRAYS

Function: This program stores data arrays in files on tape. The program is written in BASIC and is compatible with a Tektronix 4051 microprocessor.

U U U U U U U U U U U U U U U U U U U U

C-3

ORIGINAL PAGE IS  
OF POOR QUALITY

```

100 REM PROGRAM FOR STORING DATA ARRAYS-----
110 PAGE
120 INIT A(18,4)
130 DIM A(18,4)
140 FOR I=1 TO 18
150 FOR J=1 TO 4
160 PRINT "A(";I;";";J;")=?";
170 INPUT A(I,J)
180 NEXT J
190 NEXT I
200 PAGE
210 FOR I=1 TO 18
220 PRINT USING 230:A(I,1),A(I,2),A(I,3),A(I,4)
230 IMAGE 4(6D.2D,1X)
240 NEXT I
250 STOP
260 REM MAKE CORRECTIONS ABOVE OR STORE DATA BELOW-----
270 PRINT "DATA STORAGE FILE?";
280 INPUT F
290 FIND F
295 FOR I=1 TO 18
300 PRINT @33:A(I,1),A(I,2),A(I,3),A(I,4)
301 NEXT I
305 CLOSE
310 STOP
320 REM CHECK STORED DATA FILE IN REST OF PROGRAM-----
330 PAGE
340 INIT
350 PRINT "FILE NO.?"
360 INPUT G
370 FIND G
375 FOR I=1 TO 18
380 INPUT @33:A(I,1),A(I,2),A(I,3),A(I,4)
385 NEXT I

```

=====





TABLE G-2  
 LIST OF PI TERMS FOR ROCKETING FRAGMENT

$\pi_1$	$\gamma$
$\pi_2$	$\frac{R_M T}{gV^{1/3}}$
$\pi_3$	$V_v/V_1$
$\pi_4$	$\alpha$
$\pi_5$	$\frac{A}{V^{2/3}}$
$\pi_6$	$\frac{Mg}{PV^{2/3}}$
$\pi_7$	$\frac{u}{g^{1/2}V^{1/6}}$
$\pi_8$	$\frac{P}{P_a}$
$\pi_9$	$\frac{X}{V^{1/3}}$



Therefore, one finds that the distance traveled by a fragment experiencing rocketing due to the expansion of a single gas (propane in this case), depends upon the relative volumes of the vapor and liquid at fracture ( $V_v/V_l$ ), the launch angle ( $\alpha$ ), a vent area to fragment volume ( $A/V^{2/3}$ ), and a ratio of inertial force to the force of the gas inside the vessel ( $Mg/PV^{2/3}$ ). Representing these observations in equation form, one has

$$\frac{X}{V^{1/3}} = f \left( \frac{V_v}{V_l}, \alpha, \frac{A}{V^{2/3}}, \frac{Mg}{PV^{2/3}} \right) \quad (G-1)$$

Several computer runs were made to simulate actual accidents recorded in accident reports. Because these accidents were not experimental tests, some parameters such as launch angle and internal pressure of the tank at rupture had to be assumed. In spite of these obvious obstacles, the predicted values for distance traveled by the fragments, in most instances, correlated well with accident report observations. A summary of these comparative computer runs is contained in Table G-3. When one observes the sensitivity of fragment range to launch angle in this table and in Table 4-2 and keeps in mind the limitations on predicting launch angle from the accident reports, one can readily appreciate the apparent accuracy of the computer program.

Due to the complexity of the thrusting process (explained in greater detail in Appendix F) and limitations on the number of computer runs performed, no reduction of the five parameter space described by Equation (G-1) was readily apparent. Until further analysis can be performed for propane and other gases, it is recommended that the reader use the results contained in Table G-3 and Table 4-2 where appropriate or actually exercise the computer program.



TABLE G-3. COMPARISON OF COMPUTER PREDICTED RANGES AND REPORTED RANGES FOR ACCIDENTS INVOLVING ROCKETING FRAGMENTS

EXAMPLE NUMBER	SOURCE OF ACTUAL DATA	INITIAL PRESSURE (P <sub>a</sub> )	VOLUME OF CONTAINER (m <sup>3</sup> )	VOLUME OF FRAGMENT ENCLOSURE (m <sup>3</sup> )	VOLUME OF LIQUID BEFORE RUPTURE (m <sup>3</sup> )	VOLUME OF VAPOR BEFORE RUPTURE (m <sup>3</sup> )	EXIT AREA (m <sup>2</sup> )	MASS OF FRAGMENT (kg)	LAUNCH ANGLE (degrees)	CALCULATED IMPACT VELOCITY (m/s)	CALCULATED RANGE (m)	ACTUAL RANGE (m)	PERCENT DIFFERENCE IN RANGE (%)	BEST ESTIMATE FOR LAUNCH ANGLE (degrees)
1	NTSB-HAR-76-4 4/29/75	701,197	38.02	28.23	33.10	4.916	3.75	3885	5	194	426	314	36	5
2	NTSB-HAR-73-4 9/21/72	1,034,214	37.85	30.32	27.29	10.56	3.41	5083	5	189	471	398	18	5
3	NTSB-HAR-73-4 9/21/72	1,034,214	37.85	1.28	27.29	10.56	3.41	652	5	94	154	165	-6.7	5
4a	Propane Tank Explosion in San Antonio	1,378,951	1.8927	0.5513	1.586	0.3067	2.336	171	5	159	450	123	266	5-10
4b	Propane Tank Explosion in San Antonio	1,378,951	1.8927	0.5513	1.586	0.3067	2.336	171	10	154	846	123	-588	5-10
4c	Propane Tank Explosion in San Antonio	1,378,951	1.8927	0.2002	1.586	0.3067	0.6567	171	5	72	90	123	-27	5-10
4d	Propane Tank Explosion in San Antonio	1,378,951	1.8927	0.2002	1.586	0.3067	0.6567	171	10	71	179	123	66	5-10

## APPENDIX H

### Accident Data and Statistical Fitting to Fragment Data

A literature search was conducted in which accident reports and other available, related data sources were reviewed for information on characteristics of fragments and pressure waves of bursting thick-wall, compressed fluid storage and transportation vessels. Fluids and gases considered in the survey were propane, anhydrous ammonia, oxygen, argon, air and propylene. Organizations and contractors contributing sources included the National Transportation Safety Board, Naval Surface Weapons Center, NASA Langley Research Center, Department of Transportation, National Technical Information Service and Ballistic Research Laboratory. Also, an incident which occurred in San Antonio, Texas during the accumulation of data, in which a propane storage tank exploded, was personally investigated by two staff members, W. E. Baker and L. M. Vargas, for information on energy release. The missile map developed as a result of this investigation proved very useful in determining effects of fragment impact. Data obtained from this literature were organized in a logical manner for the subsequent analysis. Records of the data include the reference and date of the explosion; the quantity of the explosion source; the estimated energy release; the shape, volume, mass, material and dimensions of the container vessel; the number of fragments; the masses, ranges, trajectory elevations (if given), drag coefficients and shapes of the fragments; and any additional pertinent information. Each vessel is assigned an identifying number. Twenty-five vessel explosions form the data base. These data are given in Tables H-1 and H-2.

In order to uncover any trends in terms of different variables which affect the characteristics and effects of fragment impact and pressure waves, all the data were tabulated in terms of absolute numbers, percentiles, means, standard deviations and variations in information. The tabulations and analyses of different combinations of variables follow. A bibliography of sources utilized is also included.

#### Derivation of Fragment Range Distributions

(Figures 4-6 and 4-7)

The fragment range data for each of the six event groups (see Table 4-3) were sorted in ascending order. For event groups 1, 2, 3, 4 and 6, the values for the range for the 10th to the 90th percentile in 10% steps were identified. For event group 5, the values from the 14.3 percentile to the 85.7 percentile in 14.3% steps were identified. Table H-3 is a listing of these values.



TABLE H-1. LISTING OF EXPLOSION EVENT SOURCE AND VESSEL DATA

I. D. NUMBER	REFERENCE	EXPLOSION SOURCE				VESSEL				
		MATERIAL	QUANTITY (M <sup>3</sup> OR KG)	OTHER DATA	ESTIMATED ENERGY (JOULES)	SHAPE	DIMENSIONS	VOLUME (M <sup>3</sup> )	MASS (KG)	MATERIAL
1	NTSB-RAR-72-2	Propane	62,700 kg =	Temp: 83°F	5.417 x 10 <sup>5</sup> Joules	Railroad Tank	Inside	30.07m <sup>3</sup>	235,000 kg	A 212GrB Steel
	Train		31,300 m <sup>3</sup>	Specific Gravity:		Car #27 with	diameter:			
	Derailment					Hemispherical	2.61m & 3.06m			
	6-21-70			0.507		heads	Surface			
							Area:			
							183.14m <sup>2</sup>			
							Thickness			
							sheets 0.019m			
							0.02m			
							Outage:			
							0.34m			
							Length: 21m			
2	NTSB RAR-72-2	Propane	64,900 kg = 32,400m <sup>3</sup>	Temp: 88°F	5.954 x 10 <sup>5</sup> Joules	Tank car #28	Inside	20.71m <sup>3</sup>	162,000 kg	TC128GrB Steel
	Train			Specific Gravity:		with	Diameter:			
	Derailment			0.507		Hemispherical	3.02m			
	6-21-70					heads	Surface			
							Area:			
							181.53m <sup>2</sup>			
							Thickness			
							sheets:			
							0.016m			
							0.011m			
							Outage: 0.30m			
							Length:			
							19.1m			

TABLE H-1. LISTING OF EXPLOSION EVENT SOURCE AND VESSEL DATA (CONT.)

I.D. NUMBER	EXPLOSION SOURCE						VESSEL				
	REFERENCE	MATERIAL	QUANTITY (M <sup>3</sup> OR KG)	OTHER DATA	ESTIMATED ENERGY (JOULES)	SHAPE	DIMENSIONS	VOLUME (M <sup>3</sup> )	MASS (KG)	MATERIAL	
3	NTSB- RAR-72-2 Train Derailment 6-21-70	Propane	64,800 kg 32,300m <sup>3</sup>	Temp = 78°F Specific Gravity: 0.507	1.272 x 10 <sup>5</sup> Joules	Tank Car #30 with Hemispheri- cal heads	Inside Diameter: 3.01m Surface Area: 182.18m <sup>2</sup> Thickness sheets: 0.019m, 0.02m Outage: 0.36m	4.19m <sup>3</sup>	32,800 kg	TC128GrB Steel	
4	NTSB- RAR-72-2 Train Derailment 6-21-70	Propane	64,600 kg = 32,200m <sup>3</sup>	Temp: 80°F Specific Gravity: 0.507	3.030 x 10 <sup>5</sup> Joules	Tank Car #32 with hemispheri- cal heads	Length: 19.3m Inside Diameter: 2.66m-2.96m Surface Area: 618.13m <sup>2</sup> Outage: 0.36m Length: 70m	12.21m <sup>3</sup>	95,600 kg	AZ12GrB steel	

TABLE H-1. LISTING OF EXPLOSION EVENT SOURCE AND VESSEL DATA (CONT.)

I.D. NUMBER	REFERENCE	EXPLOSION SOURCE					VESSEL				
		MATERIAL	QUANTITY (M <sup>3</sup> OR KG)	OTHER DATA	ESTIMATED ENERGY (JOULES)	SHAPE	DIMENSIONS	VOLUME (M <sup>3</sup> )	MASS (KG)	MATERIAL	
5	NTSB BAR-72-2 Train Derailment 6-21-70	Propane	65,400 kg = 32,600m <sup>3</sup>	Temp: 80° F Specific Gravity: 0.507	1,288 x 10 <sup>6</sup> Joules	Tank Car #33 with hemispherical heads	Inside Diameter: 2.997m Surface Area: 604.42m <sup>2</sup> Thickness: Sheets 0.016m, 0.017m Outage: 0.36m Length: 64.2m	10.73m <sup>3</sup>	83,900 kg	TC128GrB Steel	
6	NTSB 1-25-69 Train Derailment (wheel fracture)	LPG	116m <sup>3</sup>	Specific Gravity: 0.505 Temp: 157°F	3814 Joules	Section of Tank car (POTX car 261) with hemispherical heads	About 18.29m long	3.253m <sup>3</sup> (estimated from BRL report)	25,400kg	ASTMA212 Grade B or AAR TC128 Grade B steel	
7	NTSB 1-25-69 Train Derailment (wheel fracture)	LPG	116m <sup>3</sup>	Specific Gravity: 0.505 Temp: 157°F	3814 Joules	Section of tank car with hemispherical heads (POTX 269)	About 18.29m long	3.253m <sup>3</sup> (estimated from BRL report)	25,400 kg	ASTMA212 Grade B or AAR TC128 Grade B steel	

TABLE H-1. LISTING OF EXPLOSION EVENT SOURCE AND VESSEL DATA (CONT.)

I.D. NUMBER	REFERENCE	EXPLOSION SOURCE					VESSEL				
		MATERIAL	QUANTITY (M <sup>3</sup> OR KG)	OTHER DATA	ESTIMATED ENERGY (JOULES)	SHAPE	DIMENSIONS	VOLUME (M <sup>3</sup> )	MASS (KG)	MATERIAL	
8	NTSB	LPG	114m <sup>3</sup>	Specific Gravity: 0.505	3814 Joules	Section of tank car with hemispherical heads (GALX car 557)	About 18.29m long	3.253m <sup>3</sup> (estimated from BRL report)	25,400 kg	ASTM A212	
	1-25-69									Grade B or AAR TC128	
	Train			Temp: 157°F						Grade B steel	
	Derailment (wheel fracture)										
9	NTSB	LPG	114m <sup>3</sup>	Specific Gravity: 0.505	3814 Joules	Section of Tank car with hemispherical heads (POTX 162)	About 18.29m long	3.253m <sup>3</sup> (estimated from BRL report)	25,400 kg	ASTM A212	
	1-25-69									Grade B or AAR TC128	
	Train			Temp: 157°F						Grade B Steel	
	Derailment (wheel Fracture)										
10	NTSB	LPG	114m <sup>3</sup>	Specific Gravity: 0.505	3814 Joules	Section of tank car with hemispherical heads (GATX 89971)	About 18.29m long	3.253m <sup>3</sup> (estimated from BRL report)	25,400 kg	ASTM A212	
	1-25-69									Grade B or AARTC 128	
	Train			Temp: 157°F						Grade B steel	
	Derailment (wheel fracture)										

TABLE H-1. LISTING OF EXPLOSION EVENT SOURCE AND VESSEL DATA (CONT.)

I.D. NUMBER	REFERENCE	EXPLOSION SOURCE				VESSEL				
		MATERIAL	QUANTITY (M <sup>3</sup> OR KG)	OTHER DATA	ESTIMATED ENERGY (JOULES)	SHAPE	DIMENSIONS	VOLUME (M <sup>3</sup> )	MASS (KG)	MATERIAL
11	NTSB PAR-75-3 Pipeline Accident 3-15-74	Natural gas		Pressure: 3.427 x 10 <sup>6</sup> Pa Temp: 40°F-50°F		Cylindrical pipe	Diameter: 0.3048m Thickness: 0.00254m (corroded from 0.0064m) Length?			Steel (pipe was not cathodically protected)
12	NTSB PAR-76-2 Pipeline Accident 4-22-74	AIR (Tank partially filled with water)		Pressure: 1.2066 x 10 <sup>6</sup> Pa		Cylindrical tank; concave bottom, convex top; designed to operate at maximum pressure of 75 psig	1.524m high Diameter: 0.61m Length: ?	0.45m <sup>3</sup>	3520 kg	Steel
13	NTSB PAR-76-8 9-1-75	LPG	125m <sup>3</sup>	Pressure: 2.41 x 10 <sup>6</sup> Pa Temp: 157°F (estimated from BRL report)	3920 Joules	Cylindrical tank car #27 with hemispherical heads (NATX34071)	None given	3.253m <sup>3</sup> (estimated from BRL report)	25,400kg	DOT 112A340W & DOT 114A340W Tank cars steel

TABLE H-1. LISTING OF EXPLOSION EVENT SOURCE AND VESSEL DATA (CONT.)

I.D. NUMBER	EXPLOSION SOURCE					VESSEL					
	REFERENCE	MATERIAL	QUANTITY (M <sup>3</sup> OR KG)	OTHER DATA	ESTIMATED ENERGY (JOULES)	SHAPE	DIMENSIONS	VOLUME (M <sup>3</sup> )	MASS (KG)	MATERIAL	
14	NTSB-76-8	LPG	125m <sup>3</sup>	Tank	3920	Cylindrical	None	3.253m <sup>3</sup>	25,400kg	DOT 112A340W 4	
	BAR-76-8			Pressure: 2.41 x 10 <sup>6</sup> Pa	Joules	tank car #32	given	(estimated from BRL report)	DOT 114A340W		
	9-1-75			Temp: 157° F		with hemispherical heads (GATX 83367)			tank cars	steel	
				(estimated from BRL report)							
15	NTSB-76-8	LPG	125m <sup>3</sup>	Tank	3920	Cylindrical	None	3.253m <sup>3</sup>	25,400kg	DOT 112A340W 6	
	BAR-76-8			Pressure: 2.41 x 10 <sup>6</sup> Pa	Joules	tank car #33	given	(estimated from BRL report)	DOT 114A340W		
	9-1-75			Temp: 157° F		with hemispherical heads (GATX 83340)			Tank cars	steel	
				(estimated from BRL report)							
16	NTSB-71-6	Liquidified Oxygen (LOX)	8.21m <sup>3</sup>	Pressure in tank: at time of delivery	?	Cargo tank assembly with hemispherical heads	None	8.97m <sup>3</sup>	70,200kg	Tank surrouned by about 0.15m of powdered inert insulating material contained in a steel jacket	
	5-30-70			68,948Pa-82,737Pa							
				Temp: was refrigerated							
				in tank at 290° F							
			Purity in tank: 99.73%								



TABLE H-1. LISTING OF EXPLOSION EVENT SOURCE AND VESSEL DATA (CONT.)

I. D. NUMBER	REFERENCE	EXPLOSION SOURCE					VESSEL				
		MATERIAL	QUANTITY (M <sup>3</sup> OR KG)	OTHER DATA	ESTIMATED ENERGY (JOULES)	SHAPE	DIMENSIONS	VOLUME (M <sup>3</sup> )	MASS (KG)	MATERIAL	
18	NTSB-	Anhydrous ammonia	72,400 kg = 93,800m <sup>3</sup>	Temp: 4°F (ambient temp)	1.487 x 10 <sup>5</sup> Joules	Cylindrical Tank	18.26m long	3.263m <sup>3</sup>	25,500 kg	Steel plate	
	BAR-71-2					car with hemispherical heads					
	Train					3.023m in-diameter shell					
	Deraillment & Collision			Pressure: 1.37 x 10 <sup>5</sup>		other train derailed;					
	2-18-69					released gas to form ammonia cloud					
						thickness: 0.017m					
						car length: 19.28m					
						wheels = 0.91m					
						100 ton trucks					
						15.95m apart					
						other train was traveling about 52 mph at time of deraillment(max speed at that section of track was 50 mph)					

TABLE H-1. LISTING OF EXPLOSION EVENT SOURCE AND VESSEL DATA (CONT.)

I.D. NUMBER	REFERENCE	EXPLOSION SOURCE				VESSEL				
		MATERIAL	QUANTITY (M <sup>3</sup> OR KG)	OTHER DATA	ESTIMATED ENERGY (JOULES)	SHAPE	DIMENSIONS	VOLUME (M <sup>3</sup> )	MASS (KG)	MATERIAL
19	BRL R 1935 September 1976	LPG (97.96% Propane)	About 125m <sup>3</sup>	Pressure: 9.63 x 10 <sup>5</sup> Pa Temp: 70°F tank pressure at rupture: 2.41 x 10 <sup>6</sup> Pa	3920 Joules	Cylindrical tank car with ellipsoidal heads (RAX 201)	18.3m long 3.05m in diameter shell thickness 0.0159m Avg. tank temp: 157°F	3.253m <sup>3</sup>	25,400 kg	TC-128 steel
20	NTSB- BAR-73-4 Multiple- vehicle collision 9-21-72	Propylene LPG	27.29m <sup>3</sup>	Vapor Pressure: 1.034 x 10 <sup>6</sup> Pa Temp: 65°F Weight: 14,217.7 kg	?	Cylindrical cargo tank semitrailer with hemispherical heads	Cylinder wall thick- ness: 0.0119m head thick- ness: 0.00635m tank length 11.57m semitrailer length: 1.83m tank diam- eter: 2.11m (outside)	1.001m <sup>3</sup>	7840 kg	Quenched-and-tempered steel

TABLE H-1. LISTING OF EXPLOSION EVENT SOURCE AND VESSEL DATA (CONT.)

I.D. NUMBER	REFERENCE	EXPLOSION SOURCE					VESSEL				
		MATERIAL	QUANTITY (M <sup>3</sup> OR KG)	OTHER DATA	ESTIMATED ENERGY (JOULES)	SHAPE	DIMENSIONS	VOLUME (M <sup>3</sup> )	MASS (KG)	MATERIAL	
21	NSWC/	Argon	28.2 kg =	Pressure: 2.438 x 10 <sup>9</sup>	Spherical	Internal	0.0283m <sup>3</sup>	46.2 kg	T-1 steel		
	WOL/TR	15.8m <sup>3</sup>	1.034 x 10 <sup>8</sup>	radius:0.19m (Internal)							
	75-87		Pa		Shell						
	2-9-76			Temp: 17°C	thickness:						
						0.012m					
22	NSWC/	Argon	35.2 kg =	Pressure: 6.078x10 <sup>9</sup>	Spherical	Internal	0.0283m <sup>3</sup>	136 kg	T-1 steel		
	WOL/TR	19.7m <sup>3</sup>	2.068x10 <sup>8</sup> Pa	radius:0.19m (Internal)							
	75-87			Temp:17°C	Shell						
	2-9-76				thickness:						
						0.025m					
23	NSWC/	Argon	39.3 kg =	Pressure: 1.133x10 <sup>10</sup>	Spherical	Internal	0.0283m <sup>3</sup>	187 kg	T-1 steel		
	WOL/TR	22.0m <sup>3</sup>	3.447x10 <sup>9</sup> Pa	radius:0.19m (Internal)							
	75-87			Temp:17°C	Shell						
	2-9-76				thickness:						
						0.044m					
					External						
					radius:						
					0.23m						

TABLE H-1. LISTING OF EXPLOSION EVENT SOURCE AND VESSEL DATA (CONT.)

I.D. NUMBER	REFERENCE	EXPLOSION SOURCE				VESSEL				
		MATERIAL	QUANTITY (M <sup>3</sup> OR KG)	OTHER DATA	ESTIMATED ENERGY (JOULES)	SHAPE	DIMENSIONS	VOLUME (M <sup>3</sup> )	MASS (KG)	MATERIAL
24	NTSB- BAR-76-4 4-29-75	LPG (Half propane half butane)	33.11m <sup>3</sup>	Temp: 80°F	549.6 Joules	Cylindrical cargo tank on semitrailer with hemispherical heads attached to tractor	Tank length: 0.810m 10.87m Inside diameter: 2.18m Thickness: 0.0096m (min) Tank head thickness: 0.0064m Design Pressure: 1.724x10 <sup>6</sup> Pa at 150°F Actual internal pressure: 5.998x10 <sup>5</sup> Pa	0.810m <sup>3</sup>	6340 kg	U.S. Steel T-1
25	Propane tank Explosion 8-2-77	Propane	1.586m <sup>3</sup>	Relief valve triggered at 200 psi, wide at 225 psi	24.78 Joules	Cylindrical tank with hemispherical heads	External diameter .955 m Thickness: 0.0794m Head thickness: 0.0508m Tank length: 3.089m, CYL. length: 2.134m	0.0654m <sup>3</sup>	512 kg	Steel



TABLE H-2. LISTING OF EXPLOSION EVENT FRAGMENT DATA (CONT.)

I.D. NUMBER	TOTAL NUMBER FRAGMENTS	MASSES (KG)	RANGE (M)	APPARENT TRAJECTORY ELEVATION	DRAG COEFFICIENT $C_D$	SHAPES OR OTHER DESCRIPTION	REMARKS
3	2		182m		0.82	about 1/2 of the tank (north end)	destroyed 2 buildings after going through them & came to a stop in a third one
			20.0m			other end -	remained in general derailment area
							The remaining cars of the train were rear-ranged with this explosion
			0.0m	--		car split	both fragments remained stationary;
			0.0m	--		longitudinally	did not separate into hurling pieces
			5.0m			west end -	did not travel beyond general area; struck next car
			15.24m		1.20	other end -	piece bounced off #39 & ignited propane in #35





TABLE H-2. LISTING OF EXPLOSION EVENT FRAGMENT DATA (CONT.)

FRAGMENTS							
I.D. NUMBER	TOTAL NUMBER FRAGMENTS	MASSES (KG)	RANGE (M)	APPARENT TRAJECTORY ELEVATION	DRAG COEFFICIENT $C_D$	SHAPES OR OTHER DESCRIPTION	REMARKS
12	1			90°	1.20		bottom blew out of the tank, rocketing it upward to strike a 0.152m gas service line above it
13	2		0.0m		1.20	16.15m long - piece	found next to track, split open on top, up-right
			27.4m		1.20	6.096m long - piece	
14	3		4.57m		1.98	main section -	tank shell flattened into a sheet
			19.8m		1.20	end piece (a-bout 3.048m long)	found upright
			19.8m		1.20	other end (a-bout 3.048m long)	located 39.62m from first end
						piece	



TABLE H-2. LISTING OF EXPLOSION EVENT FRAGMENT DATA (CONT.)

I.D. NUMBER	TOTAL NUMBER FRAGMENTS	MASSES (KG)	RANGE (M)	APPARENT TRAJECTORY ELEVATION	DRAG COEFFICIENT $C_D$	FRAGMENTS	
						SHAPES OR OTHER DESCRIPTION	REMARKS
17	35	④ 1930kg	208m		0.82	④ 0.91m diameter cylindrical pipe	see diagram
						Thickness: 0.0095m	
						Length: ⑤ very small piece	" "
			146m		1.17	⑥ of 0.91m in diameter pipe	
						⑦ very small piece	" "
			185m		1.17	⑧ of 0.91m in diameter cylindrical pipe	
						⑨ 0.91m in diameter cylindrical pipe; thickness: 0.0095m; Length: 6.33m	
		⑩ 1340kg	40.0m		0.82	⑪ long piece of 0.91m in diameter pipe; thickness: 0.0095m	
						⑫ 0.91m in diameter pipe; thickness: 0.0095m	
		⑬ 1440kg	44.0m		1.20	⑭ long piece of 0.91m in diameter pipe; thickness: 0.0095m	
						⑮ 0.91m in diameter pipe; thickness: 0.0095m	
						⑯ Length: 6.77m	
		⑰ 1627kg	54.2m		1.20	⑱ long piece of 0.91m in diameter pipe; thickness: 0.0095m	
						⑲ Length: 7.65m	

TABLE H-2. LISTING OF EXPLOSION EVENT FRAGMENT DATA (CONT.)

I. D. NUMBER	TOTAL NUMBER FRAGMENTS	FRAGMENTS					REMARKS
		MASSES (KG)	RANGE (M)	APPARENT TRAJECTORY ELEVATION	DRAG COEFFICIENT $C_D$	SHAPES OR OTHER DESCRIPTION	
17	35	⑩ 1082kg	63.00m		1.20	⑩ 0.91m in diameter cylindrical pipe Thickness: 0.0095m	See Diagrams
cont'd.							
		⑪ 1039kg	66.4m		0.47	⑪ Length: 5.089m ⑫ 2.4m in diameter spheres; thickness = 0.032m	" "
		⑬ 2020kg	73.1m		1.20	⑬ long piece at 0.91m diameter cylindrical pipe Thickness: 0.0095m	" "
				/			
		⑭	67.7m		1.17	⑭ Length: 9.5m ⑮ very small piece of 0.91m in diameter cylindrical pipe, 0.0095m thick	" "
		⑯ 93.6kg	63.7m		1.17	⑯ small piece of 0.91m diameter cylindrical pipe; 0.0095m thick	" "
		⑰ 2007kg	68.4m		1.20	⑰ Length: 0.44m ⑱ 0.91m diameter cylindrical pipe 0.0095m thick Length: 9.44m	" "





TABLE H-2. LISTING OF EXPLOSION EVENT FRAGMENT DATA (CONT.)

I. D. NUMBER	TOTAL NUMBER FRAGMENTS	FRAGMENTS						REMARKS
		MASSES (KG)	RANGE (M)	APPARENT TRAJECTORY ELEVATION	DRAG COEFFICIENT $C_D$	SHAPES OR OTHER DESCRIPTION		
17	35	(27) 399kg	5.42m		1.20	(27) 0.91m diameter cylindrical pipe		
Cont'd.								
		(28) 242kg	292m		1.17	0.0095m thick Length: 1.88m (30) small piece of		
						0.91m diameter		
						cylindrical pipe		
						0.0095m thick		
		(29) 238kg	116m		1.20	Length: 1.13m (32) 0.91m diameter		
						cylindrical pipe		
						0.0095m thick		
						Length: 1.12m (33) very small frag-	does not appear on reconstruction picture	
		(31)	48.1m		0.82	ment very small frag-	does not appear on reconstruction picture	
		(32)	40.6m		1.20	ment very small frag-	reconstruction picture does not appear on	
		(33)	102.3m		0.52	ment very small piece	reconstruction picture	
						of 0.91m diam-		
						eter cylindrical		
						pipe, 0.0095m		
						thick		









TABLE H-2. LISTING OF EXPLOSION EVENT FRAGMENT DATA (CONT.)

I.D. NUMBER	TOTAL NUMBER FRAGMENTS	FRAGMENTS					REMARKS
		MASSES (KG)	RANGE (M)	APPARENT TRAJECTORY ELEVATION	DRAG COEFFICIENT $C_D$	SHAPES OR OTHER DESCRIPTION	
22	2 each for 2 shots	(Shot No.) 7a 42.4kg	0.0m		0.165	top	both found inside the arena; average velocity for bottom section = 83.52m/sec
		7b 49.0kg	0.0m		0.165	bottom	
23	2 each for 2 shots	(Shot No.) 4a 117kg	0.0m		0.165	large portion -	found inside arena; avg velocity = 63.86m/sec never found both found inside the arena
		4b 70.3kg	max. of 220.07m	78°	0.165	small portion -	
		5a 123kg	0.0m		0.165	large portion	
		5b 64.4kg	0.0m		0.165	small portion	
24	25	1	504m			large forward -	struck on elevated sign first hit ground at 313.64m, bounced up, touched again after 84.73m and demolished a mobile home; bounced into the air & went another 105.77m over a second mobile home which caught fire & struck a third mobile home to stop 504.14m from explosion point
						section	





TABLE H-2. LISTING OF EXPLOSION EVENT FRAGMENT DATA (CONT.)

I. D. NUMBER	TOTAL NUMBER FRAGMENTS	FRAGMENTS						REMARKS
		MASSES (KG)	RANGE (M)	APPARENT TRAJECTORY ELEVATION	DRAG COEFFICIENT $C_D$	SHAPES OR OTHER DESCRIPTION		
25	11	(Fragment ID) ① 104kg	31.4m to wall, then another 4.57m		0.47	hemispherical end cap; diameter = .0144m, .00508m thick	struck wall 2.8448m above ground level; impact on wall also included	
		① 171.1kg	123m		1.20	main portion of cylinder; 2.1336m long; .07144m circum-ference; .07144m thick	one attached end cap	
		① 52.2kg	119m		0.47	section of end cap (about 1/2)	located in creek 3.05m from the main portion of the cylinder	
		① 0.0341kg	31.4m		1.05	cubical section of cement block	tank was sitting on these concrete blocks	
		② 1.56kg	40.2m		1.55	fairly rectangular		
		③ 1.22kg	17.7m		2.05	section of block		
		④ 0.998kg	25.2m		1.55	pie-shaped piece of block	12.2m from a van	
		⑤ 1.22kg	15.2m		0.80	sort of cubical section of block		
		⑥ 0.967kg	28.3m		2.05	rectangular section of block		



TABLE H-3. PERCENTILES FOR PLOTTING FRAGMENT RANGES OF THE SIX EVENT GROUPS

Percent	Event Group Numbers					
	1	2	3	4	5	6
10.0	20.00	15.24	22.35	32.00		15.24
14.3					168.27	
20.0	40.00	19.81	40.64	51.51		17.68
28.6					202.69	
30.0	60.96	27.43	54.19	60.65		25.20
40.0	91.44	30.48	66.38	76.02		28.35
42.9					220.07	
50.0	161.00	60.96	68.41	85.04		31.39
57.1					346.25	
60.0	182.88	94.50	88.05	136.86		41.76
70.0	182.88	133.40	109.73	164.59		58.83
71.4					423.37	
80.0	228.60	167.64	115.82	238.96		119.79
85.7					512.06	
90.0	487.68	335.28	206.59	373.73		122.83

U U U U E E U U E U E U U U U U U U U U U



Figures H-1 through H-6 are plots of the percentile points on log normal probability paper for each of the respective six events groups.

Table H-4 is a listing of the estimated means and standard deviations for the log normal (to the base e) distributions.

A "W" statistic [see Hahn and Shapiro (1967)] for goodness of fit was calculated for each of the distributions. The approximate probability of obtaining the calculated test statistic, given that the chosen distribution is correct, was then determined. The results are shown in Table H-5.

#### Deviation of Fragment Mass Distributions

(Figures 4-8 and 4-9)

Sufficient pertinent mass data were available only from event groups 2, 3 and 6. Table H-6 is a listing of the percentiles of these event groups.

Figures H-7 through H-9 are plots of the percentile points on log normal probability paper for each of the respective event groups.

Table H-7 is a listing of the estimated means and standard deviations for the log normal (to the base e) distributions.

The calculated "W" statistic along with the approximate probability of obtaining the calculated test statistic, given that the chosen distribution is correct are presented for each of the three event groups in Table H-8.

#### Correlation Analyses of Fragment Range and Fragment Mass Within Event Groups

(Figures 4-11 and 4-12)

For each of the three event groups (2, 3 and 6) with sufficient fragment range and mass data, three models were exercised to determine the degree of correlation between fragment range and mass. The three models and equivalent equations were:

- 1) Linear -

$$R = a + b M$$

- 2) Power Curve -

$$R = aM^b$$



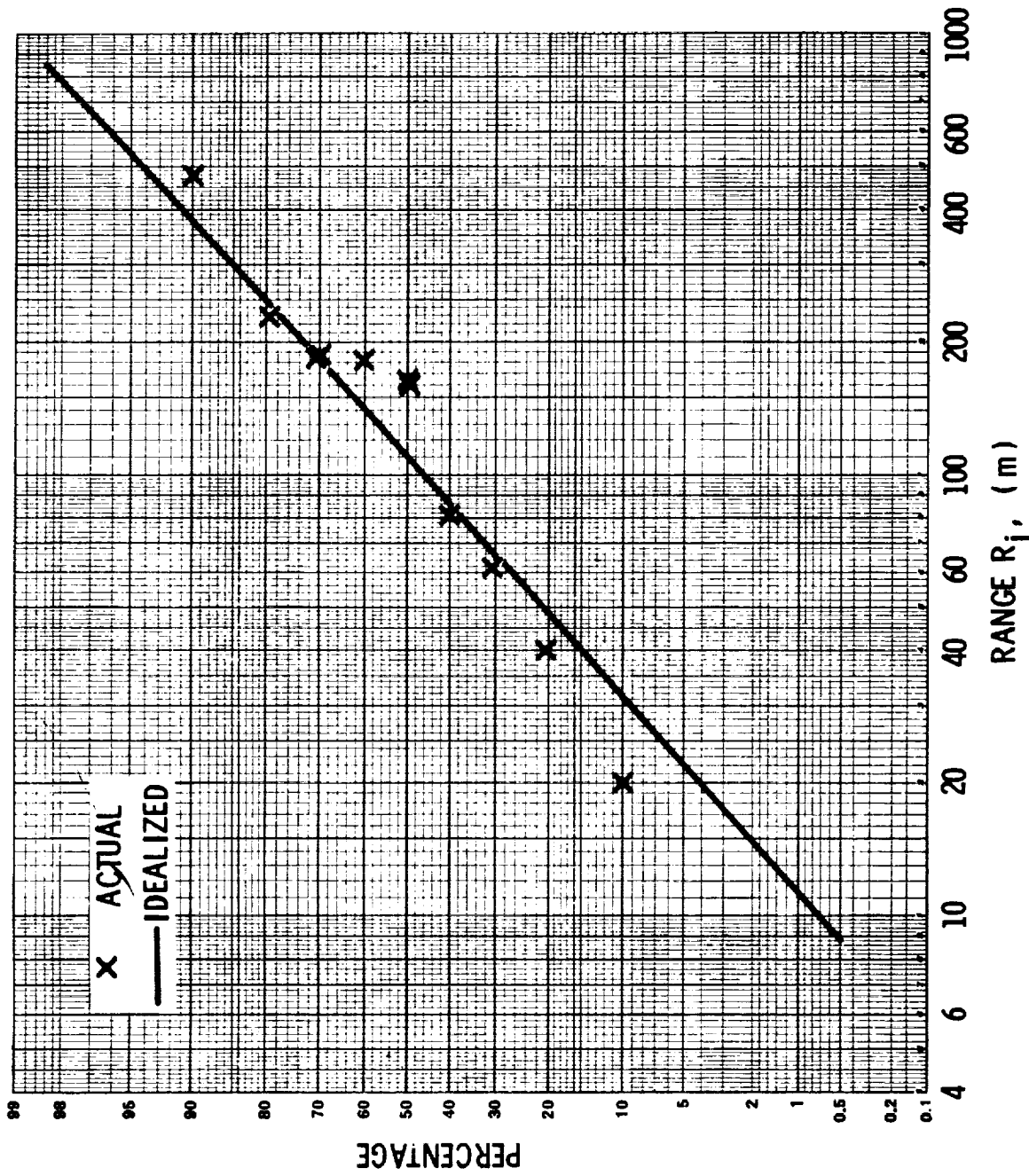


FIGURE H-1. EVENT GROUP 1 (EVENTS 1,2,3,18) PROBABILITY DISTRIBUTION RANGE

ORIGINAL PAGE IS  
 OF POOR QUALITY



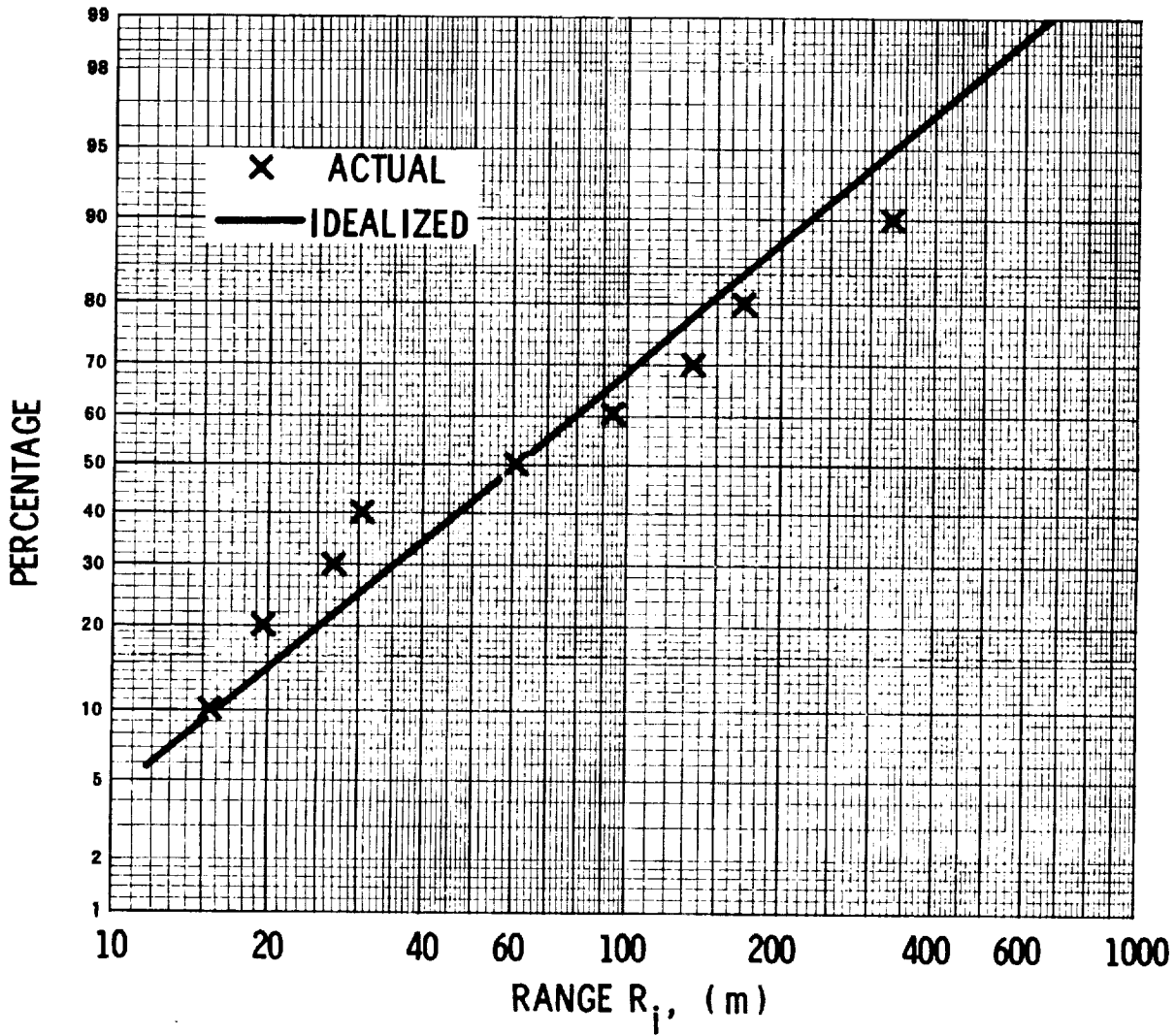


FIGURE H-2. EVENT GROUP 2 (EVENTS 6,7,8,9,10,13,14,15 and 19)  
PROBABILITY DISTRIBUTION, RANGE

U U U E U U U E U U U E U U U U U U U E U







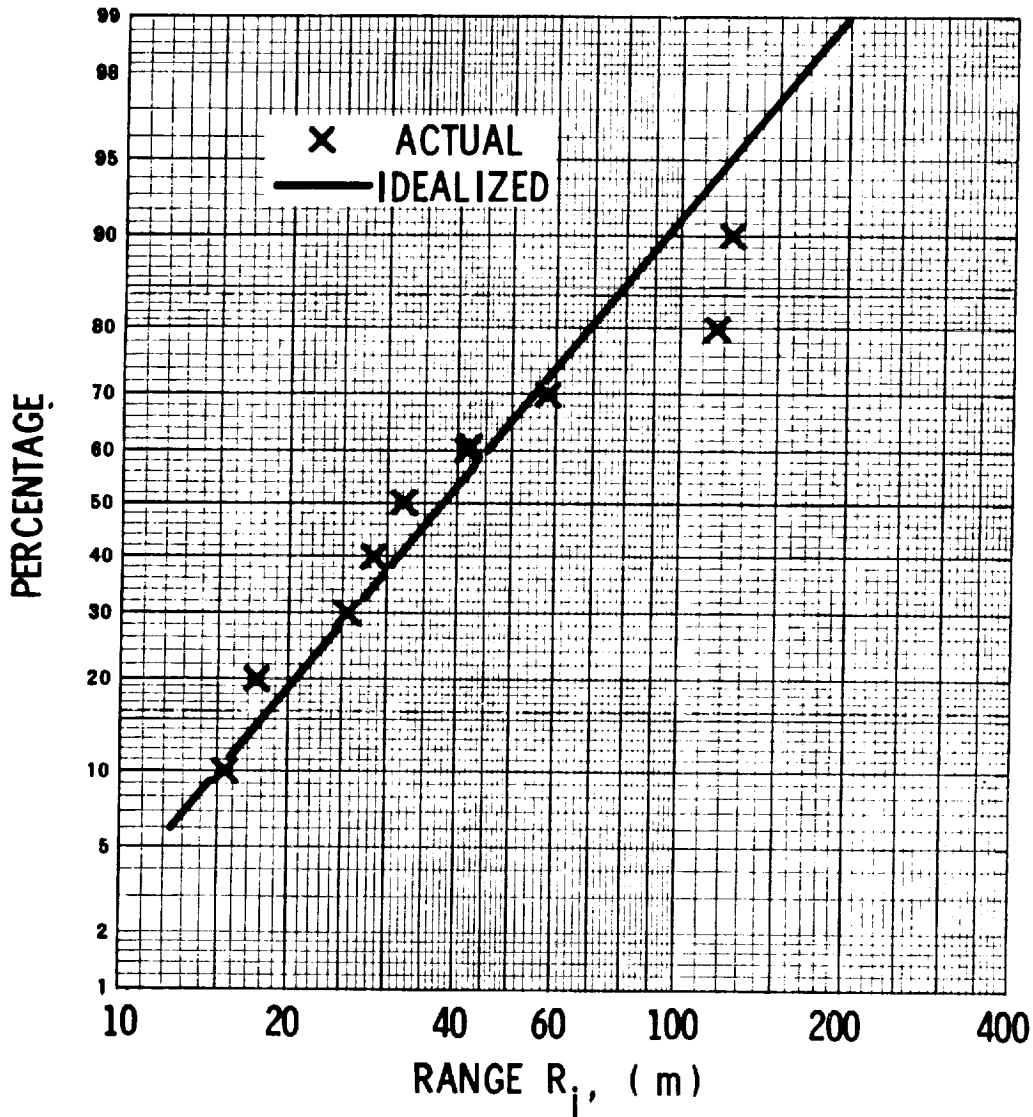


FIGURE H-6. EVENT GROUP 6 (EVENT 25) PROBABILITY DISTRIBUTION, RANGE

U U U E U U E U U E U U E U U E U U E U

TABLE H-4. LISTING OF ESTIMATED MEANS AND STANDARD DEVIATIONS FOR LOG-NORMAL RANGE DISTRIBUTIONS (TO THE BASE e) FOR THE SIX EVENT GROUPS

<u>Event Group No.</u>	<u>Estimated Mean</u>	<u>Estimated Standard Deviation</u>
1	4.569939	0.906041
2	4.103086	1.062895
3	4.275966	0.646206
4	4.633257	0.785540
5	5.660840	0.446785
6	3.668606	0.758061



TABLE H-5. SUMMARY OF "W" TEST ON NORMALITY FOR  
 FRAGMENT RANGE DISTRIBUTIONS FOR  
 EVENT GROUPS 1 THROUGH 6

<u>Event Group No.</u>	<u>"W"</u>	<u>Probability</u>
1	.964	.82
2	.951	.68
3	.986	.98
4	.980	.95
5	.936	.57
6	.917	.28

As it is customary to consider values exceeding 2 to 10% as adequate grounds for not rejecting the hypothesis that the data belong to the chosen distribution, the fits for the six event groups are more than adequate.





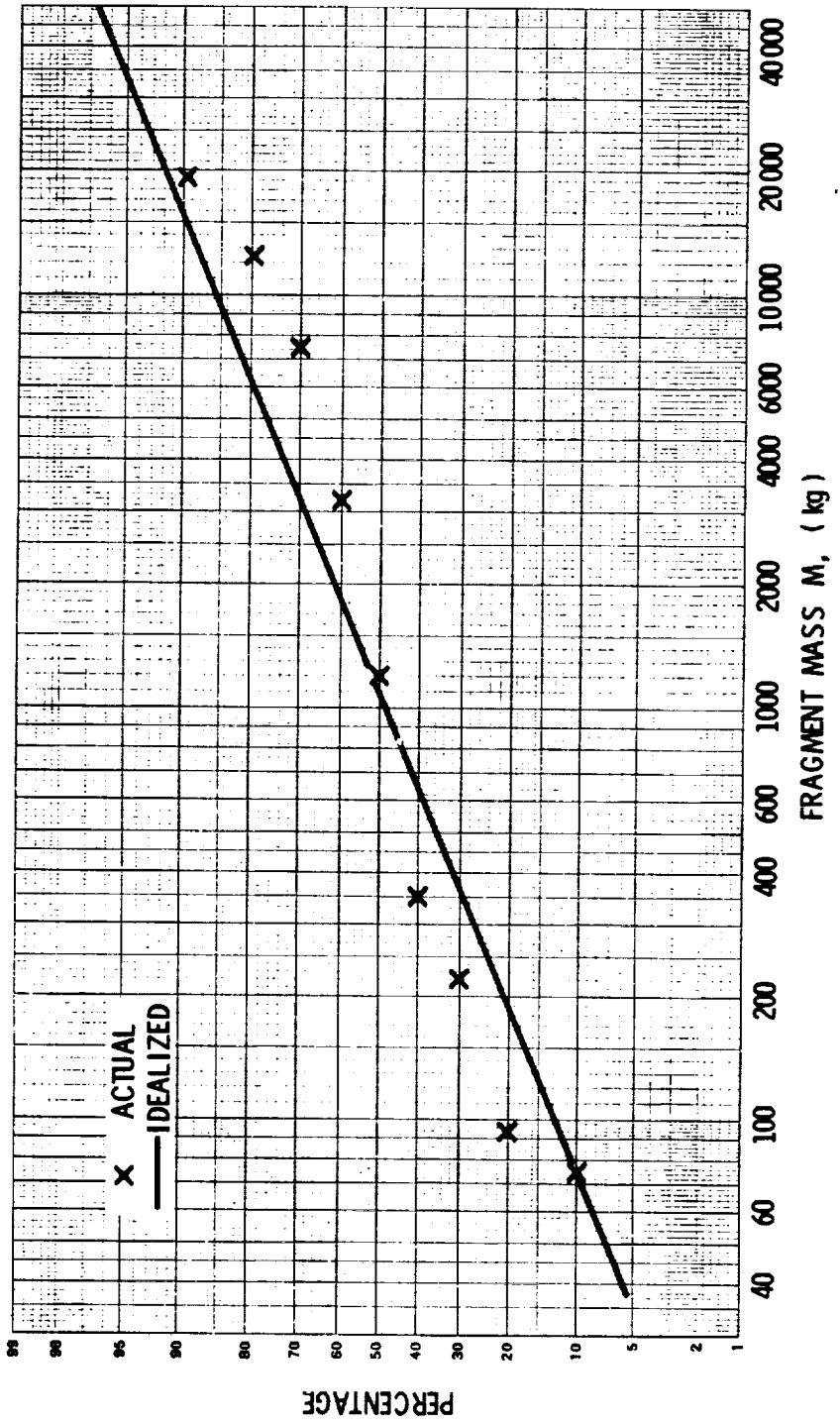


FIGURE H-7. EVENT GROUP 2 (EVENTS 6, 7, 8, 9, 10, 13, 14, 15, 19)  
PROBABILITY DISTRIBUTION, MASS





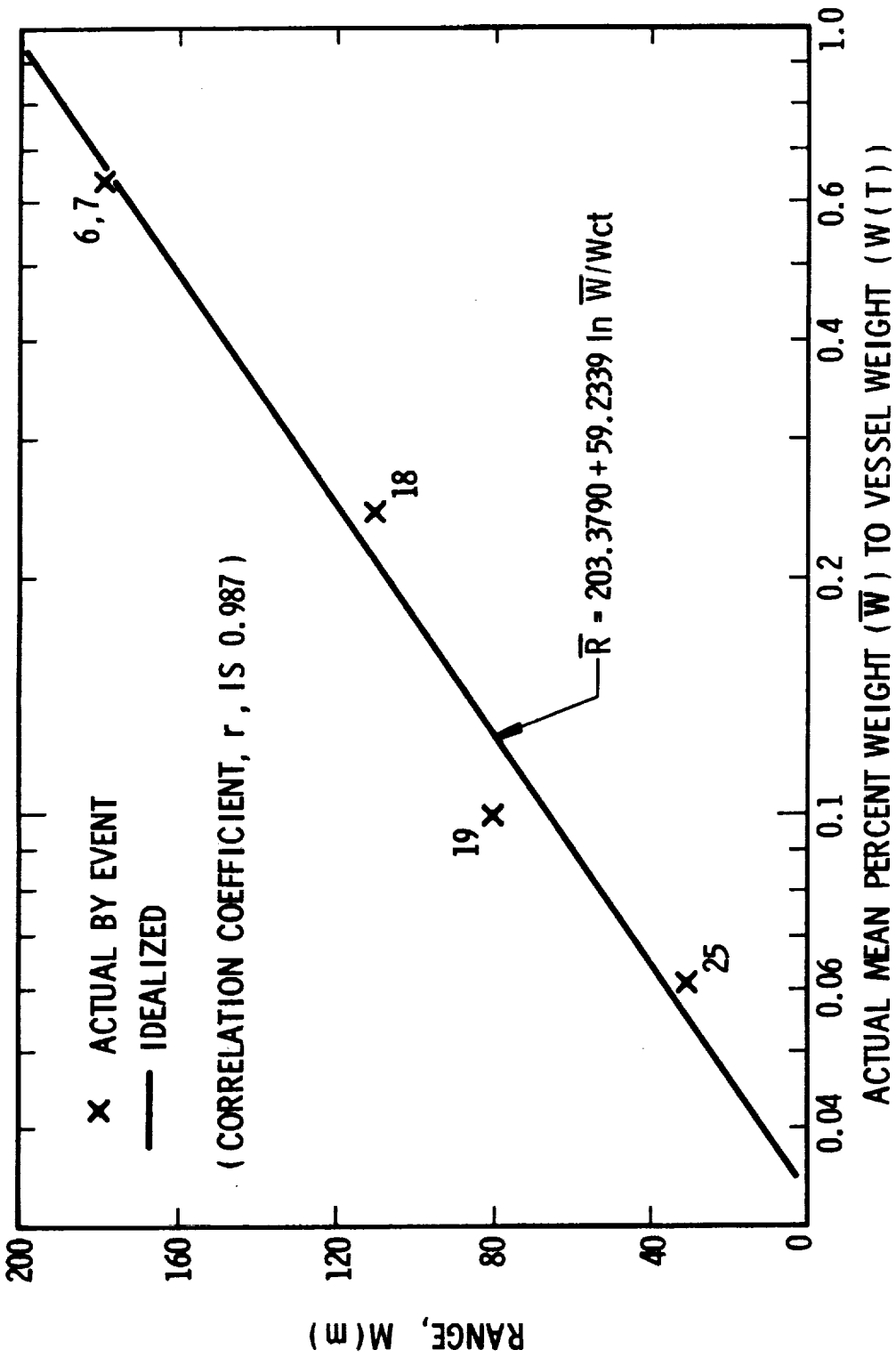


FIGURE H-10. RANGE VERSUS THE RATIO OF MEAN FRAGMENT WEIGHT TO TANK WEIGHT FOR CYLINDRICAL VESSELS (EVENTS 6 and 7, 18, 19, 25)

ORIGINAL PAGE IS  
OF POOR QUALITY



3) Logarithmic Curve -

$$R = a + b \ln M$$

Table H-9 is a listing of fragment range and mass for the three event groups. Table H-10 contains a listing of the estimated parameters and correlation coefficients for each model for each event group.

From Table H-10, the largest correlation coefficients over each of the three models are .79, .35, and .68 for the event groups 2, 3 and 6, respectively. These values of  $r$  can be transformed to a normal variate,  $Z$ , by the following formula [Arkin and Colton (1950)]:

$$Z = .5 [\ln (1 + r) - \ln (1 - r)] \quad (H-1)$$

The standard error of  $Z$ ,  $\sigma_Z$ , is:

$$\sigma_Z = 1/(N - 3) \quad (H-2)$$

where  $N$  is the number of fragment range-mass pairs in Table H-9 an event group.

A 95% confidence limit ( $L_Z$ ) on the range of sampling variation on  $Z$  can be set by:

$$L_Z = Z \pm 1.96 \sigma_Z \quad (H-3)$$

Then, the 95% confidence limit on  $r$  can be established by substituting the two values of  $L_Z$  (one at a time) into Equation (H-1) for  $Z$ , and solving for  $r$ .

The 95% confidence limits on  $r$  for the three event groups are:

- 1) Event group 2  
.70 <  $r$  < .85
- 2) Event group 3  
.39 <  $r$  < .43
- 3) Event group 6  
.61 <  $r$  < .74



TABLE H-9. LISTING OF FRAGMENT RANGE AND MASS  
FOR EVENT GROUPS 2, 3 AND 6

Event Group 2		Event Group 3		Event Group 6	
<u>Range</u>	<u>Mass</u>	<u>Range</u>	<u>Mass</u>	<u>Range</u>	<u>Mass</u>
112.9	74.8	233.0	2.22	31.39	.0341
19.9	94.8	63.37	93.61	28.35	.0967
73.6	183.0	115.82	237.66	25.2	.998
94.5	220.0	4.064	224.70	41.76	1.00
21.2	350.0	292.61	241.98	15.24	1.22
104.2	1150.0	29.13	387.18	17.68	1.22
145.7	1180.0	5.42	399.28	40.23	1.56
15.24	3183.0	206.59	470.70	58.83	9.3
30.48	6366.0	69.77	903.18	119.79	52.23
15.4	7470.0	112.44	1039.52	31.39	104.46
133.4	12200.0	66.38	1039.52	122.83	171.38
487.68	19098.0	65.70	1080.29		
335.28	19098.0	63.00	1082.13		
		110.41	1134.30		
		97.54	1281.78		
		39.96	1345.72		
		44.03	1439.81		
		54.19	1627.08		
		191.69	1703.20		
		207.94	1935.88		
		64.41	2007.72		
		73.15	2020.84		
		75.86	2223.24		
		32.51	2399.70		

U U

TABLE H-10. ESTIMATED PARAMETERS FOR REGRESSION MODELS FOR CORRELATION BETWEEN FRAGMENT RANGE AND MASS FOR EVENT GROUPS 2, 3 AND 6

Model*	Event Group								
	2			3			6		
	a	b	r	a	b	r	a	b	r
Linear	37.5572	.01558	.79	731.72	-0.5789	.18	34.2328	0.4534	.68
Power Curve	20.3775	.16782	.30	101.93	-0.0640	.09	31.3277	0.1692	.63
Logarithmic Curve	-9258.7	3472.05	.56	210.41	-17.4501	.35	32.9911	10.2442	.60

\* a is the range axis intercept

b is the slope

r is the correlation coefficient

Since one can be 95% confident that the correlation coefficient for event group 3 is less than .43, there would be little benefit in using the corresponding prediction model for fragment mass given fragment range, or vice-versa. However, for event groups 2 and 6 a sufficient degree of correlation between fragment range and fragment mass is indicated to make the prediction models worthwhile. These models are shown on Figures 4-11 and 4-12.

Correlation Analysis of Fragment Range to the Ratio of Mean  
Fragment Weight to Vessel Weight For Cylindrical Tanks

Five events with cylindrical tanks contained sufficient fragment mass information to determine the degree of correlation of fragment range to the ratio of mean fragment weight to vessel weight. It was necessary to group events 6 and 7 to have a sufficient sample size.

Table H-11 presents the data by event number, the ratio of the arithmetic mean fragment weight ( $\bar{W}$ ) to the vessel weight ( $W(T)$ ), and the arithmetic mean fragment range ( $\bar{R}$ ). Figure H-10 is a plot of the points in Table H-11 along with the prediction equation. The sample correlation coefficient is .987. Using the same techniques as described earlier, one can be 90% confident that the true population correlation coefficient is greater than .74.



TABLE H-11. MEAN RANGE AND RATIO OF MEAN FRAGMENT WEIGHT TO VESSEL WEIGHT FOR CYLINDRICAL TANKS

<u>Event</u>	<u><math>\bar{W}/W(T)</math></u>	<u><math>\bar{R}</math></u>
6,7	.644	179.83
18	.242	110.30
19	.100	80.08
25	.0612	39.20





$\left(\frac{dv}{dx}\right)_{\max}$	= maximum slope
E	= blast yield (energy); elastic modulus
E'	= blast yield (energy) for bursting pressure vessels
E <sub>c</sub>	= total heat of combustion
E <sub>e</sub>	= effective blast yield
E <sub>K</sub>	= kinetic energy of the fragment
E <sub>l</sub>	= end cap length
E <sub>o</sub>	= energy of detonation of 1 gram of TNT
E <sub>t</sub>	= end cap thickness
e	= specific energy; specific work; perforation thickness
F	= thrust; cross-sectional area; force
f' <sub>c</sub>	= ultimate concrete compressive strength
subscript <sub>f</sub>	= fluid (saturated liquid)
g	= acceleration of gravity; gravity constant
$\sqrt{g}$	= square root of the acceleration of gravity
subscript <sub>g</sub>	= gas (saturated vapor)
H	= total depth
$\bar{H}$	= scaled height
$\bar{H}_g$	= scaled gage height
h	= enthalpy; concrete panel thickness; height
h <sub>e</sub>	= enthalpy of gas at nozzle
h <sub>i</sub>	= enthalpy of gas
I	= second moment of area
$\bar{I}$	= scaled (dimensionless) impulse
I <sub>s</sub>	= side-on specific impulse



$I_s(-)$	= negative phase impulse for first shock
$I_s(+)$	= positive phase impulse for first shock
$\bar{I}_s$	= scaled (dimensionless) side-on overpressure
$i$	= impulse
$i_r$	= reflected impulse
$i_s$	= positive impulse
$K$	= coefficient of discharge; constant; concrete penetrability factor
$KE$	= impact kinetic energy
$L/D$	= length-to-diameter ratio
$L_z$	= confidence limit
$l$	= length; span
$M$	= total mass; mass of the overlying floor
$M_C$	= mass of the container
$Mg$	= force of gravity
$M_i$	= enclosed substance
$M_y$	= vertical inertial force
$M_x$	= horizontal inertial force
$(MW)$	= molecular weight
$m$	= mass of the liquid in the vessel
$N$	= number of fragment-mass pairs; projectile nose-shape factor
$n$	= number of fragments
$o$	= reservoir conditions immediately after failure
$P$	= peak applied pressure; pressure; internal pressure
$\bar{P}$	= average burst pressure



$P_a$	= atmospheric pressure
$\bar{P}_A$	= starting overpressure
$P-i$	= nondimensionalized pressure impulse
$P_{OO}$	= initial pressure
$P_r$	= peak reflected overpressure
$P_s$	= peak side-on overpressure
$\bar{P}_S$	= dimensionless overpressure
$P_{s1}$	= first shock side-on overpressure
$P_{s2}$	= second shock side-on overpressure
$\bar{P}V/E_o$	= normalized yield
$p$	= absolute pressure
$p_1$	= initial absolute pressure in the vessel
$p_1, V_1, S_1,$ $U_1, h_1$	= initial state variables
$pA$	= vertical load
$P_a$	= outside atmosphere absolute pressure; ambient pressure; atmospheric pressure
$P_c$	= critical pressure
$P_e$	= exit pressure
$P_n$	= internal pressure
$P_o$	= atmospheric pressure; back pressure
$p-v$	= pressure-volume plane
$q$	= energy expended in heating gas
$R$	= range
$\bar{R}$	= dimensionless distance; scaled distance; mean fragment range
$R_M$	= ideal gas constant





$\bar{W}$	= geometric mean fragment mass; mean fragment weight
WK	= maximum possible work
W(T)	= sphere weight, vessel weight
$W_o$	= deformation
$\dot{w}$	= mass flow rate
$w_o$	= maximum elastic deformation
x	= distance traveled by the fragment
$x_1$	= displacement distance along the axis of motion
$\ddot{X}$	= horizontal acceleration
x	= quality of the vapor; characteristic dimension; total penetration depth; the depth a missile will penetrate into an infinitely thick target
$x_1$	= initial quality
$x_2$	= final quality
$\dot{x}$	= horizontal velocity
y	= altitude
$\ddot{y}$	= vertical acceleration
$\dot{y}$	= vertical velocity
Z	= normal variate, dimensionless variable
z	= plastic section modulus

Greek Symbols

$\alpha$	= trajectory angle
$\alpha_i$	= initial trajectory angle, coefficient for simply-supported beam
$\alpha_p$	= numerical coefficient
$\gamma$	= ratio of specific heats, adiabatic exponent
$\gamma_1$	= ratio of specific heat for gas in the vessel



$\Delta t$  = small time  
 $\sigma$  = deflection  
 $\epsilon_{\max}$  = maximum strain  
 $\theta$  = trajectory angle, characteristic time, temperature  
 $\Pi$  = perimeter  
 $\rho$  = mass density  
 $\rho_*$  = gas density  
 $\rho g A$  = weight per unit length quantity  
 $\rho_0$  = density of air  
 $\sigma_{\max}$  = scaled stress  
 $\sigma_t$  = yield strength  
 $\sigma_u$  = ultimate stress  
 $\sigma_y$  = yield point  
 $\frac{\sigma_y}{E}$  = yield strain  
 $\frac{E \epsilon_{\max}}{\sigma_y}$  = scaled strain  
 $\sigma_z$  = standard error of Z  
 $\tau$  = time  
 $\psi_{p,i,\epsilon,w_0}$  = coefficients



## BIBLIOGRAPHY OF DATA SOURCES FOR MISSILE MAPS

Anonymous, "Railroad Accident Report-Derailment of Toledo, Peoria and Western Railroad Company's Train No. 20 with Resultant Fire and Tank Car Ruptures, Crescent City, Illinois, June 21, 1970," Report No. NTSB-RAR-72-2, National Transportation Safety Board, Washington, D.C., March 29, 1972.

Anonymous, "Railroad Accident Report - Southern Railway Company Train 154 Derailment with Fire and Explosion, Laurel, Mississippi, January 25, 1969," National Transportation Safety Board, Washington, D.C., October 6, 1969.

Anonymous, "Pipeline Accident Report - Southern Union Gas Company, Transmission Pipeline Failure, Near Farmington, New Mexico, March 15, 1974," Report No. NTSB-PAR-75-3, National Transportation Safety Board, Washington, D.C., December 23, 1975.

Anonymous, "Pipeline Accident Report - Consolidated Edison Company, Explosion at 305 East 45th Street, New York, New York, April 22, 1974," Report No. NTSB-PAR-76-2, National Transportation Safety Board, Washington, D.C., February 19, 1976.

Anonymous, "Railroad Accident Report Derailment of Tank Cars With Subsequent Fire and Explosion on Chicago, Rock Island and Pacific Railroad Company, Near Des Moines, Iowa, September 1, 1975," Report No. NTSB-RAR-76-8, National Transportation Safety Board, Washington, D.C., June 30, 1976.

Anonymous, "Highway Accident Report - Liquified Oxygen Tank Truck Explosion Followed by Fires in Brooklyn, New York, May 30, 1970," Report No. NTSB-HAR-71-6, National Transportation Safety Board, Washington, D.C., May 12, 1971.

Wilson, H. A., Jr., Belles, F. E., Clark, H. K., Crockett, C. D., Caplan, D. F., Shaw, R. C., Swain, R. L., Vincke, C. J., McSmith, D., "Report of Accident Investigating Board, 9 x 6 Thermal Structures Tunnel (TST), 600 PSIA Air Supply System," Report to Director, NASA Langley Research Center, Hampton, Virginia, April 1972.

Anonymous, "Railroad Accident Report - Chicago, Burlington and Quincy Railroad Company, Train 64 and Train 824, Derailment and Collision with Tank Car Explosion, Crete, Nebraska, February 18, 1969." Report No. NTSB-RAR-71-2, National Transportation Safety Board, Washington, D.C., February 24, 1971.

Anonymous, "Highway Accident Report - Multiple-Vehicle Collision, Followed by Propylene Cargo-Tank Explosion, New Jersey Turnpike, Exit 8, September 21, 1972," Report No. NTSB-HAR-73-4, National Transportation Safety Board, Washington, D.C., October 17, 1973.



BIBLIOGRAPHY OF DATA SOURCES FOR MISSILE MAPS (Cont'd.)

Anonymous, "Pipeline Accident Report - United Gas Pipe Line Company, 20-Inch Pipeline Rupture and Fire, Cartwright, Louisiana, August 9, 1976," Report No. NTSB-PAR-77-1, National Transportation Safety Board, Washington, D.C., April 26, 1977.

Anderson, C., Townsend, W., Zook, J. A., Cowgill, G., "The Effects of a Fire Environment on a Rail Tank Car Filled With LPG," BRL Report No. 1935, Aberdeen Proving Ground, Maryland, September 1976.

Pittman, J. F., "Blast and Fragments From Superpressure Vessel Rupture," Report No. NSWC/WOL/TR 75-87, Naval Surface Weapons Center, White Oak, Silver Spring, Maryland, February 1976.

U U U E U U U E U U U E U U U E U U U E U

## CONVERSION FACTORS

The following table provides multiplying factors for converting numbers and miscellaneous units to corresponding new numbers and SI units.

The first two digits of each numerical entry represent a power of 10. An asterisk follows each number which expresses an exact definition. For example, the entry "--02 2.54\*" expresses the fact that 1 inch =  $2.54 \times 10^{-2}$  meter, exactly, by definition. Most of the definitions are extracted from National Bureau of Standards documents. Numbers not followed by an asterisk are only approximate representations of definitions, or are the results of physical measurements. The accepted abbreviation in Système International (SI) is given in parentheses in the second column.

<u>To convert from</u>	<u>to</u>	<u>multiply by</u>
atmosphere	Pascal (Pa), <sup>2</sup> Newton/meter <sup>2</sup>	+05 1.013 25*
bar	Pascal (Pa), <sup>2</sup> Newton/meter <sup>2</sup>	+05 1.00*
British thermal unit (mean)	Joule (J)	+03 1.055 87
calorie (mean)	Joule (J)	+00 4.190 02
dyne	Newton (N)	-05 1.00*
erg	Joule (J)	-07 1.00*
Fahrenheit (temperature)	Celsius (C)	$t_c = (5/9)(t_F - 32)$
foot	meter (m)	-01 3.048*
inch	meter (m)	-02 2.54*
lb <sub>f</sub> (pound force, avoirdupois)	Newton (N)	+00 4.448 221 651 260 5*
lb <sub>m</sub> (pound mass, avoirdupois)	kilogram (kg)	-01 4.535 923 7*
Pascal	Newton/meter <sup>2</sup> (N/m <sup>2</sup> )	+00 1.00*
pound force (lb <sub>f</sub> avoirdupois)	Newton (N)	+00 4.448 221 615 260 5*







overpressure - pressure in a blast wave above atmospheric pressure

perforation thickness - the maximum thickness of material which will be completely penetrated by a missile at a given velocity.

reflected impulse - integral of reflected pressure-time history.

risk assessment - the estimation of effects of some potentially dangerous operation or situation; but also the estimation of the probability that the event will occur and cause some level of damage.

rocketing - propulsion of large fragments from liquid propellant vessels resulting from the change of the liquid propellant into a gas when the external pressure is released during the fracturing of the vessel.

scabbing thickness - thickness of a target required to prevent scabbing of material from the backface for a missile with a given velocity.

side-on impulse - integral of time history of side-on overpressure.

side-on overpressure - blast wave overpressure in an undisturbed blast wave.

single-revetted barricade - a mound which has been modified by a retaining wall preferably of concrete of such slope and thickness as to hold firmly in place the 3 ft. width of earth required for the top, with the earth at the natural angle on one side. All other requirements of a mound shall be applicable to the single-revetted barricades.

spalling or scabbing - the process of projection of pieces of material from impacted plates or walls by stress wave reflection.

stable buckling - bending of a column under axial impulsive load.

starting overpressure - a curve on a graph of dimensionless overpressure versus dimensionless distance used as a starting point to compute the overpressure at a given distance from the center of the vessel.

THRUST - a computer program for predicting trajectories of large parts of pressure vessels containing flash-evaporating fluids.

total penetration depth - the depth a missile will penetrate into an infinitely thick target.

TUTTI - two dimensional finite difference computer program for compressible fluids.

unconfined vapor cloud explosion - a quantity of fuel released to the atmosphere as a vapor or aerosol, subsequently mixed with air and then exploded by some ignition source.

UNQL - a computer program for predicting velocities of two unequal fragments of a failed pressure vessel.

vapor density - the ratio of the density of the vapor to that of air at standard temperature and pressure.

vapor dome - the dome-shaped curve on a plot of thermodynamic properties of a fluid which represents the boundary between wet vapor and superheat.

## BIBLIOGRAPHY

- Adamczyk, A. A. and Strehlow, R. A., (1977), "Terminal Energy Distribution of Blast Waves from Bursting Spheres", NASA CR-2903, Grant NSG 3008, September 1977.
- AISC Handbook, (1961), "Steel Construction", American Institute of Steel Construction, 5th Edition, New York, New York, 1961.
- Anderson, C., Townsend, W., Zook, J. A., Cowgill, G., (1976), "The Effects of a Fire Environment on a Rail Tank Car Filled With LPG", BRL Report No. 1935, Aberdeen Proving Ground, Maryland, September 1976.
- Anonymous, (1969), "Railroad Accident Report - Southern Railway Company Train 154 Derailment with Fire and Explosion, Laurel, Mississippi, January 25, 1969", National Transportation Safety Board, Washington, D.C., October 6, 1969.
- Anonymous, (1971a), "Railroad Accident Report - Chicago, Burlington and Quincy Railroad Company, Train 64 and Train 824, Derailment and Collision with Tank Car Explosion, Crete, Nebraska, February 18, 1969", Report No. NTSB-RAR-71-2, National Transportation Safety Board, Washington, D.C., February 24, 1971.
- Anonymous, (1971b), "Highway Accident Report - Liquified Oxygen Tank Truck Explosion Followed by Fires in Brooklyn, New York, May 30, 1970", Report No. NTSB-HAR-71-6, National Transportation Safety Board, Washington, D.C., May 12, 1971.
- Anonymous, (1972), "Railroad Accident Report-Derailment of Toledo, Peoria and Western Railroad Company's Train No. 20 with Resultant Fire and Tank Car Ruptures, Crescent City, Illinois, June 21, 1970", Report No. NTSB-RAR-72-2, National Transportation Safety Board, Washington, D.C., March 29, 1972.
- Anonymous, (1973), "Highway Accident Report - Multiple-Vehicle Collision, Followed by Propylene Cargo-Tank Explosion, New Jersey Turnpike, Exit 8, September 21, 1972", Report No. NTSB-HAR-73-4, National Transportation Safety Board, Washington, D.C., October 17, 1973.
- Anonymous, (1975), "Pipeline Accident Report - Southern Union Gas Company, Transmission Pipeline Failure, Near Farmington, New Mexico, March 15, 1974", Report No. NTSB-PAR-75-3, National Transportation Safety Board, Washington, D.C., December 23, 1975.
- Anonymous, (1976a), "Pipeline Accident Report - Consolidated Edison Company, Explosion at 305 East 45th Street, New York, New York, April 22, 1974", Report No. NTSB-PAR-76-2, National Transportation Safety Board, Washington, D.C., February 19, 1976.



BIBLIOGRAPHY (CONT'D)

Anonymous, (1976b), "Railroad Accident Report - Derailment of Tank Cars with Subsequent Fire and Explosion on Chicago, Rock Island and Pacific Railroad Company, Near Des Moines, Iowa, September 1, 1975", Report No. NTSB-RAR-76-8, National Transportation Safety Board, Washington, D.C., June 30, 1976.

Anonymous, (1977), "Pipeline Accident Report - United Gas Pipe Line Company, 20-Inch Pipeline Rupture and Fire, Cartwright, Louisiana, August 9, 1976", Report No. NTSB-PAR-77-1, National Transportation Safety Board, Washington, D.C., April 26, 1977.

Arkin, H. and Colton, R. R., (1950), Tables for Statisticians, Barnes & Noble, New York.

ASHRAE Handbook of Fundamentals, (1972), Am. Soc. of Heating, Refrigerating and Air Conditioning Engineers, Inc., New York.

Baker, W. E., (1973), Explosions in Air, University of Texas Press, Austin, Texas.

Baker, W. E., Esparza, E. D., Hokanson, J. C., Funnell, J. E., Moseley, P. K., and Deffenbaugh, D. M. (1978), "Initial Feasibility Study of Water Vessels for Arresting Lava Flow", AMSAA Contractor Report to be published.

Baker, W. E., Hokanson, J. C., and Cervantes, R. A., (1976), "Model Tests of Industrial Missiles", Final Report, SwRI Project No. 02-9153-001, Southwest Research Institute, San Antonio, Texas, May 1976.

Baker, W. E., Kulesz, J. J., Ricker, R. E., Bessey, R. L., Westine, P. S., Parr, V. B., and Oldham, G. A., (1975), "Workbook for Predicting Pressure Wave and Fragment Effects of Exploding Propellant Tanks and Gas Storage Vessels", NASA CR-134906, Contract NAS3-19231, November 1975 (reprinted September 1977).

Baker, W. E., Westine, P. S. and Dodge, F. T., (1973), Similarity Methods in Engineering Dynamics, Hayden Book Co., Rochelle Park, N.J.

Beth, R. A., (1945), "Concrete Penetration", OSRD-4856, National Defense Research Committee Report A-319, March 1945.

Boyer, W. D., Brode, H. L., Glass, I. I., and Hall, J. G. (1958), Blast From A Pressurized Sphere, UTIA Report No. 48, Institute of Aerophysics, University of Toronto, 1958.





BIBLIOGRAPHY (CONT'D)

Goodwin, R. D., Roder, H. M., and Straty, G. C., (1976), "Thermophysical Properties of Ethane, from 90 to 600 K of Pressures to 700 Bar", NBS Technical Note 684, National Bureau of Standards, August 1976.

Hahn, G. J. and Shapiro, S. S., (1967), Statistical Models in Engineering, John Wiley & Sons, Inc., N.Y.

Hammel, J., (1976), "Aircraft Impact on a Spherical Shell", Nuclear Engineering and Design, 37, 205-223.

Kennan, J. H., Keyes, F. G., Hill, P. G., and Moore, J. G., (1969), Steam Tables, John Wiley & Sons, Inc., N.Y.

Kennedy, R. P., (1976), "A Review of Procedures for the Analysis of Design of Concrete Structures to Resist Missile Impact Effects", Nuclear Engineering and Design, Vol, 37, 1976, pp 183-203.

Lee, J., Guirao, C., Chiu, K., and Bach, G., (1977), "Blast Effects from Vapor Cloud Explosions", Loss Prevention, Vol. 11, American Institute of Chemical Engineering, N.Y.

National Defense Research Committee, (1946), Effects of Impact and Explosion, Summary Technical Report of Division II, NDRC, Volume I, AD-221-586.

Parker, R. J., Pope, J. A., Davidson, J. F., and Simpson, W. J., (1974), "The Flixborough Disaster, Report of the Court of Inquiry", Her Majesty's Stationery Office London, June 1974.

Peterson, R. E., Editor, (1976), Proceedings of the Symposium on Tornadoes, Assessment of Knowledge and Implications for Man, Texas Tech. University, Lubbock, Texas, June 22-24, 1976.

Pittman, J. F., (1976), "Blast and Fragments From Superpressure Vessel Rupture", Report No. NSWC/WOL/TR 75-87, Naval Surface Weapons Center, White Oak, Silver Spring, Maryland, February 1976.

Pittman, J. F., (1972), "Blast and Fragment Hazards From Bursting High Pressure Tanks NOLTR-12-102, U. S. Naval Ordnance Laboratory, Silver Spring, Maryland, May 1972.

Robinson, C. A., Jr., (1973), "Special Report: Fuel Air Explosives, Services Ready Joint Development Plan", Aviation Week and Space Technology, February 19, 1973, pp 42-46.



BIBLIOGRAPHY (CONC'D)

- Strehlow, R. A., and Baker, W. E., (1975), "The Characterization and Evaluation of Accidental Explosions", NASA CR-134779, Grant NSG 3008, June 1975.
- Strehlow, R. A., and Baker, W. E., (1976), "The Characterization and Evaluation of Accidental Explosions", Progress in Energy and Combustion Science, 2, 1, pp 27-60.
- Strehlow, R. A., and Ricker, R. E., (1976), "The Blast Wave from a Bursting Sphere", Loss Prevention, Vol. 10, American Institute of Chemical Engineering, N.Y. pp 115-121.
- Stull, D. R., (1977), Fundamentals of Fire and Explosion, AIChE Monograph No. 10, Vol. 73, American Institute of Chemical Engineering, N.Y.
- Taylor, D. B., and Price, C. F., (1971), "Velocities of Fragments from Bursting Gas Reservoirs", ASME Transactions, Journal of Engineering for Industry, November 1971.
- Tucker, D. M., (1975), "The Explosion and Fire at Nypro (UK) Ltd., Flixborough, on 1 June 1974", Building Research Establishment, Fire Research Station, Borehamwood, Hertfordshire, England, July 1975.
- Wenzel, A. B and Bessey, R. L. (1969), "Barricaded and Unbarri-caded Blast Measurements, Final Report, Contract No. DAHC04-69-C-0028, Subcontract 1-OU-431, Southwest Research Institute, San Antonio, Texas, October 1969.
- Wilson, H. A., Jr., Belles, F. E., Clark, H. K., Crockett, C. D., Caplan, D. F., Shaw, R. C., Swain, R. L., Vincke, C. J., McSmith, D., (1972), "Report of Accident Investigating Board, 9 x 6 Thermal Structures Tunnel (TST), 600 PSIA Air Supply System", Report to Director, NASA Langley Research Center, Hampton, Virginia, April 1972.
- Zabetakis, M. G., (1965), "Flammability Characteristics of Com-bustible Gases and Vapors", Bulletin 627, Bureau of Mines, U. S. Dept. of the Interior.

☆U.S. GOVERNMENT PRINTING OFFICE: 1978-735-078/24





И И И И И И И И И И И И И И И И И И И



И И И И И И И И И И И И И И И И И И И





